


12-2016

Scaffold and Tissue Based Therapies to Improve Skeletal Muscle Regeneration After Volumetric Muscle Loss

Benjamin Kasukonis
University of Arkansas, Fayetteville

Follow this and additional works at: <http://scholarworks.uark.edu/etd>

 Part of the [Molecular, Cellular, and Tissue Engineering Commons](#)

Recommended Citation

Kasukonis, Benjamin, "Scaffold and Tissue Based Therapies to Improve Skeletal Muscle Regeneration After Volumetric Muscle Loss" (2016). *Theses and Dissertations*. 1807.
<http://scholarworks.uark.edu/etd/1807>

This Dissertation is brought to you for free and open access by ScholarWorks@UARK. It has been accepted for inclusion in Theses and Dissertations by an authorized administrator of ScholarWorks@UARK. For more information, please contact scholar@uark.edu, ccmiddle@uark.edu.

Scaffold and Tissue Based Therapies to Improve Skeletal Muscle
Regeneration After Volumetric Muscle Loss

A dissertation submitted in partial fulfillment
of the requirements for the degree of
Doctor of Philosophy in Engineering

by

Benjamin Kasukonis
University of Wisconsin – Stevens Point
Bachelor of Science in Biology, 2005
University of Arkansas
Master of Science in Biomedical Engineering, 2014

December 2016
University of Arkansas

This dissertation is approved for recommendation to the Graduate Council.

Dr. Jeffrey Wolchok
Dissertation Director

Dr. Timothy Muldoon
Committee Member

Dr. Tyrone Washington
Committee Member

Dr. Morten Jensen
Committee Member

Abstract

Volumetric muscle loss (VML) is an injury to skeletal muscle characterized by a loss of more than 20% of a muscle's volume. The combination of the bulk loss of tissue, transection and separation of myofibers proximal and distal to the injury, loss of innervation and blood supply, and the depletion of muscle progenitor cells results in permanent fibrosis and functional deficits due to loss of contractile tissue. Scaffolds, cells, and engineered constructs have been explored as potential therapeutic interventions to induce myogenesis at the site of a VML injury in animal models, in addition to limited clinical trials. This dissertation summarizes the current state of the field and explores possible strategies for repairing VML and understanding the mechanisms underlying the regenerative response of VML-damaged muscle. The challenges currently facing the skeletal muscle tissue engineering are presented along with potential approaches to further the field and deliver effective treatment options for patients and their physicians.

Acknowledgements

I would like to thank my peers in the Regenerative Biomaterials Lab at the University of Arkansas, especially Abby Terlouw and John Kim for their assistance and collaboration in this research. Special thanks is also due to my dissertation committee: Dr. Muldoon, Dr. Washington, and Dr. Jensen for their time and feedback.

And my sincerest thank you to Dr. Wolchok, for providing the opportunity and funding sources (NIH Award# R15AR064481 and Arkansas Biosciences Institute) that made all of this work possible.

Dedication

I would like to dedicate this paper to my wife, Faith, for her encouragement, patience, and resolute love.

Table of Contents

Chapter 1: Introduction.....	1
A. Overview of Skeletal Muscle Tissue.....	1
B. Repair and Regeneration of Skeletal Muscle.....	3
C. Volumetric Muscle Loss.....	7
D. Skeletal Muscle Tissue Engineering.....	10
E. Objective.....	33
References.....	35
Chapter 2: Development of an Infusion Bioreactor for the Accelerated Preparation of Decellularized Skeletal Muscle Scaffolds.....	49
A. Introduction.....	51
B. Methods.....	53
C. Results.....	61
D. Discussion.....	65
E. Conclusions.....	70
References.....	72
Figure Legend.....	77
Figures.....	80

Chapter 3: Co-delivery of Infusion Decellularized Skeletal Muscle with Minced Muscle Autografts Improved Recovery from Volumetric Muscle Loss Injury in a Rat Model.....88

A. Introduction.....90

B. Methods.....93

C. Results.....99

D. Discussion.....103

E. Conclusions.....111

References.....113

Figure Legend.....119

Figures.....123

Chapter 4: Autograft Relative Alignment Impacts the Regenerative Response of Skeletal Muscle After Volumetric Muscle Loss in a Rat Model.....133

A. Introduction.....135

B. Methods.....138

C. Results.....142

D. Discussion.....147

E. Conclusions.....151

References.....152

Figure Legend.....	156
Figures.....	159
Chapter 5: Conclusion.....	166
A. Evaluation of Muscle Regeneration.....	166
B. Further Characterization.....	169
C. Future Directions for VML.....	174
F. Remaining Challenges.....	176
References	179
Appendix.....	184

List of Published Papers

Chapter 2:

Kasukonis, B., Kim, J., Washington, T., & Wolchok, J. (2016). Development of an infusion bioreactor for the accelerated preparation of decellularized skeletal muscle scaffolds. *Biotechnology Progress*, doi:10.1002/btpr.2257

Chapter 3:

Kasukonis, B., Kim, J., Brown, L., Jones, J., Ahmadi, S., Washington, T., & Wolchok, J. (2016). Codelivery of infusion decellularized skeletal muscle with minced muscle autografts improved recovery from volumetric muscle loss injury in a rat model. *Tissue Engineering Part A*, 22(19-20), 1151-1163.

Chapter 1

Introduction

A. Overview of Skeletal Muscle Tissue

Skeletal muscle, which makes up almost half of the mass of the human body, is an organized tissue composed of muscle cells, nerves, blood vessels and connective tissue.(Lieber & Friden, 2000) Cells within skeletal muscle tissue include the multi-nucleated myofibers, regenerative satellite cells, and fibroblasts. Skeletal muscle tissue also contains the neurons, endothelial cells, and smooth muscle cells associated with the nerves and blood vessels that respectively innervate and exchange required molecules. The primary function of skeletal muscle is to provide contractile force to enable locomotion at the joints. The contractile cells of skeletal muscle are multinucleated myofibers that contract in response to acetylcholine being released into the neuromuscular junction between the muscle and a motor nerve.(Lieber & Friden, 2000) Muscle contraction causes muscle to have very high energy demands compared to most other tissues in the body and requires muscle to have an extensive blood supply. Muscle cells have such high oxygen requirements that they contain an intracellular protein, myoglobin, which has a higher affinity for oxygen than hemoglobin within red blood cells.(Wittenberg, 1970)

Skeletal muscle has a hierarchical construction in which myofibers are enclosed within a layer of connective tissue called endomysium and multiple endomysium-wrapped myofibers are surrounded by connective tissue, perimysium, to make up a structure called a fascicle.(Lieber & Friden, 2000) Multiple fascicles are then surrounded by a final layer of connective tissue known as the epimysium. The connective tissue within the muscle transmits the contractile force

collectively to musculotendinous junctions after which the force is then transferred from the tendon to bone to provide movement.(Lieber & Friden, 2000) Within this paper and unless otherwise noted, the epimysium, perimysium, and endomysium, in addition to the basement membrane, will be collectively referred to as the extracellular matrix (ECM).

The ECM of muscle provides a scaffold for cell attachment with specific architecture, a conduit for blood vessels and nerves within the belly of the muscle, and also protects myofibers from excessive stretching and distributes forces to minimize damage.(Gillies & Lieber, 2011) In addition, the ECM provides feedback from stretch and contraction to cells; mechanical stimuli has been shown to be very important for cell survival, growth, and metabolic activity.(KJÆR, 2004) Fibroblasts within muscle tissue are responsible for maintaining ECM and responding to injury when the structure of ECM is compromised. In cases when recovery from a traumatic defect is incomplete, fibroblasts will deposit an excess of ECM to create a fibrotic, non-contractile region.(Mann et al., 2011; Serrano & Muñoz-Cánoves, 2010; Tomasek, Gabbiani, Hinz, Chaponnier, & Brown, 2002)

B. Repair and Regeneration of Skeletal Muscle

When muscle receives an injury, cells within the muscle are capable of repairing and regenerating the contractile myofibers as well as the underlying ECM supporting structure.(Huard, Li, & Fu, 2002; Turner & Badylak, 2012) The normal repair process can be broken down into five stages: degradation, inflammation, regeneration, remodeling, and maturation. These stages are demarcated by the expression of different cytokines, release of growth factors, and the recruitment and activity of various cells. The initial degradation of myofibers has been linked to damage to the sarcolemma, the cell membrane of the myofiber.(Clarke & Feedback, 1996; Fredsted, Gissel, Madsen, & Clausen, 2007; Kasper, 1995) A damaged sarcolemma, which normally maintains a calcium ion gradient across the membrane, will allow an unregulated flood of calcium ions into the myofiber. These calcium ions activate proteases that will breakdown cellular components which recruit neutrophils, macrophages, and cells responsible for restoring the architecture of the muscle.(Fredsted et al., 2007) Necrotic tissue and damaged ECM also contribute to the pro-inflammatory environment present immediately after muscle damage.(Laumonier & Menetrey, 2016) Neutrophils are the first cells to arrive at the site of injury by releasing cytokines (TNF- α , IL-6), chemokines (CCL17, CCL2) and growth factors (FGF, HGF, IGF-I, VEGF; TGF- β 1).(Laumonier & Menetrey, 2016; Tidball, 1995; Toumi & Best, 2003) Neutrophils can also damage healthy muscle cells. Damaging healthy muscle cells can increase the inflammatory response by recruiting more M1 macrophages. M1 macrophages appear hours after a muscle is injured and their numbers are gradually reduced over the days that follow in the case of mild injury where complete regeneration is possible.(Arnold et al., 2007) M1 macrophages are pro-inflammatory cells which lyse cells, phagocytize cellular components, and upregulate the differentiation of myoblasts from

satellite cells. The initial wave of M1 macrophages subsides and M2 macrophages arrive at the injury site 2-4 days after the initial damage. M2 macrophages suppress the inflammatory response and stimulate the fusion of myoblasts which forms the myofibers.(Tidball & Wehling-Henricks, 2007) The interplay of M1 and M2 macrophages can lead muscle repair toward myogenesis or fibrosis depending on injury severity and the inflammatory environment.(Muñoz-Cánoves & Serrano, 2015) When muscle repair is deviated toward myogenesis, macrophage incursion into the defect site will be transient. As the inflammatory stages are taking place, regenerative processes will begin after having been initiated by immune cells that took part in clearing damaged tissue components.(Arnold et al., 2007)

Satellite cells are key cells of the regenerative stage. Satellite cells differentiate in response to factors released by the ECM upon incurring damage.(Montarras, L'honoré, & Buckingham, 2013) Factors that have been shown to activate satellite cells include: FGF(DiMario, Buffinger, Yamada, & Strohman, 1989), HGF(Allen, Sheehan, Taylor, Kendall, & Rice, 1995; Tatsumi, Anderson, Nevoret, Halevy, & Allen, 1998), IGF(Musarò et al., 2001) and TNF- α (Y. P. Li, 2003). Nitric oxide has also been shown to indirectly induce satellite cell differentiation by stimulating MMP production.(Tatsumi, 2010) Upregulating MMPs causes further degradation of the ECM, releasing more growth factors confined within the ECM.(Tatsumi, 2010) Satellite cell division must take place not only to provide the cells necessary to replace damaged myofibers, but also to renew the stockpile of satellite cells needed for future regeneration. Renewal of skeletal muscle stem cells during a myogenic event will occur through the asymmetric division of satellite cells.(Dumont, Bentzinger, Sincennes, & Rudnicki, 2015) One daughter cell will be an activated cell that will differentiate to a myoblast and the other daughter cell will remain a satellite cell. The asymmetric division of satellite cells

is characterized by the presence of Myf5 in cells committed to myogenesis and the absence of Myf5 in cells that will remain stem cells.(Knoblich, 2008) These uncommitted satellite cells can undergo symmetric division to replenish the pool of satellite cells in preparation for the next regenerative event.(Shi & Garry, 2006) Alongside stem cell activation, myogenic cell migration is also initiated by cytokines to recruit regenerative cells to the injury site. Migration of satellite cells can occur before or after activation, but studies have shown that the rate of migration is higher before activation takes place.(Schultz, Jaryszak, & Valliere, 1985; Siegel, Atchison, Fisher, Davis, & Cornelison, 2009a) A transmembrane protein, CD34, appears to be important for satellite cell migration as CD34-deficient mice have reduced satellite cell motility.(Alfaro et al., 2011) Chemotactic cytokines are not the only type of molecule responsible for myogenic cell migration, MMPs also aid in the process by degrading the ECM surrounding the satellite cells.(Kaar et al., 2008) MMP1, MMP2, and MMP9 proteolyze the collagen fibers that make up the ECM(Kaar et al., 2008), but MMP action is attenuated by an upregulation in TIMP, an MMP inhibitor. Therefore increased expression of both MMPs and TIMPs is seen during skeletal muscle regeneration to facilitate regenerative cell chemotaxis without compromising the integrity of the ECM.(Karalaki, Fili, Philippou, & Koutsilieris, 2009; Nishimura et al., 2008)

Myoblast proliferation begins after progenitor cells have been activated and migrate to the injury. A spike in pro-inflammatory cytokines, such as IL-6 and TNF- α , has been shown to take place concurrently to myoblast proliferation.(Allen et al., 1995) There are a number of pathways that can be activated or repressed to induce either proliferation of myoblasts or further differentiation. The JNK(Alter, Rozentzweig, & Bengal, 2008; Perdiguero, Ruiz-Bonilla, Serrano, & Muñoz-Cánoves, 2007) and NF-kB(Otis et al., 2014) pathways can both be activated to promote myoblast proliferation, while the JAK1/STAT1/STAT3 pathway suppresses genes

responsible for differentiation and pushes cells towards mitosis.(Sun et al., 2007) Suppressing premature complete differentiation allows for a more robust response to a skeletal muscle injury by increasing the pool of myogenic cells. The final steps of differentiation involve the repression of Pax7 and the increased expression of MyoD.(Olguin, Yang, Tapscott, & Olwin, 2007) Cells expressing MyoD will initiate the production of molecules associated with the contractility of mature myofibers.(Megoney, Kablar, Garrett, Anderson, & Rudnicki, 1996; Sabourin, Girgis-Gabardo, Seale, Asakura, & Rudnicki, 1999) Myosin heavy and light chains, troponin, α -actinin, and muscle creatine kinase will all be produced after myogenin, a downstream product of MyoD, is expressed.(Davie et al., 2007) Myotubes in turn fuse to one another to form multinucleated myofibers. These nascent myofibers are identified by cross sectional views that show centrally located nuclei, contrasted with mature myofibers in which the nuclei are located at the periphery of the fiber.

In addition to myofiber regeneration, ECM regeneration also must take place to restore the muscle to pre-injury condition. Fibroblasts within the tissue deposit new ECM when directed by cytokines released during the inflammatory stages. Muscle that receives a critical defect due to a massive wound or muscle compromised by disease will not regenerate and will instead develop a fibrotic scar. Myostatin is a pro-fibrotic growth factor responsible for inhibiting muscle regeneration and facilitating the proliferation of fibroblasts.(Z. B. Li, Kollias, & Wagner, 2008)

C. Volumetric Muscle Loss

If muscle sustains mild to moderate injury, such as contusions and small lacerations, satellite cells within the muscle are capable of replacing damaged myofibers and returning the muscle to full function.(Grogan, Hsu, & Skeletal Trauma Research Consortium, 2011; Mauro, 1961; Turner & Badylak, 2012) However, in the case of volumetric muscle loss (VML), where more than 20% of muscle volume is lost due to severe trauma, satellite cells are incapable of replacing the damaged tissue and the muscle will suffer permanent functional deficit.(Grogan et al., 2011; Sicari et al., 2012; Wu, Corona, Chen, & Walters, 2012a) The loss of volume from the muscle not only removes contractile myofibers, it also removes a significant stockpile of satellite cells. The remaining muscle undergoes fibrosis at the injury site, limiting the future contractile potential.(Corona et al., 2013a; Meyer & Lieber, 2012) The effect VML has on a muscle is dependent on the joint angle and muscle length, as found by Garg et al. in 2015. They reported that strength deficits in VML-damaged muscles may be significantly worse in joint angles in which the muscle is in a shortened position, such as dorsiflexion of the tibialis anterior (TA).(Garg et al., 2015) They also noted that VML results in a persistent reduction of fiber length. Their study highlights the complexity of VML injuries and considerations that must be understood to regenerate skeletal muscle tissue. “Not only the gross loss of muscle tissue but also architectural and histologic adaptations of the remaining tissue underlie the persistent functional deficits. Therefore, approaching full strength recovery of VML injured muscle will require therapies that maximize the functional capacity of the remaining muscle tissue, promote de novo regeneration of muscle tissue, and integrate these tissues to re-establish the intrinsic properties of the original muscle.”(Garg et al., 2015) Clinically, there are few options available to physicians to treat VML and regenerate lost tissue.(Grogan et al., 2011) Autografts have been used although

they introduce an additional surgical site and cause donor site morbidity.(Fisher & Mauck, 2013; Grogan et al., 2011)

Initial studies of skeletal muscle autografts performed over 100 years ago showed that if muscle was implanted back into the body it would undergo fibrosis and/or necrosis. Muscle was replaced in frogs, rodents, and canines with researchers eventually concluding that muscle could not remain viable after being freely transferred into an autologous or homologous host. In 1906, Hildebrandt hypothesized that muscle could be transferred as long as the tissue remained innervated. He found that muscle rapidly deteriorated and underwent fibrosis except of portions that were in contact with the healthy tissue that surrounded the implant site.(Thompson, 1971) He discovered that nascent anastomosis between the healthy tissue and implanted tissue had kept the nearest myofibers alive.(Thompson, 1971) Other early animal studies have shown that even if an autograft retains its blood supply and vasculature, gradual atrophy and fibrosis of the muscle will take place if it is not innervated. Thus, muscles that do not have a blood supply and are not receiving stimuli from a motor neuron will undergo ischemia and lose contractility. However, in 1970 Thompson showed that free muscle autografts could be successfully transplanted in humans if the autograft was reinnervated by a motor neuron from the muscles surrounding the implant site. Thompson transplanted either the palmaris longus or extensor digitorum brevis to treat facial paralysis in 8 patients.(Thompson, 1971) By implanting the free autografts in contact with functioning facial muscles, the intact motor neurons from adjacent muscles were able to branch such that the terminal buds came into contact with the motor end plate. All of the patients were able to demonstrate voluntary control of implanted muscles after 4 months and retained control through the end of the year and a half long study.(Thompson, 1971) Muscle flap autografts have been a treatment option for physicians treating VML for at least the

past 30 years.(Mase et al., 2010) Flap autografts differ from free autografts in that flap autografts remain attached to the origin of the muscle and preserve the connection to the systemic blood supply.(Klebuc & Menn, 2013) Many cases of flap autografts to repair the lower limb use the anterolateral flap to replace tissue lost in the anterior crural compartment of the lower limb.(T. Kim, Kim, Kim, & Lee, 2012; Lin, Lin, Yeh, & Chen, 2007) Functional recovery from this procedure is not expected as this intervention is used to create a favorable environment for soft tissue repair and for cosmetic reasons.(T. Kim et al., 2012) Free and flap muscle transfers are also used to improve functional outcomes of bone repair with or without bone allografts by providing a suitable environment for osteogenic repair.(N. Li, Yuan, Chen, Chen, & Jin, 2009; Masquelet, 2003) Similarly, in the upper extremity, physicians use free or flap muscle autografts to repair soft tissue damage.(Coulet, Boch, Boretto, Lazerges, & Chammas, 2011; Fan et al., 2008; Fischer, Elliott, Kozin, & Levin, 2013; Lohse, Lee, & Watson, 2014; Vekris et al., 2008) There have been isolated cases of free muscle transfers being used to restore function, specifically in restoring elbow flexion to patients that have suffered brachial plexus injuries.(Coulet et al., 2011; Fan et al., 2008; Lohse et al., 2014; Vekris et al., 2008)

D. Skeletal Muscle Tissue Engineering

Advances in tissue engineering have yielded researchers and physicians a number of treatment options for other tissues such as bone and skin.(Bi & Jin, 2013; Rossi, Pozzobon, & De Coppi, 2010) In contrast, very few options exist for skeletal muscle repair, although a number of scaffold-based and cell-based strategies are currently being developed.(Bursac, Juhas, & Rando, 2015; Laumonier & Menetrey, 2016; Qazi, Mooney, Pumberger, Geissler, & Duda, 2015) Scaffolds that are designed for skeletal muscle tissue engineering are not unlike scaffolds used for other applications in the body. They must promote the adhesion and proliferation of cells, they must be composed of biocompatible materials and they must provide the engineered tissue with properties similar to native tissue. However, skeletal muscle tissue has several additional requirements of scaffolds designed to repair skeletal muscle. Skeletal muscle tissue constructs must have parallel fibers to promote the formation of parallel myofibers, which are essential for contractile force, and must allow for vascularization and innervation in vivo.(Turner & Badylak, 2012) Vascularization is exceedingly important because cells must have access to oxygen and needed biomolecules from the moment the cells are seeded onto the scaffold.(Levenberg et al., 2005a) Innervation is necessary to provide electrical stimuli for the directed contractile force. 3D scaffold integration with host vascular and nervous networks must take place for successful regeneration of skeletal muscle.(Bursac et al., 2015) Damaged or diseased skeletal muscle can also be repaired without the use a three dimensional scaffold. Researchers have been able to repair a skeletal muscle defect using fibrin microthreads seeded with muscle-derived fibroblasts.(Page et al., 2011) The fibrin microthreads allowed the host to replace skeletal muscle tissue without forming considerable scar tissue as was seen in an untreated defect.(Page et al., 2011) The fibrin microthread treated muscle was able to regain 80-95% of original tetanic force,

whereas untreated, defected muscle only had around 55% of the original tetanic force.(Page et al., 2011)

Biologic and synthetic scaffolds have been developed to provide a stable environment for cell proliferation and the production of contractile tissue under in vitro and in vivo conditions. Biologic scaffolds include acellular extracellular matrix (ECM), collagen, hydrogels, and polymeric constructs which can be seeded with cells ranging from human stem cells to differentiated myoblasts.(Wolf, Dearth, Sonnenberg, Lobo, & Badylak, 2015) ECM scaffolds can have many different configurations; scaffolds can be therapeutically delivered as a powder, in sheets (either single-ply or laminate), as a hydrogel, or whole tissue 3D constructs.(Wolf et al., 2015) ECM has been shown to be an effective scaffold in many translational applications and, in various forms, is currently an FDA-approved biomaterial.(Chen, Xu, Wang, & Zheng, 2009) ECM not only provides a scaffold for cell attachment, but host immune degradation of the ECM also provides a pro-regenerative environment in many applications.(S. F. Badylak, Dziki, Sicari, Ambrosio, & Boninger, 2016; J. L. Dziki, Sicari, Wolf, Cramer, & Badylak, 2016)

ECM Scaffold Based Repair Strategies

In recent years, many researchers have used ECM based scaffolds to repair skeletal muscle defects in animal models. The research group out of the University of Pittsburgh led by Dr. Stephen Badylak has been using ECM derived from the small intestine submucosa (SIS) or urinary bladder submucosa of pigs a therapeutic scaffold to repair various tissues and structures since 1995.

The first studies used the SIS as a vascular graft in canines.(S. F. Badylak, Lantz, Coffey, & Geddes, 1989; Lantz, Badylak, Coffey, Geddes, & Blevins, 1990) Through these initial studies, they addressed the biocompatibility of the graft and found that by stripping the cells, they reduced the rejection response of the host's immune system, which is the principal challenge for any study involving the transplantation of whole organs or tissues. They also demonstrated decellularized porcine SIS is an effective scaffold, allowing for the infiltration of host cells while maintaining structural integrity of the entire tissue in conjunction with surrounding host tissue.(Lantz et al., 1990) The vascular grafts were gradually replaced by host cells and ECM which indicated to the researchers that complete recovery had taken place.(Sandusky Jr, Badylak, Morff, Johnson, & Lantz, 1992) This lead Badylak and his colleagues to use decellularized porcine SIS and the submucosa from the urinary bladder to repair a variety of tissues. They subsequently published papers on bladder wall, dural tissue, and esophageal repair using porcine SIS.(S. Badylak, Meurling, Chen, Spievack, & Simmons-Byrd, 2000; Cobb, Badylak, Janas, Simmons-Byrd, & Boop, 1999; Kropp et al., 1995; Kropp et al., 1996) They also used porcine SIS as a wound healing patch in a rodent model.(Prevel, Eppley, Summerlin, Sidner et al., 1995)

Within the field of musculoskeletal repair, they investigated the regenerative capabilities of an SIS bioscaffold in tendon, bone, and muscle of animal models. The tendon repair study, led by Badylak, showed that a defect within the Achilles tendon in canines could be repaired using decellularized porcine SIS.(S. F. Badylak et al., 1995) By measuring the uniaxial longitudinal tensile strength, they determined that the repaired portion of the tendon had greater strength than the proximal or distal ends of the tendon 12 weeks post-recovery. The SIS bioscaffold had been degraded and replaced by host tissue 8 weeks after implantation according to

immunohistological analysis.(S. F. Badylak et al., 1995) The initial bone repair study, led by Suckow, showed that SIS rapidly repaired a long bone defect in Sprague-Dawley rats.(Suckow, Voytik-Harbin, Terril, & Badylak, 1999) The SIS performed similarly to demineralized cortical bone treatment by first allowing for cartilage formation which was interchanged with mineralized bone.(Suckow et al., 1999) The first study investigating the regenerative potential of SIS in a muscle defect model took place in 1995 using an abdominal wall defect model.(Prevel, Eppley, Summerlin, Jackson et al., 1995) The abdominal wall defect model was developed using rats who received a 2cm x 2cm defect within the skeletal muscle of the abdominal wall. An SIS bioscaffold was placed into the defect. To assess skeletal muscle regeneration, Prevel and his group did qualitative histological analysis of thin muscle sections to determine that the SIS incorporated into the existing abdominal wall after two months with minimal inflammation and there was no evidence of host rejection of the donor tissue.(Prevel et al., 1995)

More recently, research groups associated with Dr. Badylak and the University of Pittsburgh have published research on using porcine SIS to repair VML in animal models. In one study, Turner et al. made a defect in the distal third of the gastrocnemius muscle and proximal half of the associated Achilles tendon of canines.(Turner et al., 2010) While in another study, Sicari et al. made a defect in murine quadriceps.(Sicari et al., 2012) The techniques used in determining the effectiveness of the SIS in repairing the skeletal muscle defect in both studies were similar. The researchers looked at the vascularization of the wound site, the infiltration of myoblasts and nascent myofiber formation, and they observed the progressive degradation of the SIS scaffold in the wound site. They noticed that the repair proceeded similarly to the earlier abdominal wall defect models, with a rapid degradation on the bioscaffold, neovascularization, and myoblasts forming isolated myofibers within the defect.(Sicari et al., 2012; Turner et al.,

2010) Badylak's group relies on histological evidence of wound repair and muscle formation and does not use in vivo functional testing as a measure of regeneration, although they have reported on ex vivo functional testing.(Turner et al., 2010) In addition to investigating decellularized porcine SIS as a bioscaffold to repair VML, Wolf et al. compared the regenerative performance of SIS to ECM derived from decellularized skeletal muscle.(Wolf, Daly, Reing, & Badylak, 2012) They observed differences in the biochemical composition of the ECM scaffolds, specifically: growth factors, glycosaminoglycans, and structural proteins of the basement membrane. However, using the same criteria as previous studies, they found that there was little difference between the regenerative capacities of the two bioscaffolds when used to repair an abdominal wall defect.(Wolf et al., 2012) They concluded that "superior tissue remodeling outcomes are not universally dependent upon homologous tissue derived ECM scaffold materials."(Wolf et al., 2012) Another Sicari et al. study (again within the Badylak group) published a translational study using ECM derived from porcine urinary bladder to repair VML in a rat model and in five human patients.(Sicari et al., 2014) The ECM derived from porcine urinary bladder matrix (UBM) is structurally and biochemically very similar to ECM derived from porcine SIS. The UBM elicited functional improvement in three of the five human patients.(Sicari et al., 2014) Although the authors were careful not to call the response "regeneration" and instead referred to the recovery as constructive remodeling. The distinction between these terms was more clearly explained in a recent review by Badylak et al. in 2016. The response of the host to the ECM bioscaffold is similar to innate repair mechanisms with infiltration of macrophages and a transient pro-inflammatory environment, followed by myogenesis and ECM remodeling, but the processes are not identical since current ECM-based

repair modalities are accompanied by long-lasting, though isolated, fibrosis at the injury site and no study has yet shown complete functional recovery from VML.(S. F. Badylak et al., 2016)

Badylak's group has since performed a larger clinical study with a 13 patient cohort. The patients had a variety of defect sites and mechanisms of injury but most experienced functional recovery after treatment with porcine ECM bioscaffolds (SIS, UBM, and dermal ECM). The authors reported a 37% improvement in functional strength and a 27% increase for range of motion tasks.(J. Dziki et al., 2016) This study provides evidence to justify the further exploration of ECM bioscaffolds as a therapy for VML, but the percent improvement from this study do not necessarily correspond to expected clinical outcomes due to the diversity of VML injury locations and severity. These patients also were outside the acute injury response phase and had undergone several previous surgeries for debridement and/or tenolysis.(J. Dziki et al., 2016) Animal models used for investigating VML repair typically deliver scaffolds and/or cells immediately after creation of a VML injury. Therefore it is difficult to compare functional recovery results from this human study to results seen in small or large animal models. This study also self-identifies several limitations with respect to the lack of a control treatment (scar debridement and prescribed physical therapy), the presence of varying comorbidities even with similar implantation sites, and failing to control for the placebo effect.(J. Dziki et al., 2016) However, this study, published online in July 2016, is currently the largest clinical study to date to explore ECM bioscaffold therapies for VML in human patients.

In addition to investigations with decellularized porcine submucosa scaffolds, Dr. Badylak and his group has advanced the characterization and use of decellularized scaffolds more broadly.(Gilbert, Sellaro, & Badylak, 2006) Decellularization is a process which removes the cellular components from a tissue leaving behind the intact ECM.(Gilbert et al., 2006)

Decellularized tissue is promising as a biologic scaffold because it retains the biochemical and morphological structure of the native ECM while having dramatically lower antigenicity than an allograft because it lacks foreign cell antigens.(Gilbert et al., 2006) Decellularization of tissues and whole organs can be accomplished through the use of chemical agents such as: surfactants, detergents or osmotic solutions.(Gilbert et al., 2006; Gillies, Smith, Lieber, & Varghese, 2010) Decellularization has been used to produce whole organ scaffolds for the heart(Ott et al., 2008), liver(Uygun et al., 2010), lungs(Ott et al., 2010), and kidneys(Sullivan et al., 2012). Whole organ decellularization in many cases has been achieved through the use of vascular perfusion.(Ott et al., 2008; Ott et al., 2010; Sullivan et al., 2012; Uygun et al., 2010) The major inlets and outlets (arteries and veins) and the capillary network of organs allow for perfusion of the entire organ.

One of the hallmark papers of decellularized tissue was published by Ott et al. in *Nature Medicine* in 2008. They sought to decellularize a mammalian heart and subsequently return cells to the resulting scaffold in an attempt to engineer a functional “bioartificial” heart.(Ott et al., 2008) They successfully decellularized the heart and repopulated the scaffold with neonatal cardiomyocytes, fibrocytes, endothelial cells, and smooth muscle cells. Although the bioartificial heart was responsive to electrical and chemical stimuli after 8 days, the contractile force only produced 2% of adult rat heart function. They did, however, report rhythmic depolarizations and contractions up to 5 minutes after the heart was removed from electrical pacing. The authors also stated that recellularization of the scaffold was incomplete as only 34% of tissue cross-sections were populated by injected cells.(Ott et al., 2008) While this study left a lot to be improved upon, it demonstrated the potential that decellularization had as a method for fabricating scaffolds with regenerative capacity.

While most skeletal muscle lacks the major arteries and veins used for perfusion decellularization, skeletal muscle can also be decellularized to form an ECM-based scaffold. Scaffolds composed of decellularized muscle are unique because they retain the parallel alignment of the native muscle from which they were obtained and pores for cell attachment left by the previous cells.(Wilson, Terlow, Roberts, & Wolchok, 2016) Decellularization of skeletal muscle can be accomplished through the use of chemical agents such as: surfactants, detergents or osmotic solutions.(Gilbert et al., 2006) Decellularized skeletal muscle (DSM) lacks the antigenicity of an allogenic transplant but requires the infiltration of host cells and revascularization with associated integration into the host vasculature to produce functioning myofibers.

Several research groups around the world are currently exploring the use of DSM as a scaffold to repair VML in animal models. In 2010, Merritt et al. published a study in *Tissue Engineering* in which they used DSM along with bone marrow-derived mesenchymal stem cells to repair a VML injury in the gastrocnemius of a rat.(Merritt et al., 2010) The peak isometric contractile force produced by the muscle repaired with ECM+cells was 84% of the uninjured contralateral muscle after a 42 day recovery period. The authors also noted a dense population of desmin+ cells in the defect area of ECM+cells repaired muscles as well as significantly more vWF+ blood vessel ingrowth.(Merritt et al., 2010) Results confirming this robust regenerative capacity of DSM in VML injuries have been reported in other research groups.

In a 2011 *Biomaterials* article, Perniconi et al. presented research in which most of a murine TA was removed, leaving only the distal tendon and enough muscle at the tibial origin to anchor a DSM scaffold.(Perniconi et al., 2011a) The authors did not perform any functional testing but described a pro-myogenic environment with capacity to support the *de novo*

formation of myofibers after implantation into a VML injury. The authors tracked the degradation of the acellular scaffold over four weeks and noted that it remained stable during initial macrophage invasion and was gradually degraded as host myoblasts migrated to the defect site. Centrally located nuclei were observed in the newly formed myofibers, indicative of skeletal muscle regeneration.(Perniconi et al., 2011a)

Repair of VML is not the only application which is being researched to investigate the regenerative potential of DSM. DeQuach et al. developed an injectable skeletal muscle matrix hydrogel to repair peripheral artery disease (PAD) in a rat hindlimb ischemia model.(DeQuach et al., 2012) In order to create ischemia, the femoral artery was resected in a rat model. One week post-hindlimb ischemia, either DSM hydrogel or collagen hydrogel was injected intramuscularly below the site of the initial defect. Arteriole density was significantly greater in the DSM hydrogel compared to collagen at 3, 5, and 7 days post-injection. The authors also reported a significant increase in the number of desmin+ cells that co-expressed Ki67, an indicator for proliferating satellite cell, present at the site of DSM hydrogel injection.(DeQuach et al., 2012)

Cell Based Repair Strategies

Many researchers in the field of skeletal muscle regenerative medicine tout the advantages of “off the shelf” therapies such as DSM derived ECM compared to cell-based therapies.(Swinehart & Badylak, 2016) The disadvantages of cell-based therapies include: inadequate supply of fresh donor cells, difficulty delivering cells, and potential for implanted cells to undergo transdifferentiation, leading to cancerous growth.(Dumont et al., 2015) The inadequate supply of donor cells is due to several reasons. One of which is due to the host rejection response typically associated with whole organ donation. Stem cells are usually

autologous and harvested from many different sources within the patient's body to include many different cell types. However, the first stem cell transplants were performed using allogeneic myoblasts to treat Duchenne Muscular Dystrophy (DMD). Although researchers had success initially with preclinical animal trials, the results from the first clinical trials were unsuccessful.(Huard et al., 1992; Huard et al., 1994; Kinoshita et al., 1994; Skuk, 2012) The conclusions drawn from these studies were that allogeneic myoblasts were not an effective treatment for DMD. Only 25% of the donor myoblasts remained viable after three days in two studies which was explained in a subsequent study that insufficient immunosuppressive therapy led to the host destroying most of the implanted myoblasts.(Guérette, Asselin, Skuk, Entman, & Tremblay, 1997) Almost 10 years later, Skuk et al. found that the implanted myoblasts did not migrate more than 200µm from the injection site.(Skuk et al., 2006) Another study hypothesized that the myoblasts had undergone precocious differentiation leading to a much smaller pool of myoblasts and by delaying cell cycle exit into asymmetric differentiation, the implanted pool of myoblasts was able to migrate further into the tissue.(Riederer et al., 2012) Other muscle derived cells have been indentified and studied for their impact on muscle regeneration, such as: CD133+ progenitor cells, muscle derived stem cells, multipotent perivascular progenitor cells.(Meng et al., 2014; Sampaolesi et al., 2006; Zheng et al., 2007) Studies using these cell types have been limited in scope and have not been used in clinical trials other than to determine the safety of delivery methods.(Cossu et al., 2015)

Mesenchymal stem cells (MSCs) are another broad stem cell type that have been used as a cell source for skeletal muscle tissue engineering. MSCs are precursor cells which eventually form the tissues of the mesoderm through chondrogenic, osteogenic, adipogenic, or myogenic differentiation.(Sicari, Dearth, & Badylak, 2014) The sources of donor MSCs used to investigate

muscle repair range from bone marrow and adipose tissue to placenta and umbilical cord.(Erices, Conget, & Minguell, 2000; Jiang et al., 2002; Scherjon et al., 2004; Zuk et al., 2001) Bone marrow derived MSCs (BM-MSCs) have been shown to provide a dose dependent effect on functional recovery from a crush injury.(Winkler et al., 2008) They have also been shown to interact with the microenvironment at the defect site to induce paracrine signaling with the host's own pro-inflammatory or myogenic cells.(Cizkova et al., 2011; Gang et al., 2009) Adipose derived stem cells (ADSCs) are an additional type of MSC that have been used in small animal hindlimb repair models. In 2010, Kang et al. found that injections of ADSCs into the ischemic hindlimb of a mouse improved perfusion after three days and had contributed to new myofiber formation after four weeks post-injury.(Kang et al., 2010) Work more recently by Kesireddy, has shown that while ADSCs do not increase myogenesis to the extent of muscle derived progenitor cells, they induce greater angiogenesis at the wound site and thus provide similar therapeutic outcomes within the context VML repair.(Kesireddy, 2016) Finally, umbilical cord blood (UCB) derived MSCs have been shown to have high myogenic potential by Pesce et al. when used in an ischemic hindlimb models.(Pesce et al., 2003) Like other MSCs, UBC derived MSCs have the potential to not only induce myogenesis but promote angiogenesis and deliver paracrine signals that encourage differentiation of host satellite cells and other progenitor cells.(Sicari et al., 2014)

Skeletal Muscle Repair with Minced Muscle

One novel approach for reducing the complexity of satellite cell delivery is the use of minced muscle (MM). MM is derived by mincing a small volume of muscle into pieces smaller than 1-2mm.(Corona et al., 2013b) MM differs from other cell-based therapies by delivering more than just progenitor cells to the injury site; basement membrane fragments, damaged

myofibers, and ECM captive growth factors are also present at implantation.(Corona et al., 2013b) If taken from around the area of the defect site, MM would not require an additional surgical site. In 2013, Corona et al. from the United States Army Institute of Surgical Research at Fort Sam Houston, published a paper on the use of autologous minced muscle grafts. This research further explored the regenerative capacity of minced muscle which had first been observed by Studinsky and Carlson in 1964 and 1972, respectively.(Carlson, 1968; Studitsky, 1965) Corona et al. first determined the proliferative capacity of the MM by culturing it on collagen coated dishes. They observed increasing nucleic acid out to 14 days and increasing numbers of desmin-positive cells, indicating that not only were cells proliferating but that myogenesis was occurring. Using immunohistochemical staining the authors also found that the expression of Pax7, CD31, myogenin, embryonic myosin heavy chain (emb-MHC), and CD163 were all significantly higher in MM treated VML injuries than non-repaired VML injuries.(Corona et al., 2013b) They then used a rat TA model for VML injuries and implanted the defected muscle orthotopically back into the defect site after mincing in into 1mm³ fragments. The contralateral limb was untreated to serve as a control and the rats were given an eight or sixteen week recovery period. The mass of the repaired TA was 11 and 21% heavier than unrepaired TAs after eight and sixteen weeks, respectively. The MM-treated limbs also produced ~14% more isometric torque at 16 weeks post-injury than unrepaired limbs. Motor endplates were also observed in regenerated muscle fibers using α -bungarotoxin staining at 8 weeks post-injury. They also determined that the fibers were innervated by repeatedly stimulating the muscle to deplete glycogen storage in innervated fibers. Glycogen levels of in the remaining muscle mass on the defected limb were similar to glycogen levels in the defect repair and both were significantly lower than non-stimulated muscle. Thus indicating that the nascent

myofibers within the defect area underwent glycogen depletion and were therefore innervated.(Corona et al., 2013b) The authors also identified several challenges and limitations to autologous transfer of MM to treat VML, the primary challenge being the introduction of a second surgical site on the patient to harvest skeletal muscle tissue. Nevertheless, since few other strategies to repair VML exist, Corona et al. concluded that “the use of minced muscle autografts is an appropriate standard for the future advancement of VML therapies.”(Corona et al., 2013b)

The United States Army Institute of Surgical Research at Fort Sam Houston has conducted further studies exploring the regenerative potential of MM by expanding the minced autograft in a collagen hydrogel. The rationale for this 2015 study, authored by Ward et al., was that donor muscle tissue was limited and expansion and co-delivery with a collagen hydrogel could limit the amount of donor tissue necessary to facilitate regeneration of a VML injury.(Ward, Ji, & Corona, 2015) The goal of this study was to determine the minimum volume of MM needed to obtain functional outcomes consistent with a 100% volume MM autograft.(Ward et al., 2015) The treatment groups the authors tested were 0%, 25%, 50%, and 100% MM with a volume of collagen to equal 400 μ L, the estimated size of the defect created in the TA muscle of male Lewis rats. The authors reported that the 50% autograft provided functional outcomes similar to 100% autografts with respect to peak tetanic force. However, the number of *de novo* fibers regenerating in the defect site of the 50% autograft were half the number of myofibers developing in the defect site of the 100% autograft. Another key finding was that the average fiber area was smaller in 50% and 100% autografts than fibers found in uninjured, control muscle tissue.(Ward et al., 2015)

In addition to exploring the use of MM autografts to repair VML in animal models, the United States Army Institute of Surgical Research at Fort Sam Houston, led by Dr. Corona has

contributed to the field of skeletal muscle tissue engineering by providing evidence against the use of acellular ECM implant alone to repair VML injuries. They have published several papers providing evidence counter to many of the articles published by the Badylak research group, who, as previously discussed, has promoted the use of porcine-derived SIS or UBM scaffolds to repair skeletal muscle tissue.(Aurora, Roe, Corona, & Walters, 2015; Corona et al., 2013a) In one study, authored by Aurora et al., the U.S. Army research group tested the regenerative capacity of porcine UBM and rat-derived decellularized muscle ECM (m-ECM) and compared functional outcomes and histological data to unrepaired muscle and muscle repaired using an autograft.(Aurora et al., 2015) The autograft repair in this instance was simply the muscle removed by creating the VML defect and suturing it orthotopically back into the defect site. The UBM graft improved the functional strength of the muscle by 17% after 16 weeks of recovery when compared to unrepaired muscle. However, the autograft repair group had significantly higher functional recovery than the acellular repair and after 16 weeks had produced 83% of the force generated by an uninjured contralateral limb. Histological analysis of the defect site for the treatment groups provided evidence that very little *de novo* fiber development was taking place in muscles repaired with acellular grafts.(Aurora et al., 2015) The authors reported that the number of myosin+ fibers was 100 times higher in the defect area of autograft repaired muscles compared to the defect area of muscles repaired with either UBM or m-ECM acellular grafts. They also noted that fiber formation in acellular graft repaired muscle at eight weeks post-implantation was only taking place within 200-300µm of the defect margins and that by 16 weeks, there were no early developing muscle fibers. The collagen deposition measured in the defect area of UBM repaired muscles remained consistent with values seen in unrepaired muscle, whose self-repair mechanism is permanent fibrosis. These observations led researchers to

conclude that acellular scaffolds, while providing modest functional recovery, do not facilitate myogenesis.(Aurora et al., 2015) Moreover, any improvements in muscular force output are likely due to the creation of functional fibrotic tissue that lacks the contractility of normal skeletal muscle tissue but stabilizes and links remaining contractile myofibers.(Aurora et al., 2015)

Another aspect within studies conducted by Dr. Corona's group which adds value to the field of skeletal muscle tissue engineering is that they investigate the effect rehabilitation has on functional recovery in animal VML models. They have reported that exercise, such as running wheels for rodents, does not seem to improve functional recovery for defected muscles repaired with acellular scaffolds.(Aurora et al., 2015) Animals receiving the same therapeutic intervention but with one half of the group having access to a voluntary running wheel and the other half having no access to an exercise wheel, had no significant differences in force production or tissue composition.(Aurora et al., 2015) In a previous study, Aurora et al. found that physical rehabilitation improved force production (17% improvement in peak isometric torque) and led to a 13% increase in muscle weight of animals that had an unrepaired VML injury.(Aurora, Garg, Corona, & Walters, 2014) But, wheel running did not alter the morphological characteristics of the unrepaired muscle; there was no additional myogenesis nor fiber hypertrophy in the muscles receiving a VML injury, regardless of rehabilitation.(Aurora et al., 2014) There was, however, an up-regulation of pro-fibrotic genes (Collagen I and TGF- β) in the unrepaired muscles of rats who had access to the running wheel.(Aurora et al., 2014)

Synthetic Scaffold Based Repair Strategies

Synthetic materials manufactured into scaffolds for skeletal muscle tissue engineering have been and are currently being investigated for their regenerative capacity as a therapy for VML. Synthetic scaffolds have several key advantages over biologic scaffolds from an engineering standpoint. They can be manufactured with precise specifications with respect to composition and architecture, and materials used in synthetic scaffolds have been better characterized than many biologic scaffolds.(Wolf et al., 2015) While these are advantages for the consistent, customizable, and high-throughput manufacture of tissue engineering scaffolds and allow for more precise characterization, synthetic scaffolds have not had more success than biologic scaffolds when used in animal models for skeletal muscle tissue engineering. Several types of polymers have been considered and evaluated for their potential as repair modalities for skeletal muscle trauma, they include: poly(glycolic acid) (PGA), poly(lactic acid) (PLA), poly(lactic-co-glycolic acid) (PLGA), poly(caprolactone) (PCL), polypropylene, and polyurethanes.(Wolf et al., 2015)

Polypropylene was one of the first biomaterials used for tissue engineering due to its relative bio-inertness. However, in recent years, it has not been used prevalently as bio-absorbable materials have been shown to be more appropriate due to the tendency of a host's immune system to encapsulate any material that does not degrade readily.(Anderson, Rodriguez, & Chang, 2008) Permanent encapsulation with fibrotic tissue would preclude the primary function of any material used to facilitate the regeneration of contractile muscle tissue.

PGA scaffolds have been in use for the past 17 years to repair skeletal muscle tissue. The initial PGA study, authored by Saxena et al., found that by seeding a primary cell line of myoblasts onto PGA absorbable mesh and implanting the construct into a Fisher 344 rat, they

could regenerate tissue that resembled skeletal muscle.(Saxena, Marler, Benvenuto, Willital, & Vacanti, 1999) Immunohistochemistry revealed that 45 days post-implantation, cells within the stands of the degrading synthetic graft stained positive for α -sarcomeric actin and desmin. The graft was also vascularized, however, the implantation site used in this study was the omentum.(Saxena et al., 1999) Although this paper provides evidence of the biocompatibility of the construct, it cannot be extrapolated to include myoblast-seeded PGA as an appropriate scaffold for VML unless functional testing and/or orthotopic implantation within a defected skeletal muscle is performed.

PLA has only been used as a substrate upon which C2C12 (mouse skeletal muscle cell line) and HSKM5 (human skeletal muscle cell line) were attached and their viability and proliferative response was observed and reported in a paper authored by Cronin et al..(Cronin et al., 2004) The PLA, as a fiber and as a film, was coated with either ECM gel, gelatin, fibronectin, or laminin before cells were seeded. ECM-coated PLA outperformed other scaffolds with respect to cell attachment and expression of skeletal muscle related genes.(Cronin et al., 2004) However, the *in vitro* nature of this study limits the impact PLA could potentially have as a therapeutic scaffold for skeletal muscle tissue engineering.

PLGA scaffolds are an attractive material for scaffold fabrication due to the nontoxicity of its degradation products: lactic acid and glycolic acid. Many studies have been performed under *in vitro* conditions to fabricate biomimetic constructs for a variety of applications, including skeletal muscle repair. A paper, authored by Shandalov et al., reported promising results with a stem cell seeded PLA-PLGA scaffold implanted into an abdominal wall defect model in a mouse.(Shandalov et al., 2014) Before orthotopic implantation into the abdominal wall, the researchers implanted the scaffold around the femoral artery and vein and isolated the

construct from surrounding tissue. This *in vivo* preconditioning initiated vessel formation within the scaffold and the new vasculature survived through the subsequent removal and re-implantation into the abdominal wall.(Shandalov et al., 2014) They observed anastomosis with the host vasculature and robust perfusion of the scaffold 2 weeks postimplantation. There have other *in vivo* studies in animal models using PLGA scaffolds, although results from these studies have no provided evidence of functional recovery from extremity VML repair.(Laschke et al., 2008; Levenberg et al., 2005b)

PCL is another promising synthetic biomaterial that has been investigated for its compatibility as a scaffold for skeletal muscle tissue engineering. Some of the best examples of PCL scaffolds are ones that have been fabricated using electrospinning, a method that is used to arrange synthetic constructs by extruding a polymer onto a charged plate. By varying the charge and deposition rate, researchers are able to create a scaffold with aligned microstructure, suitable for muscle progenitor cell adhesion and proliferation.(Choi, Lee, Christ, Atala, & Yoo, 2008a) Electrospun PCL scaffolds have been fabricated with aligned fibers, which has been shown to be important for myotube formation *in vitro*.(Choi et al., 2008a)

Polyurethane scaffolds have also been developed using electrospinning fabrication techniques. Researchers have reported that multiple skeletal muscle cell lines, such as: C2C12, L6, and human satellite cells, have proliferated and differentiated on polyurethane scaffolds.(S. A. Riboldi, Sampaolesi, Neuenschwander, Cossu, & Mantero, 2005) Polyesterurethane scaffolds have been developed and explored due to their favorable mechanical properties. PLA, PGA, and PLGA fibers have a high tensile modulus and researchers have suggested that this would prevent them from being used in the dynamic niche of skeletal muscle tissue engineering.(S. A. Riboldi et al., 2005) Polyesterurethane fibers are elastomeric and have been shown to provide a suitable

substrate for skeletal muscle progenitor cell attachment, proliferation, and differentiation.(S. Riboldi et al., 2008; S. A. Riboldi et al., 2005; Sirivisoot & Harrison, 2011)

One benefit to using synthetic scaffolds is that their morphology can be tuned for a specific application. Synthetic biomaterials used for skeletal muscle tissue engineering have been fibers, mesh, hydrogels, and foams. Synthetic scaffolds are designed to mimic the ECM with respect to the alignment of fibers and pore size.(Klumpp, Horch, Kneser, & Beier, 2010)

Although synthetic scaffolds may not have the exact biochemical composition of native ECM, researchers are able to direct the organization of the fibers.(Avis, Gough, & Downes, 2010; Choi et al., 2008a) Hydrogels lack any organization for cell attachment and researchers must modify the surface with microfabrication techniques if a hydrogel is to be used in skeletal muscle tissue engineering. Micropatterning with soft photolithography, a technique used in microfluidics, can create channels on which cells can adhere and proliferate.(Huang, Lee, & Li, 2010a)

Many synthetic scaffolds proposed as alternatives to repair skeletal muscle tissue trauma have only been characterized under in vitro conditions and only with a cursory knowledge of skeletal muscle tissue morphology and physiology. Although cell viability and proliferation is important to establish for any skeletal muscle scaffold suggested for implantation into even a small animal model, more rigorous in vivo testing must be undertaken before synthetic and tissue engineered skeletal muscle have any translational applications. Skeletal muscle regeneration after a VML injury is a complicated process with many spatio-temporal considerations to address. Synthetic scaffold research to this point has been focused on developing in vitro biomimetic skeletal muscle, but little advancement has taken place in terms of in vivo testing within skeletal muscle tissue beyond biocompatibility and host cell infiltration analysis,

excluding work done in abdominal wall defect models. However, there are some tissue engineered constructs that have been studied for contractile force production in vivo and even within a VML injury.

Engineered Skeletal Muscle Tissue

In addition to developing scaffolds, some researchers have sought to engineer skeletal muscle tissue from cells. Tissue engineered skeletal muscle can function as a model for pharmacological research, a tool for understanding embryological development and/or myogenesis, or a therapeutic intervention for repairing skeletal muscle trauma. Two separate groups have been using tissue engineered skeletal muscle under in vivo conditions and, more importantly, within skeletal muscle tissue. Dr. Juhas and Dr. Bursac from Duke University and Dr. Larkin from the University of Michigan have developed constructs that produce contractile force and, in the case of Dr. Larkin's research, have successfully integrated into damaged host muscle. Juhas et al. fabricated engineered skeletal muscle by first molding a MatriGel hydrogel with primary rat myoblasts in a PDMS mold. The authors noted the first objective was to create an in vitro environment that more accurately reproduces the in vivo environment of the myogenic tissue niche. Satellite cell proliferated and differentiated under in vitro conditions and the researchers directed the development of cells into an engineering skeletal muscle tissue. The engineered construct was capable of contractile force generation before it was implanted into a dorsal window on a rat. At 2 week postimplantation, the construct was producing 3.5x more contractile force than the pre-implanted engineered muscle. The engineered muscle also showed robust vascular ingrowth from the host vasculature and a 40.7% increase in myofiber diameter. The authors reported that engineered muscle appeared to have a myogenic response to

implantation even though it was not within a skeletal muscle niche. In addition, the authors reported vigorous recovery from an *in vitro* cardiotoxin injury. Juhas et al. concluded that the results from their research supports using *in vitro* engineered muscle as a tool for drug and toxicology studies.

Dr. Larkin's group has also developed tissue engineered muscle tissue and have used their construct to specifically repair VML in an animal model. In a paper authored by VanDusen et al., they report that a rat TA muscle with a VML injury receiving therapeutic intervention with their construct produced significantly more *in vivo* tetanic contractile force than an unrepaired TA. (VanDusen, Syverud, Williams, Lee, & Larkin, 2014a) The fabrication of their engineered muscle used techniques similar to those by Dr. Bursac's group. Muscle progenitor cells, along with isolated bone marrow cells, were harvested from the soleus muscle of 120 – 150 g female Fisher 344 rats. Bone marrow cells were cultured in appropriate media to produce engineered bone-tendon anchors used to implant the engineered muscle tissue. The muscle progenitor cells were grown to confluence until elongating myotubes began to form and the monolayer was delaminated and rolled into a cylindrical muscle construct. In addition to determining *in vivo* peak tetanic force, the researchers also evaluated the regenerative potential of the engineered muscle through histological data. Fluorescent imaging revealed aligned myofibers that had developed advanced sarcomeric structure. At 28 days post-implantation, there was evidence of innervation of the engineered construct through IHC staining for pan-axonal filaments and the presence of ACh receptors through α -bungarotoxin staining. Immunostaining with CD-31 also showed the presence of a well-developed capillary network throughout the engineered muscle tissue. The capillary network was morphologically similar to those found in native muscle, with vessels running parallel to the muscle fibers. The results from this study and others performed by

Dr. Larkin's group have motivated further investigations using engineered muscle tissue to repair VML in larger volume models and to explore entire muscle replacement.

As previously discussed, skeletal muscle tissue is highly aligned and the force production of a muscle is heavily influenced by the muscles architecture. Muscle architecture, the arrangement of muscle fibers in relation to the axis of force generation, is constrained by the length of the muscle, the length of myofibers, the pennation angle, and the physiological cross sectional area (PCSA).(Lieber & Friden, 2000) Even in pennate muscles, adjacent myofibers have parallel alignment and the surrounding ECM is highly uniform in direction. When designing bioreactors for tissue engineered skeletal muscle, researchers are deliberate in developing alignment within their constructs.(Aubin et al., 2010; Aviss et al., 2010; Huang, Lee, & Li, 2010b; Vandeburgh & Karlisch, 1989) Parallel alignment of myofibers has been shown to be important for developing phenotypically normal muscle tissue under *in vitro* conditions.(Aubin et al., 2010; Lam, Huang, Birla, & Takayama, 2009; Vandeburgh & Karlisch, 1989; Wang, Wu, Guo, & Ma, 2015) Researchers obtain parallel alignment through micropatterning(Cimetta et al., 2009; Flaibani et al., 2009; Huang et al., 2010a; Shimizu, Fujita, & Nagamori, 2009), aligned deposition of fibers(Aviss et al., 2010; Choi, Lee, Christ, Atala, & Yoo, 2008b; Wang et al., 2015), or by selecting a scaffold that has native parallel alignment. Myofiber alignment indicative of a mature muscle phenotype has also been induced *in vitro* using bioreactors that deliver mechanical or electrical stimulation to cells and/or tissue constructs.(Ahadian et al., 2013; Boonen et al., 2010a; Donnelly et al., 2010; Flaibani et al., 2009; Grossi, Yadav, & Lawson, 2007; Langelaan et al., 2011; Powell, Smiley, Mills, & Vandeburgh, 2002; Vandeburgh & Karlisch, 1989)

Table 2: Highlighted VML repair studies.

VML Repair Strategy	Animal Model	Outcome	Authors
DSM + MSCs	Rat (Gastroc.)	Improved contractile force. Evidence of myogenesis with addition of MSCs.	Merritt et al., 2010
SIS	Canine (Gastroc.)	No improvement in contractile force. Neovascularization and formation of isolated myofibers within defect.	Turner et al., 2010
DSM	Murine (TA) (Whole muscle)	Gradual degradation of ECM scaffold. Myoblast migration to defect. Centrally located nuclei in myofibers.	Perniconi et al., 2011
SIS	Murine (Quadriceps)	Rapid degradation of ECM scaffold. Vascularization and nascent myofiber formation at the defect site.	Sicari et al., 2012
DSM	Rat (Abdominal wall)	No remarkable difference between SIS and DSM. Isolated <i>de novo</i> myofiber formation and fibrosis at defect site.	Wolf et al., 2012
SIS			
MM	Rat (TA)	Greater contractile force. Motor endplates in new myofibers.	Corona et al., 2013
Engineered Skeletal Muscle	Rat (TA)	Significant improvement in contractile force when compared to unrepaired VML muscle. Blood vessel ingrowth and innervation.	VanDusen et al., 2014
MM + collagen hydrogel	Rat (TA)	50% MM produced contractile force similar to 100% MM, but had fewer new myofibers. Average fiber area smaller than control muscle.	Ward et al., 2015
Autograft	Rat (TA)	Autograft had greatest force recovery (83%) compared to acellular scaffolds. Myofiber formation only 200-300 μ m from defect margins. UBM treated muscle had fibrosis similar to unrepaired muscle.	Aurora et al., 2015
UBM			
DSM			

E. Objective

The foundational goal of this research is to provide additional evidence to the following hypothesis: ECM provides a therapeutic platform to aid in the regeneration of skeletal muscle after volumetric muscle loss.

What is proposed is to improve methods of obtaining DSM, use DSM to repair VML in an animal model, and to explore the effect of alignment and misalignment of VML repair strategies within a defected muscle. We will use minced muscle as a source of cells and additional signaling molecules to improve muscle regeneration. The use of minced muscle alone has been shown to improve muscle regeneration and we intend to further explore its potential when co-delivered with DSM. We will then explore the microenvironment between an autograft and a muscle with a VML injury. In doing so, we hope to study the effect alignment has on fibrosis and/or myogenesis at the interface of the graft and damaged muscle.

We seek to further explore VML repair by investigating the effect scaffold alignment has at the interface of the damaged muscle and tissue repair construct. While many researchers have established the importance of alignment when engineering or selecting an effective scaffold, no studies have investigated the effect of alignment or misalignment between the myofibers of the autograft and the myofibers of muscle that has sustained a VML injury. By first investigating the effect of autograft alignment within a VML defect on the functional recovery, we hope to guide our future repair strategies including DSM and cell-derived ECM scaffolds.

A brief outline of the approach is as follows:

- A perfusion decellularization system will be developed to produce skeletal muscle ECM scaffolds.
- Scaffolds (diffusion and perfusion decellularized) will be characterized to ensure the perfusion process does not negatively alter ECM.
- DSM with and without the addition of MM will be implanted within a defected muscle to repair VML in an animal model.
- The final portion of this study will be to explore the effect of alignment has on the regenerative potential of an autograft to repair VML.

References

- Ahadian, S., Ramon-Azcon, J., Ostrovidov, S., Camci-Unal, G., Kaji, H., Ino, K., . . . Matsue, T. (2013). A contactless electrical stimulator: Application to fabricate functional skeletal muscle tissue. *Biomedical Microdevices*, *15*(1), 109-115. doi:10.1007/s10544-012-9692-1; 10.1007/s10544-012-9692-1
- Alfaro, L. A. S., Dick, S. A., Siegel, A. L., Anonuevo, A. S., McNagny, K. M., Megeney, L. A., . . . Rossi, F. (2011). CD34 promotes satellite cell motility and entry into proliferation to facilitate efficient skeletal muscle regeneration. *Stem Cells*, *29*(12), 2030-2041.
- Allen, R. E., Sheehan, S. M., Taylor, R. G., Kendall, T. L., & Rice, G. M. (1995). Hepatocyte growth factor activates quiescent skeletal muscle satellite cells in vitro. *Journal of Cellular Physiology*, *165*(2), 307-312.
- Alter, J., Rozentzweig, D., & Bengal, E. (2008). Inhibition of myoblast differentiation by tumor necrosis factor alpha is mediated by c-jun N-terminal kinase 1 and leukemia inhibitory factor. *The Journal of Biological Chemistry*, *283*(34), 23224-23234. doi:10.1074/jbc.M801379200 [doi]
- Anderson, J. M., Rodriguez, A., & Chang, D. T. (2008). Foreign body reaction to biomaterials. *Seminars in Immunology*, *20*(2) 86-100.
- Arnold, L., Henry, A., Poron, F., Baba-Amer, Y., van Rooijen, N., Plonquet, A., . . . Chazaud, B. (2007). Inflammatory monocytes recruited after skeletal muscle injury switch into antiinflammatory macrophages to support myogenesis. *The Journal of Experimental Medicine*, *204*(5), 1057-1069. doi:jem.20070075 [pii]
- Aubin, H., Nichol, J. W., Hutson, C. B., Bae, H., Sieminski, A. L., Cropek, D. M., . . . Khademhosseini, A. (2010). Directed 3D cell alignment and elongation in microengineered hydrogels. *Biomaterials*, *31*(27), 6941-6951.
- Aurora, A., Roe, J. L., Corona, B. T., & Walters, T. J. (2015). An acellular biologic scaffold does not regenerate appreciable de novo muscle tissue in rat models of volumetric muscle loss injury. *Biomaterials*, *67*, 393-407.
- Aurora, A., Garg, K., Corona, B. T., & Walters, T. J. (2014). Physical rehabilitation improves muscle function following volumetric muscle loss injury. *BMC Sports Science, Medicine and Rehabilitation*, *6*(1), 41-1847-6-41. eCollection 2014. doi:10.1186/2052-1847-6-41 [doi]
- Aviss, K. J., Gough, J. E., & Downes, S. (2010). Aligned electrospun polymer fibres for skeletal muscle regeneration. *Euro. Cells and Mater.*, *19*, 193-204.

- Badylak, S. F., Dziki, J. L., Sicari, B. M., Ambrosio, F., & Boninger, M. L. (2016). Mechanisms by which acellular biologic scaffolds promote functional skeletal muscle restoration. *Biomaterials*, *103*, 128-136.
- Badylak, S. F., Lantz, G. C., Coffey, A., & Geddes, L. A. (1989). Small intestinal submucosa as a large diameter vascular graft in the dog. *Journal of Surgical Research*, *47*(1), 74-80.
- Badylak, S. F., Tullius, R., Kokini, K., Shelbourne, K. D., Klootwyk, T., Voytik, S. L., . . . Simmons, C. (1995). The use of xenogeneic small intestinal submucosa as a biomaterial for achille's tendon repair in a dog model. *Journal of Biomedical Materials Research*, *29*(8), 977-985.
- Badylak, S., Meurling, S., Chen, M., Spievack, A., & Simmons-Byrd, A. (2000). Resorbable bioscaffold for esophageal repair in a dog model. *Journal of Pediatric Surgery*, *35*(7), 1097-1103.
- Bi, H., & Jin, Y. (2013). *Current progress of skin tissue engineering: Seed cells, bioscaffolds, and construction strategies* doi:10.4103/2321-3868.118928
- Boonen, K. J., Langelaan, M. L., Polak, R. B., van der Schaft, Daisy WJ, Baaijens, F. P., & Post, M. J. (2010). Effects of a combined mechanical stimulation protocol: Value for skeletal muscle tissue engineering. *Journal of Biomechanics*, *43*(8), 1514-1521.
- Bursac, N., Juhas, M., & Rando, T. A. (2015). Synergizing engineering and biology to treat and model skeletal muscle injury and disease. *Annual Review of Biomedical Engineering*, *17*, 217-242. doi:10.1146/annurev-bioeng-071114-040640 [doi]
- Carlson, B. M. (1968). Regeneration of the completely excised gastrocnemius muscle in the frog and rat from minced muscle fragments. *Journal of Morphology*, *125*(4), 447-471.
- Chen, J., Xu, J., Wang, A., & Zheng, M. (2009). Scaffolds for tendon and ligament repair: Review of the efficacy of commercial products. *Expert Review of Medical Devices*, *6*(1), 61-73.
- Choi, J. S., Lee, S. J., Christ, G. J., Atala, A., & Yoo, J. J. (2008a). The influence of electrospun aligned poly(epsilon-caprolactone)/collagen nanofiber meshes on the formation of self-aligned skeletal muscle myotubes. *Biomaterials*, *29*(19), 2899-2906. doi:10.1016/j.biomaterials.2008.03.031 [doi]
- Choi, J. S., Lee, S. J., Christ, G. J., Atala, A., & Yoo, J. J. (2008b). The influence of electrospun aligned poly(epsilon-caprolactone)/collagen nanofiber meshes on the formation of self-aligned skeletal muscle myotubes. *Biomaterials*, *29*(19), 2899-2906. doi:10.1016/j.biomaterials.2008.03.031; 10.1016/j.biomaterials.2008.03.031

- Cimetta, E., Pizzato, S., Bollini, S., Serena, E., De Coppi, P., & Elvassore, N. (2009). Production of arrays of cardiac and skeletal muscle myofibers by micropatterning techniques on a soft substrate. *Biomedical Microdevices*, *11*(2), 389-400.
- Cizkova, D., Vávrová, J., Micuda, S., Filip, S., Brckova, E., Bruckova, L., & Mokry, J. (2011). Role of transplanted bone marrow cells in response to skeletal muscle injury. *Folia Biologica*, *57*(6), 232.
- Clarke, M. S., & Feeback, D. L. (1996). Mechanical load induces sarcoplasmic wounding and FGF release in differentiated human skeletal muscle cultures. *FASEB Journal : Official Publication of the Federation of American Societies for Experimental Biology*, *10*(4), 502-509.
- Cobb, M. A., Badylak, S. F., Janas, W., Simmons-Byrd, A., & Boop, F. A. (1999). Porcine small intestinal submucosa as a dural substitute. *Surgical Neurology*, *51*(1), 99-104.
- Corona, B. T., Wu, X., Ward, C. L., McDaniel, J. S., Rathbone, C. R., & Walters, T. J. (2013a). The promotion of a functional fibrosis in skeletal muscle with volumetric muscle loss injury following the transplantation of muscle-ECM. *Biomaterials*, *34*(13), 3324-3335.
- Corona, B. T., Garg, K., Ward, C. L., McDaniel, J. S., Walters, T. J., & Rathbone, C. R. (2013b). Autologous minced muscle grafts: A tissue engineering therapy for the volumetric loss of skeletal muscle. *American Journal of Physiology. Cell Physiology*, *305*(7), C761-75. doi:10.1152/ajpcell.00189.2013 [doi]
- Cossu, G., Previtali, S. C., Napolitano, S., Cicalese, M. P., Tedesco, F. S., Nicastro, F., . . . Ciceri, F. (2015). Intra-arterial transplantation of HLA-matched donor mesoangioblasts in duchenne muscular dystrophy. *EMBO Molecular Medicine*, *7*(12), 1513-1528. doi:10.15252/emmm.201505636 [doi]
- Coulet, B., Boch, C., Boretto, J., Lazerges, C., & Chammas, M. (2011). Free gracilis muscle transfer to restore elbow flexion in brachial plexus injuries. *Orthopaedics & Traumatology: Surgery & Research*, *97*(8), 785-792.
- Cronin, E. M., Thurmond, F. A., Bassel-Duby, R., Williams, R. S., Wright, W. E., Nelson, K. D., & Garner, H. R. (2004). Protein-coated poly (l-lactic acid) fibers provide a substrate for differentiation of human skeletal muscle cells. *Journal of Biomedical Materials Research Part A*, *69*(3), 373-381.
- Davie, J. K., Cho, J., Meadows, E., Flynn, J. M., Knapp, J. R., & Klein, W. H. (2007). Target gene selectivity of the myogenic basic helix-loop-helix transcription factor myogenin in embryonic muscle. *Developmental Biology*, *311*(2), 650-664.
- DeQuach, J. A., Lin, J. E., Cam, C., Hu, D., Salvatore, M. A., Sheikh, F., & Christman, K. L. (2012). Injectable skeletal muscle matrix hydrogel promotes neovascularization and muscle

- cell infiltration in a hindlimb ischemia model. *European Cells & Materials*, 23, 400-12; discussion 412. doi:vol023a31 [pii]
- DiMario, J., Buffinger, N., Yamada, S., & Strohman, R. C. (1989). Fibroblast growth factor in the extracellular matrix of dystrophic (mdx) mouse muscle. *Science (New York, N.Y.)*, 244(4905), 688-690.
- Donnelly, K., Khodabukus, A., Philp, A., Deldicque, L., Dennis, R. G., & Baar, K. (2010). A novel bioreactor for stimulating skeletal muscle in vitro. *Tissue Engineering.Part C, Methods*, 16(4), 711-718. doi:10.1089/ten.TEC.2009.0125; 10.1089/ten.TEC.2009.0125
- Dumont, N. A., Bentzinger, C. F., Sincennes, M., & Rudnicki, M. A. (2015). Satellite cells and skeletal muscle regeneration. *Comprehensive Physiology*,
- Dziki, J. L., Sicari, B. M., Wolf, M. T., Cramer, M. C., & Badylak, S. F. (2016). Immunomodulation and mobilization of progenitor cells by extracellular matrix bioscaffolds for volumetric muscle loss treatment. *Tissue Engineering Part A*, 22(19-20), 1129-1139.
- Dziki, J., Badylak, S., Yabroudi, M., Sicari, B., Ambrosio, F., Stearns, K., . . . Brown, E. H. (2016). An acellular biologic scaffold treatment for volumetric muscle loss: Results of a 13-patient cohort study. *Npj Regenerative Medicine*, 1, 16008.
- Erices, A., Conget, P., & Minguell, J. J. (2000). Mesenchymal progenitor cells in human umbilical cord blood. *British Journal of Haematology*, 109(1), 235-242.
- Fan, C., Jiang, P., Fu, L., Cai, P., Sun, L., & Zeng, B. (2008). Functional reconstruction of traumatic loss of flexors in forearm with gastrocnemius myocutaneous flap transfer. *Microsurgery*, 28(1), 71-75.
- Fischer, J. P., Elliott, R. M., Kozin, S. H., & Levin, L. S. (2013). Free function muscle transfers for upper extremity reconstruction: A review of indications, techniques, and outcomes. *The Journal of Hand Surgery*, 38(12), 2485-2490.
- Fisher, M. B., & Mauck, R. L. (2013). Tissue engineering and regenerative medicine: Recent innovations and the transition to translation. *Tissue Engineering Part B: Reviews*, 19(1), 1-13.
- Flaibani, M., Boldrin, L., Cimetta, E., Piccoli, M., Coppi, P. D., & Elvassore, N. (2009). Muscle differentiation and myotubes alignment is influenced by micropatterned surfaces and exogenous electrical stimulation. *Tissue Engineering Part A*, 15(9), 2447-2457.
- Fredsted, A., Gissel, H., Madsen, K., & Clausen, T. (2007). Causes of excitation-induced muscle cell damage in isometric contractions: Mechanical stress or calcium overload? *American Journal of Physiology.Regulatory, Integrative and Comparative Physiology*, 292(6), R2249-58. doi:00415.2006 [pii]

- Gang, E. J., Darabi, R., Bosnakovski, D., Xu, Z., Kamm, K. E., Kyba, M., & Perlingeiro, R. C. (2009). Engraftment of mesenchymal stem cells into dystrophin-deficient mice is not accompanied by functional recovery. *Experimental Cell Research*, 315(15), 2624-2636.
- Garg, K., Ward, C. L., Hurtgen, B. J., Wilken, J. M., Stinner, D. J., Wenke, J. C., . . . Corona, B. T. (2015). Volumetric muscle loss: Persistent functional deficits beyond frank loss of tissue. *Journal of Orthopaedic Research*, 33(1), 40-46.
- Gilbert, T. W., Sellaro, T. L., & Badylak, S. F. (2006). Decellularization of tissues and organs. *Biomaterials*, 27(19), 3675-3683. doi:<http://dx.doi.org/10.1016/j.biomaterials.2006.02.014>
- Gillies, A. R., & Lieber, R. L. (2011). Structure and function of the skeletal muscle extracellular matrix. *Muscle & Nerve*, 44(3), 318-331.
- Gillies, A. R., Smith, L. R., Lieber, R. L., & Varghese, S. (2010). Method for decellularizing skeletal muscle without detergents or proteolytic enzymes. *Tissue Engineering Part C: Methods*, 17(4), 383-389.
- Grogan, B. F., Hsu, J. R., & Skeletal Trauma Research Consortium. (2011). Volumetric muscle loss. *The Journal of the American Academy of Orthopaedic Surgeons*, 19 Suppl 1, S35-7. doi:19/suppl_1/S35 [pii]
- Grossi, A., Yadav, K., & Lawson, M. A. (2007). Mechanical stimulation increases proliferation, differentiation and protein expression in culture: Stimulation effects are substrate dependent. *Journal of Biomechanics*, 40(15), 3354-3362.
- Guérette, B., Asselin, I., Skuk, D., Entman, M., & Tremblay, J. P. (1997). Control of inflammatory damage by anti-LFA-1: Increase success of myoblast transplantation. *Cell Transplantation*, 6(2), 101-107.
- Huang, N. F., Lee, R. J., & Li, S. (2010a). Engineering of aligned skeletal muscle by micropatterning. *American Journal of Translational Research*, 2(1), 43-55.
- Huang, N. F., Lee, R. J., & Li, S. (2010b). Engineering of aligned skeletal muscle by micropatterning. *American Journal of Translational Research*, 2(1), 43-55.
- Huard, J., Bouchard, J., Roy, R., Malouin, F., Dansereau, G., Labrecque, C., . . . Tremblay, J. (1992). Human myoblast transplantation: Preliminary results of 4 cases. *Muscle & Nerve*, 15(5), 550-560.
- Huard, J., Roy, R., Guérette, B., Verreault, S., Trèmbly, G., & Tremblay, J. P. (1994). Human myoblast transplantation in immunodeficient and immunosuppressed mice: Evidence of rejection. *Muscle & Nerve*, 17(2), 224-234.
- Huard, J., Li, Y., & Fu, F. H. (2002). Muscle injuries and repair: Current trends in research. *The Journal of Bone and Joint Surgery.American Volume*, 84-A(5), 822-832.

- Jiang, Y., Jahagirdar, B. N., Reinhardt, R. L., Schwartz, R. E., Keene, C. D., Ortiz-Gonzalez, X. R., . . . Blackstad, M. (2002). Pluripotency of mesenchymal stem cells derived from adult marrow. *Nature*, *418*(6893), 41-49.
- Kaar, J. L., Li, Y., Blair, H. C., Asche, G., Koepsel, R. R., Huard, J., & Russell, A. J. (2008). Matrix metalloproteinase-1 treatment of muscle fibrosis. *Acta Biomaterialia*, *4*(5), 1411-1420.
- Kang, Y., Park, C., Kim, D., Seong, C., Kwon, K., & Choi, C. (2010). Unsorted human adipose tissue-derived stem cells promote angiogenesis and myogenesis in murine ischemic hindlimb model. *Microvascular Research*, *80*(3), 310-316.
- Karalaki, M., Fili, S., Philippou, A., & Koutsilieris, M. (2009). Muscle regeneration: Cellular and molecular events. *In Vivo (Athens, Greece)*, *23*(5), 779-796. doi:23/5/779 [pii]
- Kasper, C. E. (1995). Sarcolemmal disruption in reloaded atrophic skeletal muscle. *Journal of Applied Physiology (Bethesda, Md.: 1985)*, *79*(2), 607-614.
- Kesireddy, V. (2016). Evaluation of adipose-derived stem cells for tissue-engineered muscle repair construct-mediated repair of a murine model of volumetric muscle loss injury. *International Journal of Nanomedicine*, *11*, 1461.
- Kim, T., Kim, I., Kim, Y., & Lee, J. (2012). Reconstruction of lower extremity complex wounds with combined free tissue transfer using the anterolateral thigh flap as a link. *Microsurgery*, *32*(7), 575-579.
- Kinoshita, I., Vilquin, J., GuéRette, B., Asselin, I., Roy, R., & Tremblay, J. P. (1994). Very efficient myoblast allotransplantation in mice under FK506 immunosuppression. *Muscle & Nerve*, *17*(12), 1407-1415.
- KJÆR, M. (2004). Role of extracellular matrix in adaptation of tendon and skeletal muscle to mechanical loading. *Physiological Reviews*, *84*(2), 649-698. doi:10.1152/physrev.00031.2003
- Klebuc, M., & Menn, Z. (2013). Muscle flaps and their role in limb salvage. *Methodist DeBakey Cardiovascular Journal*, *9*(2), 95-99.
- Klumpp, D., Horch, R. E., Kneser, U., & Beier, J. P. (2010). Engineering skeletal muscle tissue--new perspectives in vitro and in vivo. *Journal of Cellular and Molecular Medicine*, *14*(11), 2622-2629. doi:10.1111/j.1582-4934.2010.01183.x; 10.1111/j.1582-4934.2010.01183.x
- Knoblich, J. A. (2008). Mechanisms of asymmetric stem cell division. *Cell*, *132*(4), 583-597.
- Kropp, B. P., Eppley, B. L., Prevel, C., Rippy, M., Harruff, R., Badylak, S., . . . Keating, M. (1995). Experimental assessment of small intestinal submucosa as a bladder wall substitute. *Urology*, *46*(3), 396-400.

- Kropp, B. P., Rippy, M. K., Badylak, S. F., Adams, M. C., Keating, M. A., Rink, R. C., & Thor, K. B. (1996). Regenerative urinary bladder augmentation using small intestinal submucosa: Urodynamic and histopathologic assessment in long-term canine bladder augmentations. *The Journal of Urology*, *155*(6), 2098-2104.
- Lam, M. T., Huang, Y. C., Birla, R. K., & Takayama, S. (2009). Microfeature guided skeletal muscle tissue engineering for highly organized 3-dimensional free-standing constructs. *Biomaterials*, *30*(6), 1150-1155. doi:10.1016/j.biomaterials.2008.11.014; 10.1016/j.biomaterials.2008.11.014
- Langelaan, M. L., Boonen, K. J., Rosaria-Chak, K. Y., van der Schaft, Daisy WJ, Post, M. J., & Baaijens, F. (2011). Advanced maturation by electrical stimulation: Differences in response between C2C12 and primary muscle progenitor cells. *Journal of Tissue Engineering and Regenerative Medicine*, *5*(7), 529-539.
- Lantz, G. C., Badylak, S. F., Coffey, A. C., Geddes, L. A., & Blevins, W. E. (1990). Small intestinal submucosa as a small-diameter arterial graft in the dog. *Journal of Investigative Surgery*, *3*(3), 217-227.
- Laschke, M., Rücker, M., Jensen, G., Carvalho, C., Mülhaupt, R., Gellrich, N., & Menger, M. (2008). Incorporation of growth factor containing matrigel promotes vascularization of porous PLGA scaffolds. *Journal of Biomedical Materials Research Part A*, *85*(2), 397-407.
- Laumonier, T., & Menetrey, J. (2016). Muscle injuries and strategies for improving their repair. *Journal of Experimental Orthopaedics*, *3*(1), 15.
- Levenberg, S., Rouwkema, J., Macdonald, M., Garfein, E. S., Kohane, D. S., Darland, D. C., . . . D'Amore, P. A. (2005a). Engineering vascularized skeletal muscle tissue. *Nature Biotechnology*, *23*(7), 879-884.
- Levenberg, S., Rouwkema, J., Macdonald, M., Garfein, E. S., Kohane, D. S., Darland, D. C., . . . D'Amore, P. A. (2005b). Engineering vascularized skeletal muscle tissue. *Nature Biotechnology*, *23*(7), 879-884.
- Li, N., Yuan, R., Chen, T., Chen, L., & Jin, X. (2009). Effect of platelet-rich plasma and latissimus dorsi muscle flap on osteogenesis and vascularization of tissue-engineered bone in dogs. *Journal of Oral and Maxillofacial Surgery*, *67*(9), 1850-1858.
- Li, Y. P. (2003). TNF-alpha is a mitogen in skeletal muscle. *American Journal of Physiology. Cell Physiology*, *285*(2), C370-6. doi:10.1152/ajpcell.00453.2002 [doi]
- Li, Z. B., Kollias, H. D., & Wagner, K. R. (2008). Myostatin directly regulates skeletal muscle fibrosis. *The Journal of Biological Chemistry*, *283*(28), 19371-19378. doi:10.1074/jbc.M802585200 [doi]

- Lieber, R. L., & Friden, J. (2000). Functional and clinical significance of skeletal muscle architecture. *Muscle & Nerve*, *23*, 1647-1666.
- Lin, C. H., Lin, Y. T., Yeh, J. T., & Chen, C. T. (2007). Free functioning muscle transfer for lower extremity posttraumatic composite structure and functional defect. *Plastic and Reconstructive Surgery*, *119*(7), 2118-2126. doi:10.1097/01.prs.0000260595.85557.41 [doi]
- Lohse, G. R., Lee, D. H., & Watson, J. T. (2014). Muscle transfer to restore elbow flexion. *The Journal of Hand Surgery*, *39*(4), 761-764. doi:10.1016/j.jhssa.2013.12.029 [doi]
- Mann, C. J., Perdiguero, E., Kharraz, Y., Aguilar, S., Pessina, P., Serrano, A. L., & Muñoz-Cánoves, P. (2011). Aberrant repair and fibrosis development in skeletal muscle. *Skeletal Muscle*, *1*(1), 1.
- Mase, V. J., Hsu, J. R., Wolf, S. E., Wenke, J. C., Baer, D. G., Owens, J., . . . Walters, T. J. (2010). Clinical application of an acellular biologic scaffold for surgical repair of a large, traumatic quadriceps femoris muscle defect. *Orthopedics*, *33*(7)
- Masquelet, A. (2003). Muscle reconstruction in reconstructive surgery: Soft tissue repair and long bone reconstruction. *Langenbeck's Archives of Surgery*, *388*(5), 344-346.
- Mauro, A. (1961). Satellite cell of skeletal muscle fibers. *The Journal of Biophysical and Biochemical Cytology*, *9*, 493-495.
- Megeney, L. A., Kablar, B., Garrett, K., Anderson, J. E., & Rudnicki, M. A. (1996). MyoD is required for myogenic stem cell function in adult skeletal muscle. *Genes & Development*, *10*(10), 1173-1183.
- Meng, J., Chun, S., Asfahani, R., Lochmüller, H., Muntoni, F., & Morgan, J. (2014). Human skeletal muscle-derived CD133 cells form functional satellite cells after intramuscular transplantation in immunodeficient host mice. *Molecular Therapy*, *22*(5), 1008.
- Merritt, E. K., Cannon, M. V., Hammers, D. W., Le, L. N., Gokhale, R., Sarathy, A., . . . Farrar, R. P. (2010). Repair of traumatic skeletal muscle injury with bone-marrow-derived mesenchymal stem cells seeded on extracellular matrix. *Tissue Engineering. Part A*, *16*(9), 2871-2881. doi:10.1089/ten.TEA.2009.0826; 10.1089/ten.TEA.2009.0826
- Meyer, G. A., & Lieber, R. L. (2012). Skeletal muscle fibrosis develops in response to desmin deletion. *American Journal of Physiology. Cell Physiology*, *302*(11), C1609-20. doi:10.1152/ajpcell.00441.2011 [doi]
- Montarras, D., L'honoré, A., & Buckingham, M. (2013). Lying low but ready for action: The quiescent muscle satellite cell. *FEBS Journal*, *280*(17), 4036-4050.
- Muñoz-Cánoves, P., & Serrano, A. L. (2015). Macrophages decide between regeneration and fibrosis in muscle. *Trends in Endocrinology & Metabolism*, *26*(9), 449-450.

- Musarò, A., McCullagh, K., Paul, A., Houghton, L., Dobrowolny, G., Molinaro, M., . . . Rosenthal, N. (2001). Localized igf-1 transgene expression sustains hypertrophy and regeneration in senescent skeletal muscle. *Nature Genetics*, 27(2), 195-200.
- Nishimura, T., Nakamura, K., Kishioka, Y., Kato-Mori, Y., Wakamatsu, J., & Hattori, A. (2008). Inhibition of matrix metalloproteinases suppresses the migration of skeletal muscle cells. *Journal of Muscle Research and Cell Motility*, 29(1), 37-44.
- Olguin, H. C., Yang, Z., Tapscott, S. J., & Olwin, B. B. (2007). Reciprocal inhibition between Pax7 and muscle regulatory factors modulates myogenic cell fate determination. *The Journal of Cell Biology*, 177(5), 769-779. doi:jcb.200608122 [pii]
- Otis, J. S., Niccoli, S., Hawdon, N., Sarvas, J. L., Frye, M. A., Chicco, A. J., & Lees, S. J. (2014). Pro-inflammatory mediation of myoblast proliferation. *PloS One*, 9(3), e92363.
- Ott, H. C., Matthiesen, T. S., Goh, S., Black, L. D., Kren, S. M., Netoff, T. I., & Taylor, D. A. (2008). Perfusion-decellularized matrix: Using nature's platform to engineer a bioartificial heart. *Nature Medicine*, 14(2), 213-221.
- Ott, H. C., Clippinger, B., Conrad, C., Schuetz, C., Pomerantseva, I., Ikonomidou, L., . . . Vacanti, J. P. (2010). Regeneration and orthotopic transplantation of a bioartificial lung. *Nature Medicine*, 16(8), 927-933.
- Page, R. L., Malcuit, C., Vilner, L., Vojtic, I., Shaw, S., Hedblom, E., . . . Dominko, T. (2011). Restoration of skeletal muscle defects with adult human cells delivered on fibrin microthreads. *Tissue Engineering. Part A*, 17(21-22), 2629-2640. doi:10.1089/ten.TEA.2011.0024; 10.1089/ten.TEA.2011.0024
- Perdiguerro, E., Ruiz-Bonilla, V., Serrano, A. L., & Muñoz-Cánoves, P. (2007). Genetic deficiency of p38 α reveals its critical role in myoblast cell cycle exit: The p38 α -JNK connection. *Cell Cycle*, 6(11), 1298-1303.
- Perniconi, B., Costa, A., Aulino, P., Teodori, L., Adamo, S., & Coletti, D. (2011). The pro-myogenic environment provided by whole organ scale acellular scaffolds from skeletal muscle. *Biomaterials*, 32(31), 7870-7882.
- Pesce, M., Orlandi, A., Iachininoto, M. G., Straino, S., Torella, A. R., Rizzuti, V., . . . Capogrossi, M. C. (2003). Myoendothelial differentiation of human umbilical cord blood-derived stem cells in ischemic limb tissues. *Circulation Research*, 93(5), e51-62. doi:10.1161/01.RES.0000090624.04507.45 [doi]
- Powell, C. A., Smiley, B. L., Mills, J., & Vandeburgh, H. H. (2002). Mechanical stimulation improves tissue-engineered human skeletal muscle. *American Journal of Physiology. Cell Physiology*, 283(5), C1557-65. doi:10.1152/ajpcell.00595.2001 [doi]

- Prevel, C. D., Eppley, B. L., Summerlin, D., Jackson, J. R., McCarty, M., & Badylak, S. F. (1995). Small intestinal submucosa: Utilization for repair of rodent abdominal wall defects. *Annals of Plastic Surgery*, 35(4), 374-380.
- Prevel, C. D., Eppley, B. L., Summerlin, D., Sidner, R., Jackson, J. R., McCarty, M., & Badylak, S. F. (1995). Small intestinal submucosa: Utilization as a wound dressing in full-thickness rodent wounds. *Annals of Plastic Surgery*, 35(4), 381-388.
- Qazi, T. H., Mooney, D. J., Pumberger, M., Geissler, S., & Duda, G. N. (2015). Biomaterials based strategies for skeletal muscle tissue engineering: Existing technologies and future trends. *Biomaterials*, 53, 502-521.
- Riboldi, S., Sadr, N., Pignini, L., Neuenschwander, P., Simonet, M., Mognol, P., . . . Mantero, S. (2008). Skeletal myogenesis on highly orientated microfibrillar polyesterurethane scaffolds. *Journal of Biomedical Materials Research Part A*, 84(4), 1094-1101.
- Riboldi, S. A., Sampaolesi, M., Neuenschwander, P., Cossu, G., & Mantero, S. (2005). Electrospun degradable polyesterurethane membranes: Potential scaffolds for skeletal muscle tissue engineering. *Biomaterials*, 26(22), 4606-4615.
- Riederer, I., Negroni, E., Bencze, M., Wolff, A., Aamiri, A., Di Santo, J. P., . . . Mouly, V. (2012). Slowing down differentiation of engrafted human myoblasts into immunodeficient mice correlates with increased proliferation and migration. *Molecular Therapy*, 20(1), 146-154.
- Rossi, C. A., Pozzobon, M., & De Coppi, P. (2010). Advances in musculoskeletal tissue engineering: Moving towards therapy. *Organogenesis*, 6, 1-6.
- Sabourin, L. A., Girgis-Gabardo, A., Seale, P., Asakura, A., & Rudnicki, M. A. (1999). Reduced differentiation potential of primary MyoD^{-/-} myogenic cells derived from adult skeletal muscle. *The Journal of Cell Biology*, 144(4), 631-643.
- Sampaolesi, M., Blot, S., D'antona, G., Granger, N., Tonlorenzi, R., Innocenzi, A., . . . Barthélémy, I. (2006). Mesoangioblast stem cells ameliorate muscle function in dystrophic dogs. *Nature*, 444(7119), 574-579.
- Sandusky Jr, G., Badylak, S., Morff, R., Johnson, W., & Lantz, G. (1992). Histologic findings after in vivo placement of small intestine submucosal vascular grafts and saphenous vein grafts in the carotid artery in dogs. *The American Journal of Pathology*, 140(2), 317.
- Saxena, A. K., Marler, J., Benvenuto, M., Willital, G. H., & Vacanti, J. P. (1999). Skeletal muscle tissue engineering using isolated myoblasts on synthetic biodegradable polymers: Preliminary studies. *Tissue Engineering*, 5(6), 525-531.

- Scherjon, S. A., Kleijburg-van der Keur, C., de Groot-Swings, G. M., Claas, F. H., Fibbe, W. E., & Kanhai, H. H. (2004). Isolation of mesenchymal stem cells of fetal or maternal origin from human placenta. *Stem Cells*, 22(7), 1338-1345.
- Schultz, E., Jaryszak, D. L., & Valliere, C. R. (1985). Response of satellite cells to focal skeletal muscle injury. *Muscle & Nerve*, 8(3), 217-222.
- Serrano, A. L., & Muñoz-Cánoves, P. (2010). Regulation and dysregulation of fibrosis in skeletal muscle. *Experimental Cell Research*, 316(18), 3050-3058.
- Shandalov, Y., Egozi, D., Koffler, J., Dado-Rosenfeld, D., Ben-Shimol, D., Freiman, A., . . . Levenberg, S. (2014). An engineered muscle flap for reconstruction of large soft tissue defects. *Proceedings of the National Academy of Sciences of the United States of America*, 111(16), 6010-6015. doi:10.1073/pnas.1402679111 [doi]
- Shi, X., & Garry, D. J. (2006). Muscle stem cells in development, regeneration, and disease. *Genes & Development*, 20(13), 1692-1708. doi:20/13/1692 [pii]
- Shimizu, K., Fujita, H., & Nagamori, E. (2009). Alignment of skeletal muscle myoblasts and myotubes using linear micropatterned surfaces ground with abrasives. *Biotech. and Bioeng.*, 103, 631-638.
- Sicari, B. M., Agrawal, V., Siu, B. F., Medberry, C. J., Dearth, C. L., Turner, N. J., & Badylak, S. F. (2012). A murine model of volumetric muscle loss and a regenerative medicine approach for tissue replacement. *Tissue Engineering Part A*, 18(19-20), 1941-1948.
- Sicari, B. M., Dearth, C. L., & Badylak, S. F. (2014). Tissue engineering and regenerative medicine approaches to enhance the functional response to skeletal muscle injury. *The Anatomical Record*, 297(1), 51-64.
- Sicari, B. M., Rubin, J. P., Dearth, C. L., Wolf, M. T., Ambrosio, F., Boninger, M., . . . Badylak, S. F. (2014). An acellular biologic scaffold promotes skeletal muscle formation in mice and humans with volumetric muscle loss. *Science Translational Medicine*, 6(234), 234ra58. doi:10.1126/scitranslmed.3008085 [doi]
- Siegel, A. L., Atchison, K., Fisher, K. E., Davis, G. E., & Cornelison, D. (2009). 3D timelapse analysis of muscle satellite cell motility. *Stem Cells*, 27(10), 2527-2538.
- Sirivisoot, S., & Harrison, B. S. (2011). Skeletal myotube formation enhanced by electrospun polyurethane carbon nanotube scaffolds. *International Journal of Nanomedicine*, 6, 2483-2497. doi:10.2147/IJN.S24073 [doi]
- Skuk, D. (2012). Acute rejection of myofibers in nonhuman primates: Key histopathologic features. *Journal of Neuropathology and Experimental Neurology*, 71(5), 398-412. doi:10.1097/NEN.0b013e31825243ae [doi]

- Skuk, D., Goulet, M., Roy, B., Chapdelaine, P., Bouchard, J. P., Roy, R., . . . Tremblay, J. P. (2006). Dystrophin expression in muscles of duchenne muscular dystrophy patients after high-density injections of normal myogenic cells. *Journal of Neuropathology and Experimental Neurology*, 65(4), 371-386. doi:10.1097/01.jnen.0000218443.45782.81 [doi]
- Studitsky, A. (1965). Free auto-and homografts of muscle tissue in experiments on animals. *Annals of the New York Academy of Sciences*, 120(2), 789-801.
- Suckow, M. A., Voytik-Harbin, S., Terril, L., & Badylak, S. (1999). Enhanced bone regeneration using porcine small intestinal submucosa. *Journal of Investigative Surgery*, 12(5), 277-287.
- Sullivan, D. C., Mirmalek-Sani, S., Deegan, D. B., Baptista, P. M., Aboushwareb, T., Atala, A., & Yoo, J. J. (2012). Decellularization methods of porcine kidneys for whole organ engineering using a high-throughput system. *Biomaterials*, 33(31), 7756-7764. doi:<http://dx.doi.org/10.1016/j.biomaterials.2012.07.023>
- Sun, L., Ma, K., Wang, H., Xiao, F., Gao, Y., Zhang, W., . . . Wu, Z. (2007). JAK1-STAT1-STAT3, a key pathway promoting proliferation and preventing premature differentiation of myoblasts. *The Journal of Cell Biology*, 179(1), 129-138. doi:jcb.200703184 [pii]
- Swinehart, I. T., & Badylak, S. F. (2016). Extracellular matrix bioscaffolds in tissue remodeling and morphogenesis. *Developmental Dynamics*,
- Tatsumi, R. (2010). Mechano-biology of skeletal muscle hypertrophy and regeneration: Possible mechanism of stretch-induced activation of resident myogenic stem cells. *Animal Science Journal*, 81(1), 11-20.
- Tatsumi, R., Anderson, J. E., Nevoret, C. J., Halevy, O., & Allen, R. E. (1998). HGF/SF is present in normal adult skeletal muscle and is capable of activating satellite cells. *Developmental Biology*, 194(1), 114-128.
- Thompson, N. (1971). Autogenous free grafts of skeletal muscle: A preliminary experimental and clinical study. *Plastic and Reconstructive Surgery*, 48(1), 11-27.
- Tidball, J. G., & Wehling-Henricks, M. (2007). Macrophages promote muscle membrane repair and muscle fibre growth and regeneration during modified muscle loading in mice in vivo. *The Journal of Physiology*, 578(1), 327-336.
- Tidball, J. G. (1995). Inflammatory cell response to acute muscle injury. *Medicine and Science in Sports and Exercise*, 27(7), 1022-1032.
- Tomasek, J. J., Gabbiani, G., Hinz, B., Chaponnier, C., & Brown, R. A. (2002). Myofibroblasts and mechano-regulation of connective tissue remodelling. *Nature Reviews Molecular Cell Biology*, 3(5), 349-363.

- Toumi, H., & Best, T. M. (2003). The inflammatory response: Friend or enemy for muscle injury? *British Journal of Sports Medicine*, 37(4), 284-286.
- Turner, N. J., & Badylak, S. F. (2012). Regeneration of skeletal muscle. *Cell and Tissue Research*, 347(3), 759-774.
- Turner, N. J., Yates Jr, A. J., Weber, D. J., Qureshi, I. R., Stolz, D. B., Gilbert, T. W., & Badylak, S. F. (2010). Xenogeneic extracellular matrix as an inductive scaffold for regeneration of a functioning musculotendinous junction. *Tissue Engineering Part A*, 16(11), 3309-3317.
- Uygun, B. E., Soto-Gutierrez, A., Yagi, H., Izamis, M., Guzzardi, M. A., Shulman, C., . . . Berthiaume, F. (2010). Organ reengineering through development of a transplantable recellularized liver graft using decellularized liver matrix. *Nature Medicine*, 16(7), 814-820.
- Vandenburgh, H. H., & Karlisch, P. (1989). Longitudinal growth of skeletal myotubes in vitro in a new horizontal mechanical cell stimulator. *In Vitro Cellular & Developmental Biology*, 25(7), 607-616.
- VanDusen, K. W., Syverud, B. C., Williams, M. L., Lee, J. D., & Larkin, L. M. (2014). Engineered skeletal muscle units for repair of volumetric muscle loss in the tibialis anterior muscle of a rat. *Tissue Engineering Part A*, 20(21-22), 2920-2930.
- Vekris, M. D., Beris, A. E., Lykissas, M. G., Korompilias, A. V., Vekris, A. D., & Soucacos, P. N. (2008). Restoration of elbow function in severe brachial plexus paralysis via muscle transfers. *Injury*, 39(3), 15-22.
- Wang, L., Wu, Y., Guo, B., & Ma, P. X. (2015). Nanofiber yarn/hydrogel Core-Shell scaffolds mimicking native skeletal muscle tissue for guiding 3D myoblast alignment, elongation, and differentiation. *ACS Nano*, 9(9), 9167-9179.
- Ward, C. L., Ji, L., & Corona, B. T. (2015). An autologous muscle tissue expansion approach for the treatment of volumetric muscle loss. *BioResearch Open Access*, 4(1), 198-208.
- Wilson, K., Terlouw, A., Roberts, K., & Wolchok, J. C. (2016). The characterization of decellularized human skeletal muscle as a blueprint for mimetic scaffolds. *Journal of Materials Science: Materials in Medicine*, 27(8), 1-15.
- Winkler, T., von Roth, P., Matziolis, G., Mehta, M., Perka, C., & Duda, G. N. (2008). Dose-response relationship of mesenchymal stem cell transplantation and functional regeneration after severe skeletal muscle injury in rats. *Tissue Engineering Part A*, 15(3), 487-492.
- Wittenberg, J. B. (1970). Myoglobin-facilitated oxygen diffusion: Role of myoglobin in oxygen entry into muscle. *Physiological Reviews*, 50(4), 559-636.

- Wolf, M. T., Dearth, C. L., Sonnenberg, S. B., Lobo, E. G., & Badylak, S. F. (2015). Naturally derived and synthetic scaffolds for skeletal muscle reconstruction. *Advanced Drug Delivery Reviews*, 84, 208-221.
- Wolf, M. T., Daly, K. A., Reing, J. E., & Badylak, S. F. (2012). Biologic scaffold composed of skeletal muscle extracellular matrix. *Biomaterials*, 33(10), 2916-2925.
doi:10.1016/j.biomaterials.2011.12.055
- Wu, X., Corona, B. T., Chen, X., & Walters, T. J. (2012). A standardized rat model of volumetric muscle loss injury for the development of tissue engineering therapies. *BioResearch Open Access*, 1(6), 280-290.
- Zheng, B., Cao, B., Crisan, M., Sun, B., Li, G., Logar, A., . . . Cassino, T. (2007). Prospective identification of myogenic endothelial cells in human skeletal muscle. *Nature Biotechnology*, 25(9), 1025-1034.
- Zuk, P. A., Zhu, M., Mizuno, H., Huang, J., Futrell, J. W., Katz, A. J., . . . Hedrick, M. H. (2001). Multilineage cells from human adipose tissue: Implications for cell-based therapies. *Tissue Engineering*, 7(2), 211-228.

Chapter 2

Development of an Infusion Bioreactor for the Accelerated Preparation of Decellularized Skeletal Muscle Scaffolds

Submitted as an original article by:

Ben Kasukonis¹, John Kim¹, Tyrone Washington², and Jeffrey Wolchok¹

¹ Department of Biomedical Engineering, College of Engineering, University of Arkansas

² Department of Health, Human Performance, and Health Professionals, College of Education
and Health Professionals, University of Arkansas

Corresponding Author:

Jeff Wolchok

125 Engineering Hall

Department of Biomedical Engineering

University of Arkansas

Fayetteville, AR 72701

jwolchok@uark.edu

479 575-2850

Abstract

The implantation of decellularized tissue has shown effectiveness as a strategy for the treatment of volumetric muscle loss (VML) injuries. The preparation of decellularized tissue typically relies on the diffusion driven removal of cellular debris. For bulky tissues like muscle, the process can be lengthy, which introduces opportunities for both tissue contamination and degradation of key ECM molecules. In this study we report on the accelerated preparation of decellularized skeletal muscle (DSM) scaffolds using an infusion system and examine scaffold performance for the repair of VML injuries. The preparation of DSM scaffolds using infusion was dramatically accelerated. As the infusion rate (1% SDS) was increased from 0.1 to 1 and 10ml/hr, the time needed to remove intracellular myoglobin and actin decreased from a maximum of 140 ± 3 hrs to 45 ± 3 hrs and 10 ± 2 hrs respectively. Although infusion appeared to remove cellular debris more aggressively, it did not significantly decrease the collagen or glycosaminoglycan composition of DSM samples when compared to un-infused controls. Infusion prepared DSM samples retained the aligned network structure and mechanical integrity of control samples. Infusion prepared DSM samples supported the attachment and in-vitro proliferation of myoblast cells and was well tolerated by the host when examined in-vivo.

Keywords: decellularization, extracellular matrix, skeletal muscle, scaffold

A. Introduction

Our group is pursuing the development of biomaterials targeting the repair of damaged skeletal muscle tissue. Skeletal muscle has a strong capacity for repair, yet this capacity can be overwhelmed when damage is severe. Following mild injuries like strains and contusions, in which the myocytes are damaged but the underlying muscle structure and satellite cell population is preserved, regeneration is robust and surgical intervention is not indicated (Mauro 1961, Hill, Wernig et al. 2003). However, when significant muscle volume is lost (trauma or surgical resection) the underlying structure and progenitor cell pool is absent and regeneration is poor. Termed volumetric muscle loss (VML), the bulk loss (>20%) of muscle tissue overwhelms the capacity for repair, leading to the formation of non-contractile scar tissue at the defect site and functional impairment for the patient (Terada, Takayama et al. 2001). The poor outcome following VML injury, motivates the need for a treatment option. A promising approach is restoration of the chemical and physical cues provided by the extracellular matrix (ECM).

To restore these cues, our group is exploring the use of ECM biomaterials derived from skeletal muscle. To improve the isolation of ECM from whole muscle tissue, a new decellularization approach was explored in this study. Commonly, the decellularization of whole tissues employs detergents (ex: sodium dodecyl sulfate) to lyse cell membranes and remove intracellular proteins, followed by DNase/RNase rinses to remove residual nucleic acids (Gilbert, Sellaro et al. 2006, Badylak, Freytes et al. 2009). The initial removal of intracellular proteins using detergents is typically a diffusion driven process, which for thicker tissues like skeletal muscle can be lengthy, requiring two weeks or more (Merritt, Cannon et al. 2010). This introduces opportunities for both tissue contamination and degradation of key ECM molecules.

In an effort to accelerate the process, the active delivery of detergents into whole organs has been achieved via vascular perfusion. The major inlets and outlets (arteries and veins) along with capillary networks are utilized to perfuse the entire organ. Perfusion decellularization has been used to produce whole organ scaffolds for the heart (Ott, Matthiesen et al. 2008), liver (Uygun, Soto-Gutierrez et al. 2010), lungs (Ott, Clippinger et al. 2010), kidneys (Sullivan, Mirmalek-Sani et al. 2012), and recently even entire limbs (Jank, Xiong et al. 2015).

Skeletal muscle tissue lacks the easily accessible major arteries and veins that are found in whole organs, motivating an alternative delivery approach. The common utilization of intramuscular injection would suggest that fluid infusion through skeletal muscle might provide a viable delivery route for decellularization agents. Towards this end, our group has developed a scalable bench top infusion platform that uses a needle rather than the vascular system to deliver detergents deep into muscle tissue with the goal of accelerating the removal of intracellular proteins. The system also explores the distinct color change (red to white) that occurs within skeletal muscle tissue as myoglobin is removed during decellularization as a means to non-invasively monitor the removal of intracellular proteins. The design/fabrication of the device, characterization of its performance, and measurement of infusion prepared decellularized skeletal muscle (DSM) properties are described in this report. Ultimately, we believe these materials could find utility as scaffolds for the repair of VML injuries.

B. Methods

Absorbance Properties of Skeletal Muscle

A visible light absorbance sweep was performed on rat (Sprague Dawley) gastrocnemius muscle samples in order to characterize the optical properties of whole and decellularized skeletal muscle. The changes in muscle absorbance properties that occur with decellularization would be utilized during the subsequent design of an optical monitoring approach. Rat muscle was selected based on its past use in muscle regeneration animal studies and the anticipated area of application for this device (Merritt, Hammers et al. 2010). All whole muscle tissues used in this study were collected from cadaveric animals that had been previously euthanized using methods approved by the University of Arkansas Institutional Animal Care and Use Committee (IACUC) approved study (protocol #12026). All tissues were stored at -20°C until required for testing. In preparation for testing, gastrocnemius muscle samples were dissected, and from each whole muscle sample a central core was harvested using a biopsy punch (diameter = 6mm) and trimmed to a thickness of 2mm. Cylindrical muscle sample cores were incubated in a 1% sodium dodecyl sulfate (SDS) solution (10mM Tris HCL) with agitation for 24 and 48 hours at room temperature following published protocols (Mirsadraee, Wilcox et al. 2006). Untreated muscle samples were maintained as controls (n=4 / sample group). At the prescribed time points (24, and 48 hours) muscle core samples were loaded into 96 well plates (one sample per well) and a spectral sweep of tissue absorbance was measured (400-900nm, step size = 5nm) with the aid of a spectrophotometer (Synergy H1, BioTek, Winooski, VT). For comparison, the absorbance of myoglobin, an abundant intracellular skeletal muscle protein, was also characterized (0.1, 0.3, and 0.6% in phosphate buffered saline). Absorbance versus wavelength data for all muscle and

myoglobin samples were plotted and examined for the presence of decellularization sensitive absorbance features.

Infusion Bioreactor Design and Fabrication

The design goal was to combine continuous tissue infusion and real time optical monitoring into a single bench top device. The two primary components of the device are the muscle infusion units and optical detection collars with integrated data collection hardware and software. The infusion units, optical monitoring collars, and data collection hardware are housed within and mounted onto a custom fabricated (Replicator 2, MakerBot Industries, New York City, NY) two-piece enclosure (**Figure 1**). The enclosure was designed to accommodate four individual infusion units each capable of accommodating a single muscle tissue sample. The closure also isolates the optical monitoring collars from ambient light. Each of the four modular infusion units consists of a rigid acrylic cylinder (ID = 10mm; length = 40mm) that forms a translucent infusion chamber. The inlet and outlet of each chamber is enclosed by watertight ports fashioned with Leur lock style fittings and fabricated in acrylic with the aid of a 3-D printer (Objet 30, Objet, Israel). The inlet port incorporates a removable 26-ga stainless steel hypodermic needle (length = 20 mm). The needle is used to deliver solution into the interior of individual whole muscle samples. The flow of fluid into each infusion unit was controlled via a commercial multi-syringe pump (#552219, Harvard Apparatus, Holliston, MA) capable of delivering fluid to all four chambers over the range of flow rates (0.1 to 10ml/hr) that would be evaluated during device characterization. Waste decellularization solution is collected in a reservoir for disposal or evaluation.

The optical collar was fitted with a single light emitting diode (LED) producing a peak emittance centered at 535nm. Peak LED wavelength selection was motivated by the results of the previously described muscle optical property characterization. The light output of the LED is directed across the diameter of the optical collar. A light detecting resistor (LDR) was positioned opposite to the LED. The LDR converts light intensity in photons to resistance in ohms. The optical collar with integrated LED and LDR can be positioned along the length of the infusion unit. During infusion, the collar is positioned over the muscle sample, such that muscle tissue impedes the light path from the LED emitter to the LDR detector. Analog voltages collected from the LDR were converted to digital values using an 8-bit analog-to-digital converter (ADC) (Adafruit Industries, New York, NY). A miniaturized single board computer (Raspberry Pi Foundation, United Kingdom) was used to power the LEDs and to control collection of the digitized LDR voltage signal from the ADC. Custom designed software (Python) was created to collect the voltage data and log it to an online spreadsheet. Optical data was collected from the LDR every five minutes. The complete system, including syringe pump and flat screen monitor, occupies a 0.5m X 0.5m footprint, a space that is compatible with typical laboratory workbenches.

Bioreactor Characterization

For all device characterization testing, medial gastrocnemius muscle tissue was harvested from cadaveric Sprague Dawley rats and stored at -20°C until needed for testing. Prior to testing all muscles were thawed and rinsed briefly in DI water to remove any superficial blood or loosely adhered tissue. Whole muscle samples were loaded into infusion chambers, one muscle per chamber. The position of the muscle was adjusted until the needle tip was located at the mid-

belly (thickest) region of the muscle. Based on static decellularization pilot testing and guided by published methods (Mirsadraee, Wilcox et al. 2006), muscle samples (n=4) were infused using a 1% SDS solution at a flow rate of 1ml/hr while LDR output was recorded and plotted. Samples were collected when muscle optical properties (LDR output) were unchanged (<0.1% difference from the previous recording) for five continuous recordings (25 minutes).

To examine the effectiveness of infusion treatment as a method for intracellular protein removal, representative infusion treated and untreated whole muscle samples were embedded in tissue freezing media (Triangle Biomedical Sciences, Durham, NC), sectioned at 8µm with a cryostat, and mounted onto glass microscope slides. Mounted sections were immune-reacted for the presence of myoglobin (rabbit IgG₁, 1:500, Sigma, St. Louis, MO) and actin (phalloidin, 1:40, Sigma, St. Louis, MO) followed by incubation with the appropriate fluorescently labeled secondary antibodies (Alexafluor, 1:500, Fisher Scientific). Sections were counterstained with the nuclear staining reagent DAPI, and then microscopically imaged (Ci-L, Nikon, Troy, NY). Digital images were captured, stored, and examined for the presence of intracellular proteins and nuclear remnants.

To explore the influence of key infusion parameters (flow rate and SDS solution concentration) on myoglobin removal, medical gastrocnemius muscle samples were perfused at flow rates of either 0.1, 1, or 10ml/hr using SDS solutions at concentrations of 0.2% or 1%. A total of 6 parameter combinations were explored (n= 4/ parameter condition). Throughout infusion testing the optical properties of each muscle was measured and digitally logged every 5 minutes. As previously described, the time at which intracellular protein removal was considered complete and samples were removed was recorded as the time at which sample optical properties were unchanged for five continuous recording.

From the infusion data, the time to reach steady state optical properties (y) was modeled with a two factor (1: flow rate, 2: SDS concentration) regression model of the type

$$y = b_0 + b_1x_1 + b_2x_2 + b_{12}x_1x_2 \quad (1)$$

The regression coefficients (b_i) were solved for using commercially available data analysis software (JMP, SAS Institute, Cary, NC). From the model, the relationship of infusion time to each of the infusion parameters was calculated.

To determine whether infusion influenced the retention of key ECM molecules, the sulfated glycosaminoglycans (sGAG) concentration was quantified using a published procedure (Barbosa, Garcia et al. 2003). For comparison, control DSM samples were statically (non-infused) incubated in 1% SDS at room temperature with gentle agitation using rocker platform, for a duration of two weeks (Merritt, Cannon et al. 2010). All infusion and control samples were lyophilized and stored at -20°C until needed for analysis. To extract sGAG, lyophilized samples ($n=4/\text{sample group}$) were digested in a solution containing $50 \mu\text{g/mL}$ proteinase K in $100 \text{ mM K}_2\text{HPO}_4$ at a pH of 8.0 at 55°C for 16 hours. The samples were then centrifuged and filtered to isolate tissue fragments. A 1,9-dimethylmethylene blue (DMMB) solution was added to produce an insoluble GAG-DMMB complex. The solution was centrifuged, the supernatant was removed, and the GAG-DMMB complex was dissolved with a decomplexation solution. The absorbance of the resulting solution was read at 656 nm with the aid of a microplate reader (Synergy H1, BioTek, Winooski, VT). Samples were tested in triplicate and compared against a standard curve to determine sGAG concentration.

The collagen content of control and infusion samples ($n=4/\text{sample group}$) was quantified using a modified version of the hydroxyproline assay procedure reported by Edwards (Edwards

and O'Brien 1980). Briefly, all tissue samples were hydrolyzed in 6N HCl for 16-20 hours at 115°C, then cooled to room temperature and diluted 1:5 in distilled water. Hydrolyzed samples were mixed with a chloramine T solution (1:2) and incubated at room temperature for 20 minutes. A dimethyl-aminobenzaldehyde assay solution was added (1:2) and the mixture was incubated at 60°C for 15 minutes to develop a red chromophore. Sample absorbance was read at 570 nm using a microplate reader. Samples were tested in triplicate and compared against a standard curve to determine collagen concentration. To visualize and validate the retention of collagen within infusion prepared tissue, a representative sample was immunoreacted for the presence of collagen type I (mouse IgG₁, 1:500, Sigma, St. Louis, MO) and type III (rabbit IgG₁, 1:1000, AbCam, UK) followed by incubation with the appropriate fluorescently labeled secondary antibodies (Alexafluor, 1:500, Fisher Scientific).

To explore the influence of infusion treatment on DSM physical properties, control and infusion (1% SDS for 12 hours at 10ml/hr) DSM sample (n=4/sample group) mechanical properties were measured with the aid of a uni-axial tensile tester (UStretch, CellScale, Ontario, Canada) using techniques familiar to our group (Wolchok, Brokopp et al. 2009, Lasher, Wolchok et al. 2010, Wolchok and Tresco 2010). Hydrated (PBS, pH=7.4) sample strips (12 mm X 3 mm) were deformed at a constant strain rate of 1%/s until failure using a 5N load cell while the load and displacement values were recorded. For each sample, engineering stress versus strain curves were generated from load and elongation data. Strain was determined using grip displacement values. From each curve the tangent modulus was calculated from a linear fit to the stress-strain curve. The ultimate strength was calculated as the peak stress achieved by each sample prior to failure.

Additional control and infusion prepared DSM samples (n=4/sample groups) were embedded in tissue freezing medium and sectioned transversely (8 μ m) with the aid of a cryostat. Sections were mounted onto glass slides, stained with hematoxylin and eosin (H&E) and microscopically imaged (100x). Three representative images from each sample were used to measure porosity (% open space) and network alignment (average orientation angle) using image analysis software (ImageJ) and guided by published techniques (Liu, Qu et al. 2008, Huang, Lee et al. 2010). For DSM sample orientation analysis, the direction of muscle contraction (long axis of the gastrocnemius muscle) was selected to correspond to an orientation angle of 0 degrees.

In-Vitro and in-Vivo Biocompatibility

To create DSM samples for implantation, Sprague Dawley tibialis anterior (TA) muscle was infusion treated (1% SDS for 12 hours at 10ml/hr) using the previously described and characterized system. Following infusion treatment, samples were statically incubated overnight in a DNase / RNase solution (1kU/ml DNase in a 10mM Tris-HCL buffer; 2.5mM MgCl₂ + 0.5mM CaCl₂) and then incubated (8 hours) in a 1X penicillin/streptomycin solution to reduce the risk of infection. Samples were rinsed thoroughly (a total of six 24 hour wash steps) in PBS following each preparation step (Figure 2). Following completion of the entire decellularization protocol, the DNA concentration of representative DSM implants (n=3) was measured with the aid of a commercial quantification kit (Qubit, Fisher Scientific). DSM implants were lyophilized and stored at -20C until needed for implantation.

A direct contact assay was used to evaluate cellular attachment and proliferation upon infusion prepared DSM substrates. DSM material islands (diameter = 6mm) were created on

glass microscope slides. DSM islands were seeded with skeletal muscle myoblasts (L6, ATCC, Manassas, VA) at a density of 7K cells per island. Cell viability was evaluated at 3 and 7 days (n= 3 islands / time point) using calcein AM (Life Technologies). Three representative fields were imaged (100x) from each island and captured digitally. From the digital images, cell confluency (% surface coverage) was calculated at each time point with the aid of image analysis software (ImageJ).

In-vivo host response was examined using a dorsal subcutaneous implant site. *In-vivo* biocompatibility was assayed at short-term (4 weeks) and long-term (12 weeks) time points. Mature male Sprague Dawley rats (300+g) were used (Harlan, IN). All surgical procedures were performed in accordance with protocols approved by the University of Arkansas Institutional Animal Care and Use Committee. Anesthesia was induced using isoflurane (2-4%) in oxygen. The subcutaneous implant site was surgically exposed through a 2 cm left-right incision placed 2 finger widths caudal to the scapulae. A subcutaneous pouch was created in each animal by blunt dissection. A single perfusion prepared DSM disk (6mm diameter X 1mm thick) was implanted into each pouch (Incisions were closed using surgical adhesive (VetBond, 3M). Following surgery all animals were housed in the University of Arkansas Central Laboratory Animal Facility. At the prescribed time-points (4 and 12 weeks) all animals (n=3 / timepoint) were euthanized via inhalation of carbon dioxide. The implant site with surrounding soft tissue was harvested, fixed in 4% paraformaldehyde, paraffin embedded, sectioned (10um), and stained with H&E with the aid of the University of Arkansas Histological Core Facility. Stained sections were imaged and examined for evidence of material degradation.

Statistics

All data is represented by the mean and standard deviation. Comparisons between infusion flow rate and SDS concentration (time to stable optical properties, collagen, and sGAG analysis) were evaluated with a two-factor ANOVA. Post hoc comparisons were made using Tukey's test. The effect of treatment (infusion version control) on alignment, porosity, and mechanical properties was evaluated using a two-way student's t-test. A standard 0.05 level of significance was used for all statistical tests.

C. Results

Absorbance Properties of Skeletal Muscle

The absorbance sweeps collected from myoglobin solution samples (0.6%) were characterized by an observable peak centered at $505\pm 4\text{nm}$ (**Figure 2**). As the myoglobin concentration was decreased to 0.3% and 0.1%, the absorbance peak heights decreased by 58% and 85% respectively and the peak profiles tended to broaden. The absorbance sweeps recorded from hydrated whole muscle samples were characterized by a more modest absorbance shoulder, which when compared to myoglobin was less pronounced and shifted modestly towards a higher wavelength ($541\pm 7\text{nm}$). The whole muscle peak wavelength was positioned within the green region of the visible light spectrum. Following 24 hours of SDS incubation, the absorbance shoulder was still detectable but less pronounced. Visually, 24 hour muscle samples showed residual evidence of intracellular myoglobin (retention of a pinkish color), suggesting partial but still incomplete removal. After 48 hours of SDS treatment, the absorbance shoulder present in whole muscle samples was no longer detected and myoglobin was no longer visualized, as evidenced by a translucent appearance. Generally, the absorbance of skeletal muscle tissue at

541nm decreased as samples were progressively incubated in SDS, suggesting a valuable target wavelength for optical monitoring of intracellular myoglobin retention.

Bioreactor Characterization

Muscle sample absorbance logs (LDR voltage versus time) were characterized by a progressive reduction in tissue absorbance (decreased LDR output voltage) with increased infusion time as more light (535nm) emitted by the LED was capable of transmitting through the muscle samples and reaching the LDR. Whole muscle samples transitioned from a characteristic red color to translucent during the infusion driven removal of intracellular proteins. (**Figure 3**). LDR voltage eventually reached a steady state minimum for all samples tested, which was defined for all subsequent tests as the time to myoglobin removal. Prior to infusion treatment, intracellular myoglobin, as well as actin and nuclear remnants were visible within whole muscle sections. Once the LDR had reached a steady minimum, identified as the time at which LDR output voltage was unchanged for 25 minutes, infusion treated muscle samples (n=4) were no longer immunoreactive to myoglobin or actin. Furthermore, although not treated with nucleases during the infusion process, DAPI positive nuclei could not be detected. Overall, the histological examination of infusion treated samples suggests that the LDR voltage minimum was an effective metric of intracellular myoglobin and actin removal.

The infusion solution flow rate and SDS concentration had a statistically significant effect on the removal of intracellular myoglobin (**Figure 4**). The average infusion time required to remove myoglobin, as measured by LDR voltage and further validated through histology, was shortened in response to increases to both flow rate and SDS concentration. Flow rate had a strong influence on myoglobin removal. The removal time decreased from a maximum of

143±8hrs at the lowest flow rate of 0.1 ml/hr (0.2% SDS) to 42±3hrs and 9±1hr as the flow rate was increased to 1ml/hour and 10ml/hour respectively. Increased SDS concentration had a significant but less dramatic influence when compared to flow rate. Increasing the SDS concentration from 0.2% to 1% shortened the time from 143±8hrs to 107±6 at the lowest flow rate tested (0.1ml/hr), a reduction of 24%. At higher flow rates (1 and 10ml/hr) the effect of SDS concentration on myoglobin removal was less pronounced, but still statistically significant. When viewed as a whole, the removal of intracellular myoglobin was more responsive to flow rate than SDS concentration, however the range of flow rates tested (100 fold difference between lowest and highest) was larger than the range of SDS concentrations tested (5 fold difference). From the data collected, the relationship of myoglobin removal time (in hours) to flow rate (ml/hr) and SDS concentration (%) was modeled (**eq. 2**). When plotted over the parameter ranges tested (**Figure 4B & C**), the model accurately describes the increased influence of flow rate on myoglobin removal time observed during benchtop testing.

$$\text{Time} = 99 - 8.3 \times [\text{Flow}] - 18.0 \times [\text{SDS}] + 2.7 \times (\text{Flow} - 0.6) \times (\text{SDS} - 3.7) \quad (2)$$

Although SDS infusion accelerated the removal of intracellular myoglobin and actin, it did not significantly decrease collagen or sGAG concentration when compared to non-infused controls. No statistically significant differences in collagen or sGAG concentration were detected for any of the flow rates and SDS concentrations examined (**Figure 5**). All infusion treated collagen and GAG composition values were within 10% of control samples. Furthermore, trends indicating a relationship between ECM composition and infusion flow rate were not observed.

Infusion decellularized samples retained the highly aligned network organization characteristic of skeletal muscle (Figure 6). The dominant orientation angle of DSM samples following infusion decellularization ($7\pm 6^\circ$) was not significantly different from controls ($11\pm 5^\circ$). Both infusion prepared and control samples were aligned in the direction of contraction (designated as 0°). Control and infusion prepared samples were robust and easily tolerated handling and tensile testing. Stress versus strain curves for both materials were characterized by an initial toe-in region out to approximately 10-15% strain followed by a nearly linear ($R^2 > 0.9$) increase in stress extending out to failure at approximately 100-125% for both infusion and control DSM samples. The average tangent modulus measured from the linear region extending from 20% (post toe-in) to material failure was $225\pm 44\text{kPa}$ and $189\pm 32\text{kPa}$ for infusion and control samples respectively. Average infusion prepared DSM sample elastic moduli were not significantly different from control samples. Similarly, average ultimate strength differences between infusion and control DSM materials were not statistically significant.

In-Vitro and in-Vivo Biocompatibility

Average infusion prepared DSM sample DNA content ($2.9\pm 0.6\text{ng}$ of DNA / mg of tissue) were well below the preferred implantation threshold ($< 50\text{-}70\text{ng/mg}$) reported by others (Zhang, He et al. 2009, Crapo, Gilbert et al. 2011). The DSM samples supported the attachment and *in-vitro* proliferation of cultured myoblast cells. Viable cells were attached to all cell seeded DSM islands at both time points. Seventy-two hours after seeding, viable cells covered, on average, $8\pm 2\%$ of the DSM sample surface (Figure 7). By seven days post seeding, average cell coverage increased to $60\pm 6\%$ of the DSM sample surface. Cells cultured on DSM materials appeared well

spread and expanded upon the DSM surface at a coverage rate of approximately 13% / day. The average cell coverage difference between day three and seven was statistically significant.

All implanted animals tolerated the subcutaneous implantation surgery well and reached the prescribed study endpoints without complications (n=4 / endpoint). At four weeks post implantation, DSM materials were well incorporated into the surrounding tissue and host cells had densely penetrated the material (Figure 8). While signs of active inflammation could be observed there were no signs of tissue necrosis or exudate (pus) accumulation at the implant site. The dense cellular penetration into the DSM material was suggestive of active remodeling of the implant site. The breakdown of whole DSM disks into smaller fragments was observed. There were no signs suggesting formation of a dense fibrous encapsulation layer surrounding DSM materials. By twelve weeks post implantation, DSM materials appeared fully degraded. No evidence of DSM material could be identified in any of the implanted animals, although some residual cellularity could be seen at the implant site.

D. Discussion

As chemical decellularization schemes continue to mature and gain acceptance, the development of effective delivery platforms deserves research investment. With that goal in mind, what was explored in this study is a device and method for the preparation of decellularized skeletal muscle tissue using a non-vascular infusion delivery method. Overall, the utilization of infusion on skeletal muscle samples was highly effective at accelerating the removal of intracellular proteins. Specifically, with the aid of the infusion device, the time to clear rat lower limb gastrocnemius and TA muscles of intracellular proteins reduced from two

weeks to as short as 10 hours. This is a notable finding, and the first we are aware of that demonstrated the accelerated removal of cellular debris from bulk tissue samples using a non-vascular infusion technique. It may be possible to translate this process to other tissues, particularly musculoskeletal tissues including, tendons (Lee, Lee et al. 2013), ligaments (Harrison and Gratzner 2005), cartilage (Sutherland, Beck et al. 2015), and menisci (Chen, Chen et al. 2015) in which vascular perfusion would be difficult. The time reduction is not just important from the standpoint of process efficiency, but also may help reduce the degradation of key ECM proteins that could occur with time throughout the decellularization process. The decellularization of tissue using SDS, the most common process, is typically performed at room temperature, and while the presence of SDS limits bacterial and fungal growth, the degradation of proteins that can occur with time at room temperature is a concern (Pasella, Baralla et al. 2013, Wang, Zhu et al. 2015). Shortening the amount of time tissue is exposed to room temperatures in aqueous solutions may reduce the degradation of key ECM proteins during decellularization and improve scaffold quality.

While the device described in this study was designed for the processing of small animal tissues for use in pre-clinical research, the future application of infusion to accelerate the preparation of human or large animal tissue for clinical applications is anticipated. Particularly since the complete removal of cellular debris from large skeletal muscle tissues, like the quadriceps which can be several centimeters thick, may be prohibitively lengthy using diffusion alone. It should also be noted that human skeletal muscle tissue is rarely if ever tissue banked, and therefore represents an untapped source for implantable human ECM. Device scale-up for the processing of larger muscle tissue will require design adaptations beyond just increasing the size of the chambers. The single needle infusion chambers developed in this study were designed

for the processing of single rat hind limb skeletal muscles. The volume of rat gastrocnemius and tibialis anterior muscles (1-2 cm³) was well suited to the delivery of decellularization solution via a single hypodermic needle. However, the processing of larger animal and potentially cadaveric human muscle samples for clinical applications would require modification to incorporate a multi-needle approach. While clearly more complex, our experience with the current single needle system suggests that expansion to a multi-needle system is achievable, and in fact the current system uses multiple needles to process muscle samples in parallel. What remains unknown, is the optimal relationship between needle quantity, spacing, and tissue volume. Future bench top measurement and computer modeling of the relationship between time to decellularization and tissue volume would help determine ideal infusion needle density.

It should be possible to utilize lower SDS concentrations than those explored in this study, while still maintaining overnight to at most 1 day myoglobin removal times. At an infusion flow rate of 10ml/hr, the highest rate tested, a 5 fold decrease in SDS concentration (0.2% versus 1%) only increased the time from 7 to 9 hours suggesting an even lower SDS concentration might still be effective. A reduction in SDS concentration could be beneficial when one considers that removing SDS from tissue is challenging and the presence of residual SDS within implanted scaffolds can be cytotoxic (Cebotari, Tudorache et al. 2010). Furthermore, it is well established that exposure to SDS during the decellularization process can have a detrimental effect on tissue properties (Faulk, Carruthers et al. 2014). Eventually it may be beneficial to transition towards SDS-free decellularization approaches. If so, it seems reasonable to suggest that infusion could be utilized to decrease process duration for other solution based decellularization strategies, including SDS-free techniques that employ osmotic or physical means to disrupt cell membranes and liberate intracellular debris (Greco, Francis et al. 2015,

Xing, Yates et al. 2015). Alternatively, it may be possible to utilize a short SDS incubation step to initially lyse cells and bind intracellular proteins, followed by a longer SDS-free infusion step to wash away the intracellular debris and residual SDS. Whatever the method, it should be possible to utilize infusion as a means to minimize both the SDS concentration and exposure time during the decellularization process.

The monitoring of skeletal muscle optical properties provided a non-destructive real time means to evaluate decellularization progression. The histological results from this study suggest that the monitoring of muscle optical properties is a good indicator of intracellular myoglobin concentration. While we only looked at one additional intracellular protein (actin) it seems reasonable to speculate that if these two proteins were effectively removed other intracellular proteins were as well. One limitation is that optical monitoring of the type used the current device was designed to detect the progressive removal of the muscle specific intracellular protein myoglobin. The progressive removal of myoglobin produced an obvious shift in tissue appearance from red to clear, which could be detected in the visible region of the light spectrum using a low cost LED and LDR pairing. However, it has been suggested that removal of the nuclear debris is more crucial to implant performance than the intracellular proteins, suggesting that development of a means to monitor the removal DNA and RNA would be valuable (Gilbert, Sellaro et al. 2006). Unfortunately, the optical properties of muscle within the visible region are not affected by the removal of nuclear debris. As an adjunct to the currently monitoring approach, it may be possible to examine the optical properties of tissues at DNA/RNA sensitive wavelengths (260/280nm) to monitor the removal of nuclear debris, although using low cost LEDs to do so is not feasible.

The co-delivery of muscle progenitor (satellite) cells in combination with ECM could also help stimulate a pro-regenerative environment following VML injury. The loss of muscle tissue following VML eliminates a substantial pool of progenitor cells. The remaining satellite cell population available for migration from surrounding healthy tissue may be inadequate, and therefore supplementation of the repair site with additional progenitor cells could enhance regeneration. Towards this end, the in-vitro seeding of ECM implants with progenitor cells has been shown to improve the restoration of peak contractile force (Merritt, Cannon et al. 2010, Corona, Ward et al. 2014). With this approach in mind, infusion flow could be used as a means to seed DSM implants with progenitor cells in preparation for implantation. Infusion could help distribute cells evenly throughout the DSM network, rather than densely at the surface as is generally observed following manual seeding (Kennedy, McCandless et al. 2011). Satellite cells are difficult to amass in great quantities, and can lose their regenerative capacity when expanded *in vitro* (Montarras, Morgan et al. 2005) so improving the efficiency of in-vitro progenitor cell delivery has value.

The average DSM modulus values measured in this study are similar in magnitude to other decellularized tissue scaffolds, including commercially available porcine intestinal and bladder tissue (Dahms, Piechota et al. 1998, Tottey, Johnson et al. 2011), as well as human facial DSM material (Wang, Johnson et al. 2013). The relationship between scaffold modulus and VML repair outcome has not been investigated, but in-vitro studies have shown that muscle progenitor cells sense and respond to substrate stiffness. Muscle progenitor cell myogenesis is significantly enhanced when the cells are grown on soft substrates like ECM and reduced on stiff substrates like tissue culture plastic (Rao, Grover et al. 2013, Morrissey, Cheng et al. 2015). Similar cell-substrate stiffness interactions have been noted for other cell types including

cardiomyocytes (Ribeiro, Ang et al. 2015). Furthermore, the robust mechanical properties of DSM and other ECM scaffolds facilitate attachment (suturing) to the surrounding healthy tissue during surgical VML repair. Surgical reattachment is clinically important, because it will enable the transfer of contractile force through the repair site during healing and regeneration. This is potentially critical, since force and substrate strain have been shown to enhance muscle progenitor cell myogenesis (Egusa, Kobayashi et al. 2013, Heher, Maleiner et al. 2015).

While the ideal VML repair scheme still awaits discovery, it appears the restoration of a pro-myogenic environment may require a multifactorial approach, combining biocompatible scaffolds, with progenitor cells, soluble myogenic signaling molecules, and postoperative rehabilitation (Aurora, Garg et al. 2014, Garvey, Russ et al. 2015). The accelerated removal of intracellular proteins from skeletal muscle tissues, without sacrificing chemical or physical properties, makes the infusion preparation platform described in this study an attractive scaffold preparation strategy. Furthermore pilot study biocompatibility testing suggesting that infusion prepared DSM both supported cell attachment and was well tolerated by the host, motivates further *in-vivo* examination using a peer accepted muscle regeneration animal model (Wu, Corona et al. 2012).

E. Conclusions

The key findings of this study suggest that:

- 1) The delivery of SDS into skeletal muscle via infusion removed intracellular proteins including myoglobin and actin.

- 2) The monitoring of myoglobin absorbance was effective as an inexpensive means to non-invasively monitor the progression of intracellular protein removal during decellularization.
- 3) Infusion flow rate and SDS concentration could be adjusted to modulate the removal rate of intracellular proteins from whole muscle samples.
- 4) Infusion did not reduce the collagen or sGAG composition of DSM scaffolds.
- 5) Infusion did not influence the native network alignment or reduce the mechanical properties of DSM scaffolds.
- 6) Infusion prepared material supported the attachment and proliferation of cells and was well tolerated by the host following subcutaneous implantation.

References

- Aurora, A., K. Garg, B. T. Corona and T. J. Walters (2014). "Physical rehabilitation improves muscle function following volumetric muscle loss injury." BMC Sports Sci Med Rehabil **6**(1): 41.
- Badylak, S. F., D. O. Freytes and T. W. Gilbert (2009). "Extracellular matrix as a biological scaffold material: Structure and function." Acta Biomater **5**(1): 1-13.
- Barbosa, I., S. Garcia, V. Barbier-Chassefiere, J. P. Caruelle, I. Martelly and D. Papy-Garcia (2003). "Improved and simple micro assay for sulfated glycosaminoglycans quantification in biological extracts and its use in skin and muscle tissue studies." Glycobiology **13**(9): 647-653.
- Cebotari, S., I. Tudorache, T. Jaekel, A. Hilfiker, S. Dorfman, W. Ternes, A. Haverich and A. Lichtenberg (2010). "Detergent decellularization of heart valves for tissue engineering: toxicological effects of residual detergents on human endothelial cells." Artif Organs **34**(3): 206-210.
- Chen, Y. C., R. N. Chen, H. J. Jhan, D. Z. Liu, H. O. Ho, Y. Mao, J. Kohn and M. T. Sheu (2015). "Development and Characterization of Acellular Extracellular Matrix Scaffolds from Porcine Menisci for Use in Cartilage Tissue Engineering." Tissue Eng Part C Methods.
- Corona, B. T., C. L. Ward, H. B. Baker, T. J. Walters and G. J. Christ (2014). "Implantation of in vitro tissue engineered muscle repair constructs and bladder acellular matrices partially restore in vivo skeletal muscle function in a rat model of volumetric muscle loss injury." Tissue Eng Part A **20**(3-4): 705-715.
- Crapo, P. M., T. W. Gilbert and S. F. Badylak (2011). "An overview of tissue and whole organ decellularization processes." Biomaterials **32**(12): 3233-3243.
- Dahms, S. E., H. J. Piechota, R. Dahiya, T. F. Lue and E. A. Tanagho (1998). "Composition and biomechanical properties of the bladder acellular matrix graft: comparative analysis in rat, pig and human." Br J Urol **82**(3): 411-419.
- Edwards, C. A. and W. D. O'Brien, Jr. (1980). "Modified assay for determination of hydroxyproline in a tissue hydrolyzate." Clin Chim Acta **104**(2): 161-167.
- Egusa, H., M. Kobayashi, T. Matsumoto, J. Sasaki, S. Uraguchi and H. Yatani (2013). "Application of cyclic strain for accelerated skeletal myogenic differentiation of mouse bone marrow-derived mesenchymal stromal cells with cell alignment." Tissue Eng Part A **19**(5-6): 770-782.
- Faulk, D. M., C. A. Carruthers, H. J. Warner, C. R. Kramer, J. E. Reing, L. Zhang, A. D'Amore and S. F. Badylak (2014). "The effect of detergents on the basement membrane complex of a biologic scaffold material." Acta Biomater **10**(1): 183-193.
- Garvey, S. M., D. W. Russ, M. B. Skelding, J. E. Dugle and N. K. Edens (2015). "Molecular and metabolomic effects of voluntary running wheel activity on skeletal muscle in late middle-aged rats." Physiol Rep **3**(2).

- Gilbert, T. W., T. L. Sellaro and S. F. Badylak (2006). "Decellularization of tissues and organs." Biomaterials **27**(19): 3675-3683.
- Greco, K. V., L. Francis, M. Somasundaram, G. Greco, N. R. English, J. A. Roether, A. R. Boccaccini, P. Sibbons and T. Ansari (2015). "Characterisation of porcine dermis scaffolds decellularised using a novel non-enzymatic method for biomedical applications." J Biomater Appl **30**(2): 239-253.
- Harrison, R. D. and P. F. Gratzner (2005). "Effect of extraction protocols and epidermal growth factor on the cellular repopulation of decellularized anterior cruciate ligament allografts." J Biomed Mater Res A **75**(4): 841-854.
- Heher, P., B. Maleiner, J. Pruller, A. H. Teuschl, J. Kollmitzer, X. Monforte, S. Wolbank, H. Redl, D. Runzler and C. Fuchs (2015). "A novel bioreactor for the generation of highly aligned 3D skeletal muscle-like constructs through orientation of fibrin via application of static strain." Acta Biomater **24**: 251-265.
- Hill, M., A. Wernig and G. Goldspink (2003). "Muscle satellite (stem) cell activation during local tissue injury and repair." J Anat **203**(1): 89-99.
- Huang, N. F., R. J. Lee and S. Li (2010). "Engineering of aligned skeletal muscle by micropatterning." Am J Transl Res **2**(1): 43-55.
- Jank, B. J., L. Xiong, P. T. Moser, J. P. Guyette, X. Ren, C. L. Cetrulo, D. A. Leonard, L. Fernandez, S. P. Fagan and H. C. Ott (2015). "Engineered composite tissue as a bioartificial limb graft." Biomaterials **61**: 246-256.
- Kennedy, J. P., S. P. McCandless, A. Rauf, L. M. Williams, J. Hillam and R. W. Hitchcock (2011). "Engineered channels enhance cellular density in perfused scaffolds." Acta Biomater **7**(11): 3896-3904.
- Lasher, R. A., J. C. Wolchok, M. K. Parikh, J. P. Kennedy and R. W. Hitchcock (2010). "Design and characterization of a modified T-flask bioreactor for continuous monitoring of engineered tissue stiffness." Biotechnol Prog **26**(3): 857-864.
- Lee, K. I., J. S. Lee, J. G. Kim, K. T. Kang, J. W. Jang, Y. B. Shim and S. H. Moon (2013). "Mechanical properties of decellularized tendon cultured by cyclic straining bioreactor." J Biomed Mater Res A **101**(11): 3152-3158.
- Liu, B., M. J. Qu, K. R. Qin, H. Li, Z. K. Li, B. R. Shen and Z. L. Jiang (2008). "Role of cyclic strain frequency in regulating the alignment of vascular smooth muscle cells in vitro." Biophys J **94**(4): 1497-1507.
- Mauro, A. (1961). "Satellite cell of skeletal muscle fibers." J Biophys Biochem Cytol **9**: 493-495.
- Merritt, E. K., M. V. Cannon, D. W. Hammers, L. N. Le, R. Gokhale, A. Sarathy, T. J. Song, M. T. Tierney, L. J. Suggs, T. J. Walters and R. P. Farrar (2010). "Repair of traumatic skeletal muscle

injury with bone-marrow-derived mesenchymal stem cells seeded on extracellular matrix." Tissue Eng Part A **16**(9): 2871-2881.

Merritt, E. K., D. W. Hammers, M. Tierney, L. J. Suggs, T. J. Walters and R. P. Farrar (2010). "Functional assessment of skeletal muscle regeneration utilizing homologous extracellular matrix as scaffolding." Tissue Eng Part A **16**(4): 1395-1405.

Mirsadraee, S., H. E. Wilcox, S. A. Korossis, J. N. Kearney, K. G. Watterson, J. Fisher and E. Ingham (2006). "Development and characterization of an acellular human pericardial matrix for tissue engineering." Tissue Eng **12**(4): 763-773.

Montarras, D., J. Morgan, C. Collins, F. Relaix, S. Zaffran, A. Cumano, T. Partridge and M. Buckingham (2005). "Direct isolation of satellite cells for skeletal muscle regeneration." Science **309**(5743): 2064-2067.

Morrissey, J. B., R. Y. Cheng, S. Davoudi and P. M. Gilbert (2015). "Biomechanical Origins of Muscle Stem Cell Signal Transduction." J Mol Biol.

Ott, H. C., B. Clippinger, C. Conrad, C. Schuetz, I. Pomerantseva, L. Ikonomidou, D. Kotton and J. P. Vacanti (2010). "Regeneration and orthotopic transplantation of a bioartificial lung." Nat Med **16**(8): 927-933.

Ott, H. C., T. S. Matthiesen, S. K. Goh, L. D. Black, S. M. Kren, T. I. Netoff and D. A. Taylor (2008). "Perfusion-decellularized matrix: using nature's platform to engineer a bioartificial heart." Nat Med **14**(2): 213-221.

Pasella, S., A. Baralla, E. Canu, S. Pinna, J. Vaupel, M. Deiana, C. Franceschi, G. Baggio, A. Zinellu, S. Sotgia, G. Castaldo, C. Carru and L. Deiana (2013). "Pre-analytical stability of the plasma proteomes based on the storage temperature." Proteome Sci **11**(1): 10.

Rao, N., G. N. Grover, L. G. Vincent, S. C. Evans, Y. S. Choi, K. H. Spencer, E. E. Hui, A. J. Engler and K. L. Christman (2013). "A co-culture device with a tunable stiffness to understand combinatorial cell-cell and cell-matrix interactions." Integr Biol (Camb) **5**(11): 1344-1354.

Ribeiro, A. J., Y. S. Ang, J. D. Fu, R. N. Rivas, T. M. Mohamed, G. C. Higgs, D. Srivastava and B. L. Pruitt (2015). "Contractility of single cardiomyocytes differentiated from pluripotent stem cells depends on physiological shape and substrate stiffness." Proc Natl Acad Sci U S A **112**(41): 12705-12710.

Sullivan, D. C., S. H. Mirmalek-Sani, D. B. Deegan, P. M. Baptista, T. Aboushwareb, A. Atala and J. J. Yoo (2012). "Decellularization methods of porcine kidneys for whole organ engineering using a high-throughput system." Biomaterials **33**(31): 7756-7764.

Sutherland, A. J., E. C. Beck, S. C. Dennis, G. L. Converse, R. A. Hopkins, C. J. Berkland and M. S. Detamore (2015). "Decellularized cartilage may be a chondroinductive material for osteochondral tissue engineering." PLoS One **10**(5): e0121966.

Terada, N., S. Takayama, H. Yamada and T. Seki (2001). "Muscle repair after a transection injury with development of a gap: an experimental study in rats." Scand J Plast Reconstr Surg Hand Surg **35**(3): 233-238.

Totley, S., S. A. Johnson, P. M. Crapo, J. E. Reing, L. Zhang, H. Jiang, C. J. Medberry, B. Reines and S. F. Badylak (2011). "The effect of source animal age upon extracellular matrix scaffold properties." Biomaterials **32**(1): 128-136.

Uygun, B. E., A. Soto-Gutierrez, H. Yagi, M. L. Izamis, M. A. Guzzardi, C. Shulman, J. Milwid, N. Kobayashi, A. Tilles, F. Berthiaume, M. Hertl, Y. Nahmias, M. L. Yarmush and K. Uygun (2010). "Organ reengineering through development of a transplantable recellularized liver graft using decellularized liver matrix." Nat Med **16**(7): 814-820.

Wang, J., H. H. Zhu, J. H. Xue, S. S. Wu and Z. Chen (2015). "Effects of storage conditions on the stability of serum CD163, NGAL, HMGB1 and MIP2." Int J Clin Exp Pathol **8**(4): 4099-4105.

Wang, L., J. A. Johnson, D. W. Chang and Q. Zhang (2013). "Decellularized musculofascial extracellular matrix for tissue engineering." Biomaterials **34**(11): 2641-2654.

Wolchok, J. C., C. Brokopp, C. J. Underwood and P. A. Tresco (2009). "The effect of bioreactor induced vibrational stimulation on extracellular matrix production from human derived fibroblasts." Biomaterials **30**(3): 327-335.

Wolchok, J. C. and P. A. Tresco (2010). "The isolation of cell derived extracellular matrix constructs using sacrificial open-cell foams." Biomaterials.

Wu, X., B. T. Corona, X. Chen and T. J. Walters (2012). "A Standardized Rat Model of Volumetric Muscle Loss for the Development of Tissue Engineering Therapies." BioResearch Open Access **1**(6).

Xing, Q., K. Yates, M. Tahtinen, E. Shearier, Z. Qian and F. Zhao (2015). "Decellularization of fibroblast cell sheets for natural extracellular matrix scaffold preparation." Tissue Eng Part C Methods **21**(1): 77-87.

Zhang, Y., Y. He, S. Bharadwaj, N. Hammam, K. Carnagey, R. Myers, A. Atala and M. Van Dyke (2009). "Tissue-specific extracellular matrix coatings for the promotion of cell proliferation and maintenance of cell phenotype." Biomaterials **30**(23-24): 4021-4028.

Acknowledgments:

Research reported in this publication was supported by the National Institute Of Arthritis And Musculoskeletal And Skin Diseases of the National Institutes of Health under Award Number R15AR064481 and the Arkansas Biosciences Institute.

Author Disclosure Statement:

No competing financial interests exist for any of the authors.

Figure Legend:

Figure 1: The primary components of the as built device are the muscle infusion chambers and optical detection collars (A and B). SDS solution is delivered into muscle tissue via a hypodermic needle (not seen), infused through the muscle, and outflows to waste collection. Light produced by the LED travels across the chamber and through the muscle sample (B: dashed arrow) where it is detected and converted to a voltage output by the LDR. Infusion units, optical monitoring collars, and data collection hardware are housed within and mounted onto a custom fabricated enclosure (C and D). The enclosure was designed to accommodate four side-by-side decellularization units each capable of accommodating a single muscle tissue sample. LDR output voltage was converted to a digital signal (8-bit) and stored with the aid of integrated data collection hardware (Raspberry Pi) and software (Python).

Figure 2: Representative visible light absorbance spectra for myoglobin solutions (A) and skeletal muscle tissue samples (B). The myoglobin absorbance peak ($505\pm 4\text{nm}$) decreased as protein concentration was diluted from a high of 0.6% (in PBS) to a low of 0.1%. A less pronounced absorbance shoulder ($541\pm 7\text{nm}$) was observed for whole muscle tissue samples. The absorbance shoulder for whole muscle samples (M) was similarly reduced as muscle samples were incubated in decellularization solution (1% SDS) for either 24 or 48 hours.

Figure 3: Representative LDR voltage output (V_o) collected during whole muscle infusion treatment (A). The change in muscle color that occurs during infusion (removal of myoglobin)

permitted increased transmission of LED light (535nm) through the tissue, decreasing LDR resistance (A:inset). Decreased LDR resistance was measured and recorded as a change in output voltage (V_o). Prior to infusion, whole muscle tissue samples (B) were strongly reactive (D: left split) to antibodies/molecules directed against actin (red) myoglobin (green) and nuclei (blue). Following infusion treatment (C), recorded as the time to reach a stable output voltage minimum (A: arrow), actin, myoglobin and nuclei could not be detected in any of the samples tested (D: right split). Infusion prepared DSM samples retained the highly aligned structure of native muscle ECM (E) and were strongly immunoreactive to antibodies directed against collagen I and III (F & G). Unless noted, scale bar = 100um

Figure 4: Both infusion flow rate (ml/hr) and SDS concentration (%) had a significant effect on removal of intracellular myoglobin (A). Values shown are mean+sd. Increases in both flow rate and SDS concentration significantly reduced the time needed to remove myoglobin. * = $p < 0.05$; two factor ANOVA. The measured effects of flow (B) and concentration (C) were described using a linear model (see equation 2). Interaction effects between flow and concentration were not observed with the model or detected with ANOVA analysis.

Figure 5: Infusion treatment did not significantly decrease the collagen or sGAG concentration of DSM samples when compared to non-infused controls. Values shown are mean+sd. $p < 0.05$, two factor (flow and concentration) ANOVA.

Figure 6: H&E stained longitudinal (A) sections prepared from infusion DSM samples ($0^\circ =$

direction of muscle contraction). Representative infusion prepared DSM sample stress versus strain curve (B). When compared to controls, infusion treatment did not significantly influence (t-test $P>0.05$) DSM sample modulus, ultimate strength or alignment values (C). Values shown are mean+sd. Scale bar = 100um.

Figure 7: DSM material substrates supported the in-vitro attachment and proliferation (A and B) of viable (calcein AM) myoblast cells. The percent surface coverage (B) was evaluated at 3 and 7 days post cell seeding. Values shown are mean+sd. * $p<0.05$ compared to day 3, n=4/sample group, Scale bar = 100um

Figure 8: DSM implants were prepared for implantation using the infusion device to first remove intracellular debris followed by incubation in a DNase/RNase solution to remove nuclear debris and penicillin/streptomycin to reduce the risk of implant infection. DSM samples were rinsed in PBS (a total of five 24-hour PBS washes) to remove residual SDS, nuclease, and antibiotic solutions (A). Stained (H&E) tissue sections collected four (B) and twelve weeks (C), following subcutaneous implantation of infusion prepared DSM scaffolds into Sprague Dawley rats. Infusion prepared DSM scaffold fragments were observed within the dorsal subcutaneous implantation site at 4 weeks (*) but were degraded by 12 weeks (**) in all animals examined (n=3/time point). Scale bar = 100 μ m

Figures

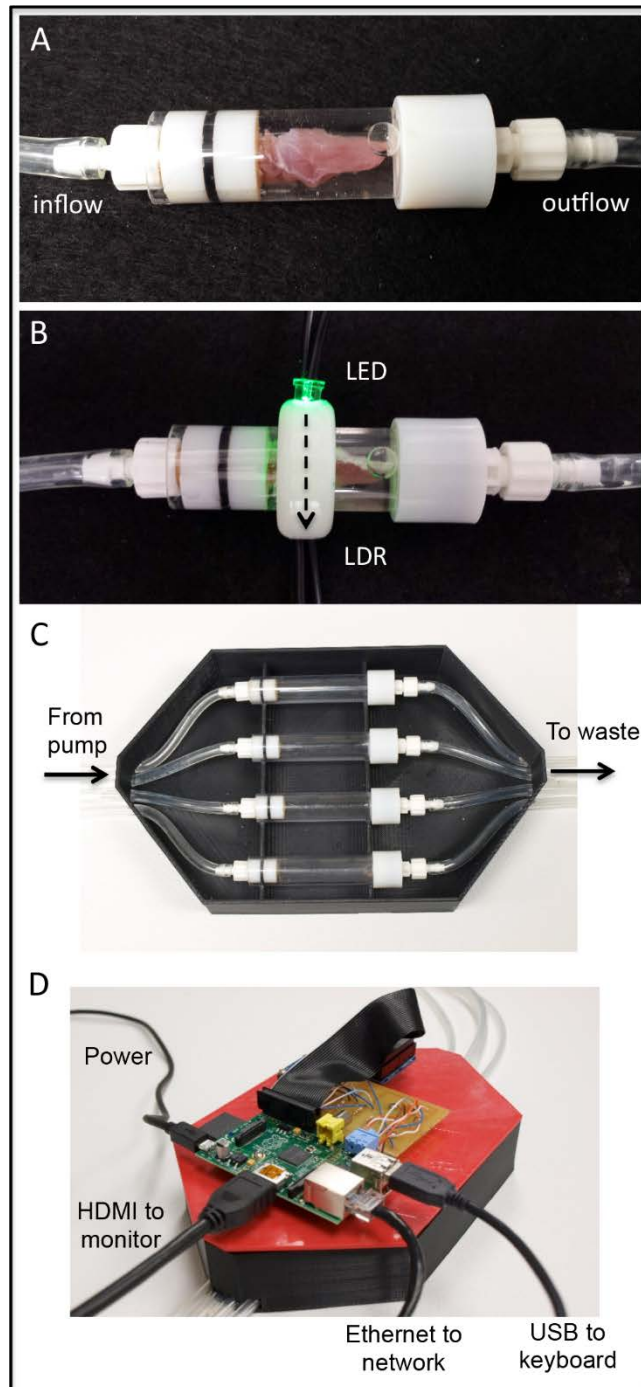


Figure 1

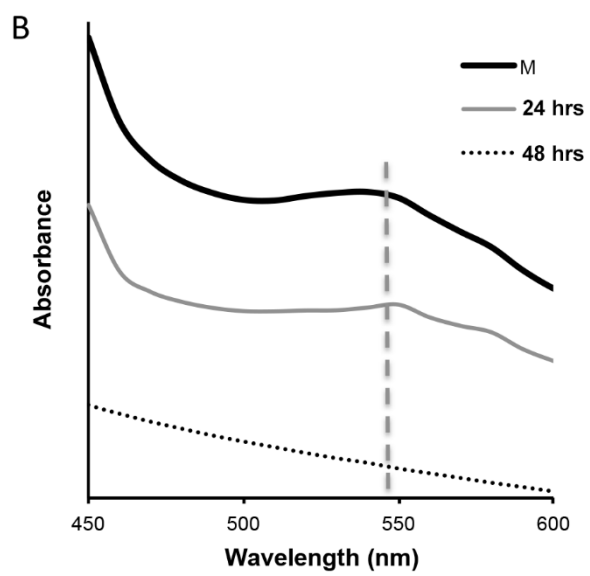
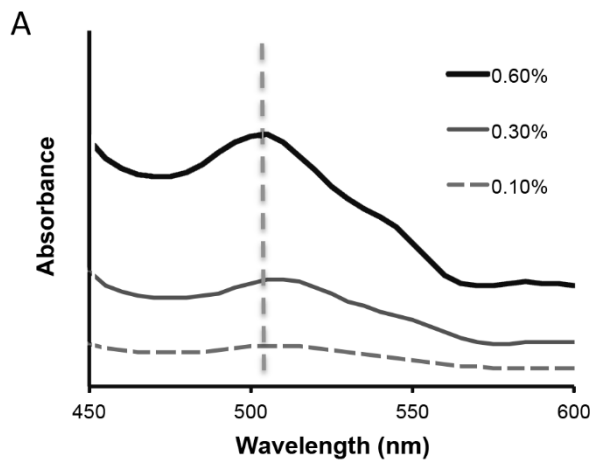


Figure 2

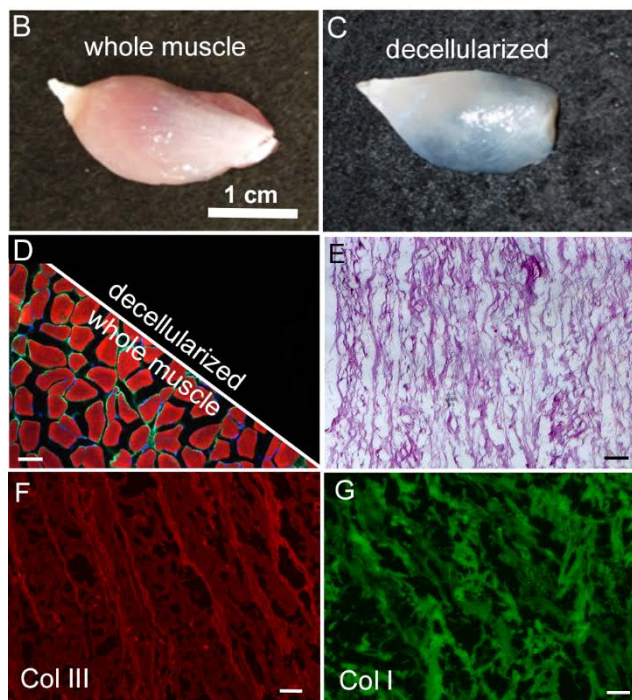
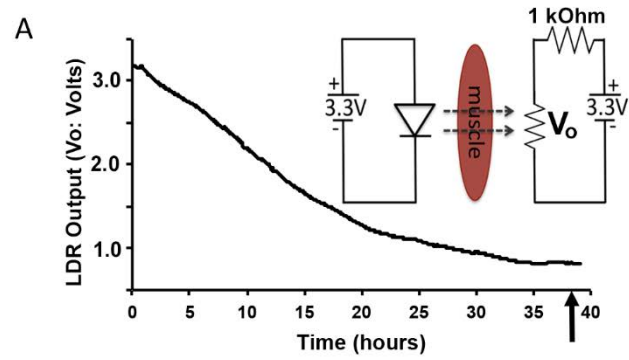


Figure 3

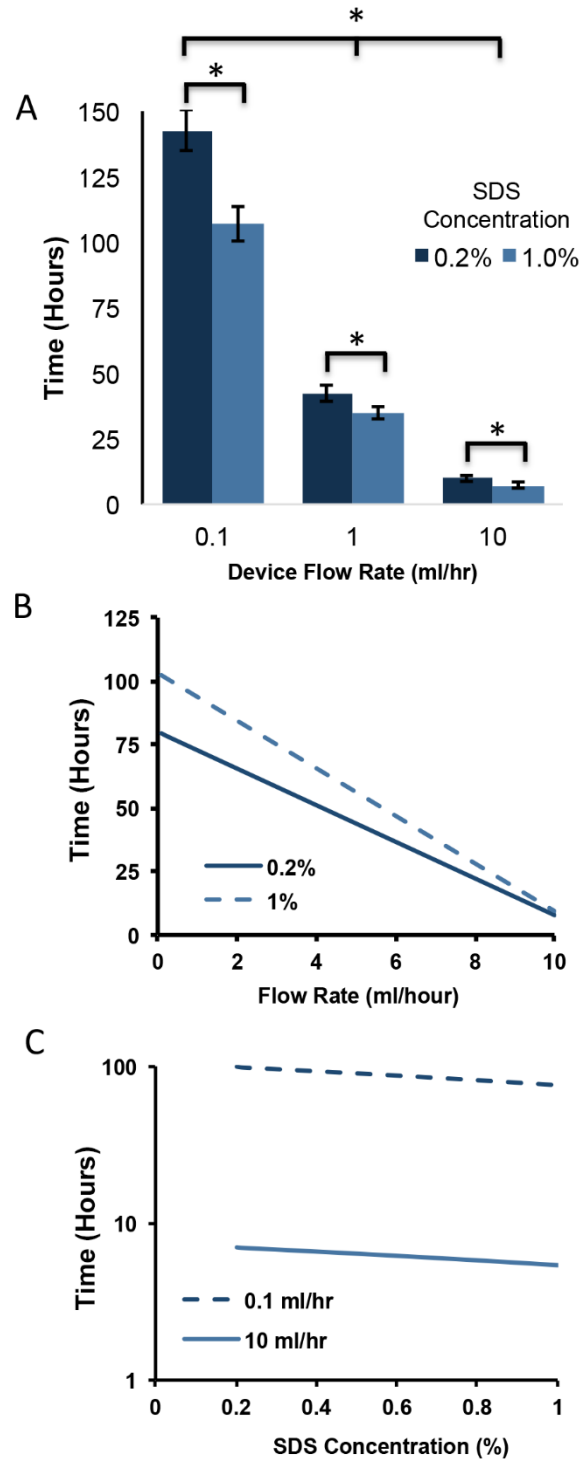


Figure 4

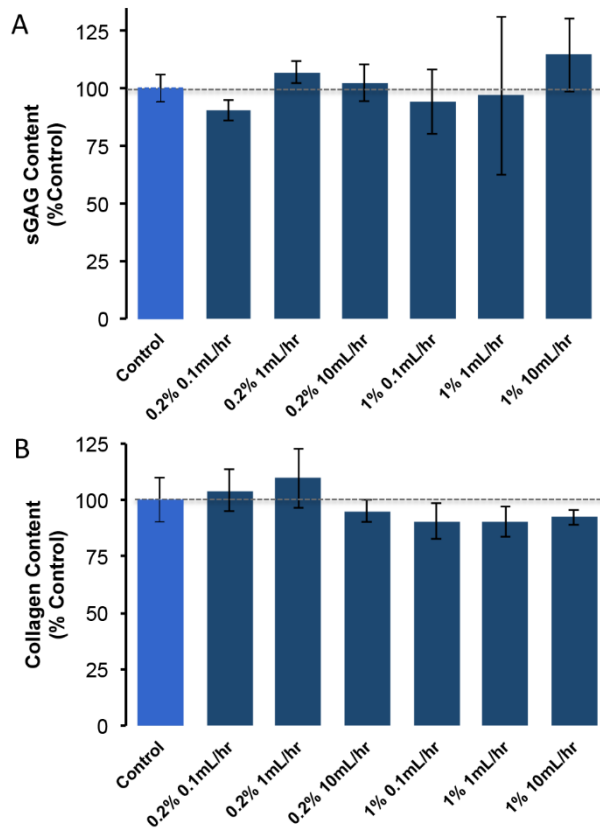


Figure 5

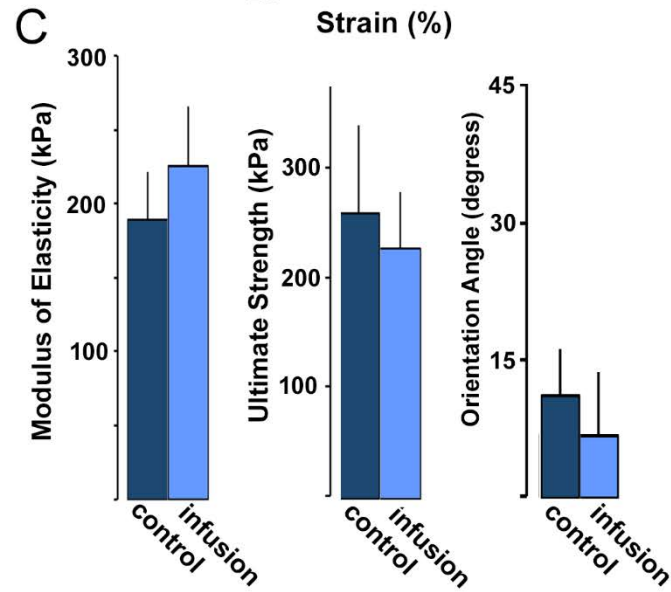
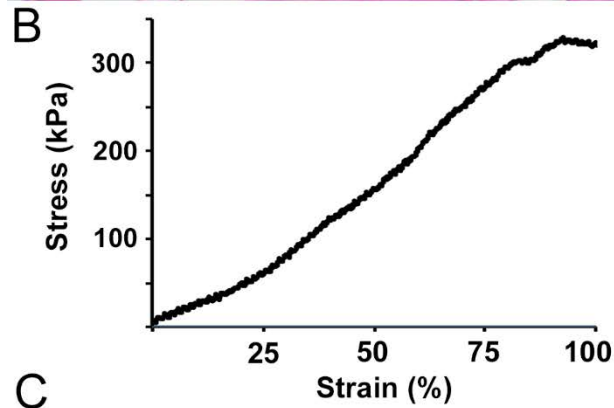
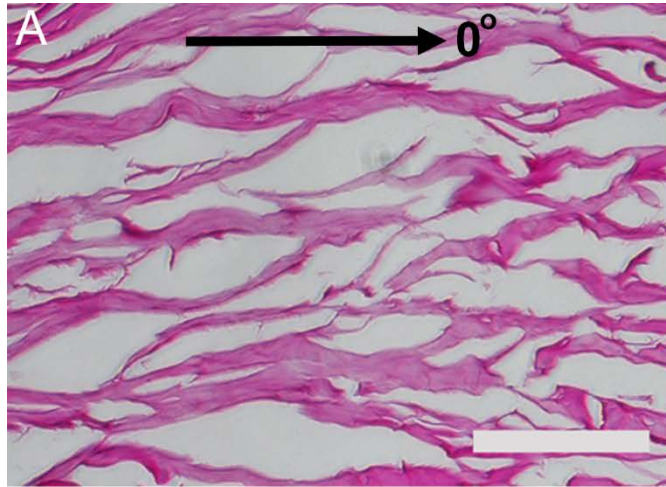


Figure 6

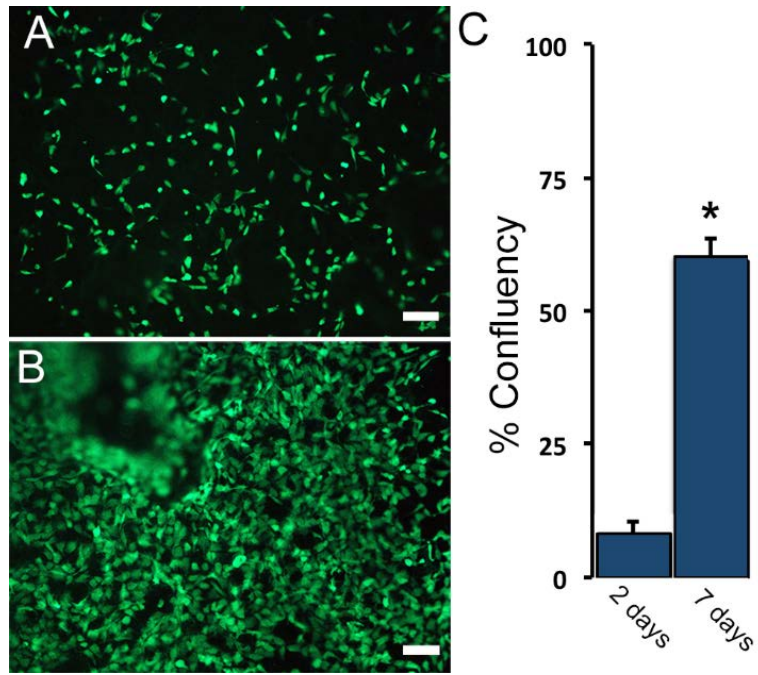


Figure 7

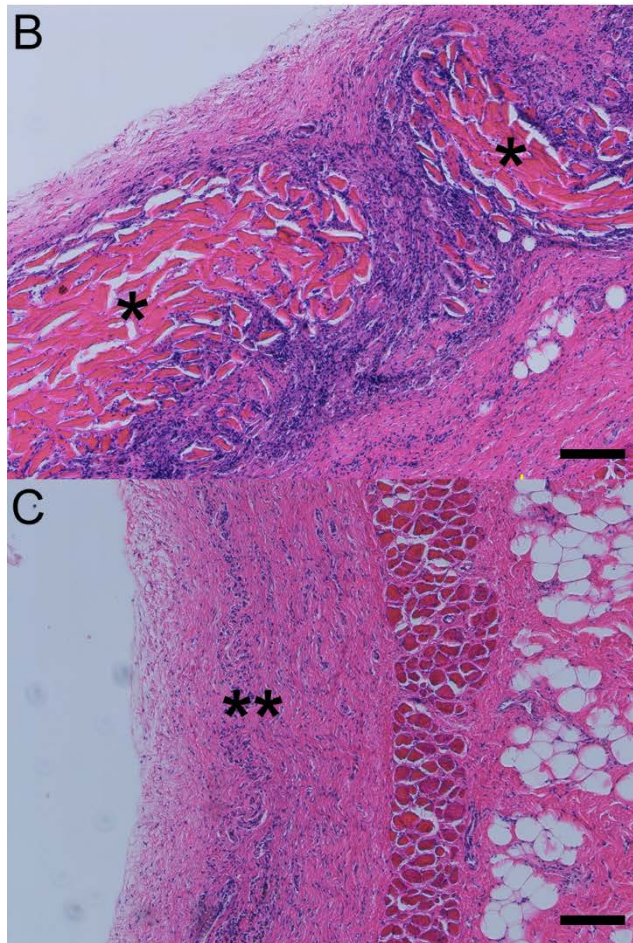
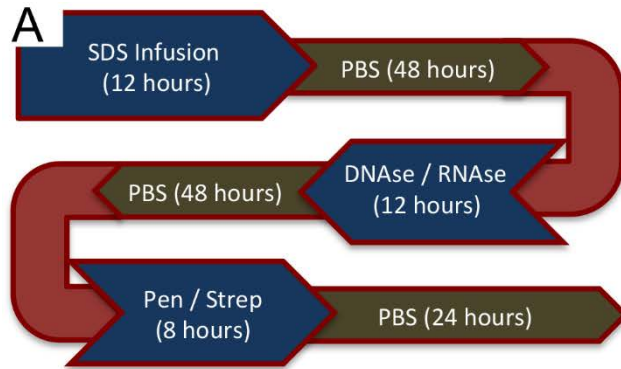


Figure 8

Chapter 3

Co-delivery of Infusion Decellularized Skeletal Muscle with Minced Muscle Autografts Improved Recovery from Volumetric Muscle Loss Injury in a Rat Model

Submitted as an original article by:

Ben Kasukonis¹, John Kim¹, Lemuel Brown², Jake Jones¹, Shahryar Ahmadi³, Tyrone Washington², and Jeffrey Wolchok¹

¹ Department of Biomedical Engineering, College of Engineering, University of Arkansas, Fayetteville, AR

² Department of Health, Human Performance, and Recreation, College of Education and Health Professions, University of Arkansas, Fayetteville, AR

³ Department of Orthopedics, University of Arkansas for Medical Sciences, Little Rock, AR

Corresponding Author:

Jeff Wolchok

125 Engineering Hall

Department of Biomedical Engineering

University of Arkansas

Fayetteville, AR 72701

jwolchok@uark.edu

479 575-2850

Abstract

Skeletal muscle is capable of robust self-repair following mild trauma, yet in cases of traumatic volumetric muscle loss (VML), where more than 20% of a muscle's mass is lost, this capacity is overwhelmed. Current autogenic whole muscle transfer techniques are imperfect, which has motivated the exploration of implantable scaffolding strategies. In this study, the use of an allogeneic decellularized skeletal muscle (DSM) scaffold with and without the addition of minced muscle (MM) autograft tissue was explored as a repair strategy using a lower-limb VLM injury model (n=8 / sample group). We found that the repair of VML injuries using DSM+MM scaffolds significantly increased recovery of peak contractile force ($81\pm 3\%$ of normal contralateral muscle) when compared to unrepaired VML controls ($62\pm 4\%$). Similar significant improvements were measured for restoration of muscle mass ($88\pm 3\%$) in response to DSM+MM repair when compared to unrepaired VML controls ($79\pm 3\%$). Histological findings revealed a marked decrease in collagen dense repair tissue formation both at and away from the implant site for DSM+MM repaired muscles. The addition of MM to DSM significantly increased MyoD expression, when compared to isolated DSM treatment (21 fold increase) and unrepaired VML (37 fold) controls. These findings support the further exploration of both DSM and MM as promising strategies for the repair of VML injury.

Keywords: extracellular matrix; scaffold; regenerative medicine; orthopedics; musculoskeletal

A. Introduction

Our group is exploring the development of strategies designed to treat volumetric muscle loss (VML) injuries. The substantial loss (>20%) of skeletal muscle tissue, either through trauma or surgical resection, appears to overwhelm the normal wound healing mechanisms that function effectively following minor muscle injuries (Terada, Takayama et al. 2001). It is generally recognized that to properly restore muscle function following VML injury, surgical intervention is required. Unfortunately, there are limited surgical options available to treat these clinically challenging VML injuries. The currently accepted surgical approach for the replacement of lost skeletal muscle is autologous muscle flap transfer (Vekris, Beris et al. 2008, Oishi and Ezaki 2010, Terzis and Kostopoulos 2010). Although frequently successful, muscle flap transfer is a highly invasive procedure that introduces significant donor site morbidity and is therefore only rarely indicated. The search for a less invasive VML repair strategy warrants research investment. Towards this end, several groups, including ours, are exploring the development of engineered extracellular matrix (ECM) scaffolds targeting VML repair (Bian and Bursac 2009, Chiron, Tomczak et al. 2012, Juhas, Engelmayr et al. 2014, Hurd, Bhatti et al. 2015, Wilson, Terlouw et al. 2016).

ECM scaffolds prepared from a variety of tissue sources have been utilized to repair a wide range of damaged tissues in animal models (Merritt, Cannon et al. 2010, Perniconi, Costa et al. 2011, Wolf, Daly et al. 2012, Corona, Ward et al. 2014) and recently in humans (Mase, Hsu et al. 2010, Sicari, Rubin et al. 2014). Within this class of tissue-derived ECM scaffolds, the application of decellularized skeletal muscle (DSM) as a repair strategy for VML injury has shown some promise (Merritt, Cannon et al. 2010, Wolf, Daly et al. 2012). The multi-molecular composition and highly aligned network architecture of DSM scaffolds are ideally suited for the

restoration of physical and chemical cues that are lost following VML injury. To improve the preparation of DSM scaffolds, our group has recently reported on a novel infusion method, which can accelerate the decellularization process, without compromising the physical, chemical, and biocompatibility properties (Kasukonis, Kim et al. 2016). Our goal is to explore the utility of these infusion prepared DSM scaffolds for the repair of VML injuries. Yet, the implantation of DSM scaffolds alone, particularly when explored in the lower extremity, appear to offer an incomplete intervention for the repair of VML injuries (Aurora, Roe et al. 2015), suggesting that other elements may be needed.

Evidence suggests that restoration of a robust pro-myogenic environment may require a multifactorial approach, which includes combining ECM scaffolds with the appropriate progenitor cells. In animal studies, the co-delivery of muscle progenitor cells in combination with ECM scaffolds has been shown to improve functional recovery following VML injury when compared to ECM scaffold delivery alone (Merritt, Cannon et al. 2010, Corona, Ward et al. 2014). The premise is that progenitor cells reestablish a needed pool of myogenic cells, which utilize the ECM implant as a substrate upon which to initiate regeneration of contractile myofibers. Cellular co-delivery has yielded promising VML regenerative results, but does introduce increased clinical complexity, as it would require surgical collection and expansion of the patient's progenitor cells prior to implantation. Our group is interested in exploring alternatives to *in-vitro* progenitor cell expansion and cultivation, with the aim of creating a single stage VML repair strategy. An attractive source of muscle progenitor cells is the collection and implantation of minced muscle (MM) autografts. MM contains several components, most notably satellite cells, necessary for the regeneration of skeletal muscle and has been shown to successfully regenerate damaged muscle tissue when examined in animal models of VML injury

(Corona, Garg et al. 2013, Ward, Ji et al. 2015). Of particular interest to our group, MM autografts can be harvested from normal muscle tissue and seeded back into the injury site during a single stage surgical procedure.

An anticipated roadblock to the clinical translation of MM autografts is the large volume of healthy muscle tissue that would be needed for grafting into a VML defect. At present the implantation of MM in quantities prepared using less than 50% of the VML defect mass has not been effective at restoring muscle function (Ward, Ji et al. 2015). While potentially less invasive than a full muscle flap transfer, the harvest of muscle tissue in volumes required to fill half the VML defect would still introduce significant donor site morbidity. Therefore, a repair strategy that reduces the amount of MM needed to stimulate functional muscle recovery would improve the clinical utility of MM autografts. Towards this end, our team is interested in exploring the co-delivery of MM autografts with infusion prepared DSM scaffolds as a VML repair strategy. We suspect that the use of DSM material as a carrier material could reduce the amount of MM autograft needed to stimulate recovery following VML injury. Specifically, the study was designed to test the hypothesis that delivery of a DSM scaffold carrier combined with a MM autograft prepared using 25% of the defect mass (1/2 the current threshold for recovery) will significantly improve functional muscle recovery (increased contractile force) and myogenesis (increased MyoD expression) following hind limb VML injury in a small animal model.

B. Methods

DSM Scaffold Preparation

To prepare DSM samples for implantation, whole tibialis anterior (TA) muscle was infusion decellularized using the previously reported (Kasukonis, Kim et al. 2016) infusion system (**Figure 1**). TA muscles were harvested from rats that had been euthanized at the completion of an unrelated study. Briefly, the wide mid-belly region of the TA muscle was positioned onto the infusion needle (27 gauge) and enclosed within a single decellularization chamber. Four TA muscles were prepared in parallel during each run. The TA samples were infused overnight (approximately 12 hours) with 1% SDS at a flow rate of 5mL/hr. Following infusion treatment, samples were incubated overnight in a DNase solution (1kU/ml DNase in a 10mM Tris-HCL buffer; 2.5mM MgCL₂ + 0.5mM CaCl₂) and then incubated (8 hours) in a 1X penicillin/streptomycin solution to reduce the risk of infection. Samples were rinsed thoroughly (a total of six 24 hour wash steps) in PBS between each preparation step. Following completion of the entire decellularization protocol, the DNA concentration of representative DSM implants (n=4) was measured with the aid of a commercial quantification kit (Qubit, Fisher Scientific). DSM implants were lyophilized and stored at -20C until utilized for implantation.

Animal Implantation

Fischer 344 rats (Harlan, Indianapolis, IN), weighing approximately 300-325g were used as the animal model for all implantation studies. Surgical procedures and DSM implant preparation methods were performed in accordance with protocols approved by the University of Arkansas IACUC (protocol #14044) and guided by published methods (Wu, Corona et al. 2012, Kim, Kasukonis et al. 2016). Anesthesia was induced using isoflurane (1-3%) in oxygen. The

implant site was surgically exposed through a 1-2 cm incision running parallel to the tibia. The TA was identified and a partial thickness VML defect (8 mm diameter x 3 mm deep) was created using a sterile biopsy punch (**Figure 2**). The muscle tissue removed from the defect site was weighed and the weight was adjusted (increased only) if needed to ensure consistent defect mass across all animals (Average defect weight = 93.4 mg). Muscle defect mass values (20% of TA mass) were based on pilot study TA muscle mass measurements (average TA mass = 470±17 mg). Muscle defect plugs were retained for use as MM autografts. Animals were randomly assigned to one of three treatment groups (n=8 animals / treatment groups)

Group 1: Unrepaired VML defect

Group 2: VML defect repaired with an isolated DSM scaffold

Group 3: VML defect repaired with a DSM scaffold supplemented with MM autograft tissue (25% of the VML defect mass)

A single infusion-prepared DSM scaffold was cut to size (average DSM mass = 4.9±0.7 mg) using surgical scissors and implanted into freshly prepared VML defects (Group 2). For animals in the DSM+MM experimental group (Group 3), 25% of the defect muscle plug was hand minced into a loose paste using a scalpel and scissors until MM fragments larger than ~1mm³ could not be visually detected. The white DSM scaffolds were manually rolled in the pink MM autograft paste until all surfaces were visibly coated. DSM+MM constructs were implanted into the VML defect. Care was taken to ensure that DSM implant network alignment was matched to TA alignment. Unrepaired VML defects (group 1) served as negative controls (n=8/ experimental group). The contralateral limb was left untreated to serve as an internal

comparative control. To remain consistent with previous MM repair techniques, the DSM scaffolds were sized to fill, but were not sutured to the surrounding muscle tissue. The deeper **fascia** and surface skin layers were separately closed using an interrupted stitch with a 5-0 absorbable suture (Vicryl, Ethicon, Summerville, MA). A single surgeon (BK) performed all implantation procedures including the preparation of MM autografts. Postoperative analgesia consisted of 0.1mg/kg buprenorphine administered subcutaneously via injection twice daily for two days. Animals also had access to the anti-inflammatory medication (Carprofen) via a single dietary gel cup (Medigel CPF, ClearH₂O, Westbrook, ME) added to each cage following surgery. Animal consumption of the gel was voluntary and any uneaten gel was removed from the cage at 1-week post surgery. Following surgery, animals were housed in standard-sized rat cages with unrestricted movement. The animals were allowed to bear weight on the operative extremity as tolerated. All animals were housed for a 12-week recovery period.

Contractile Force Measurement

At the completion of the 12 week recovery period, the peak tetanic contractile force was measured in situ as described in Corona et al (Corona, Garg et al. 2013). Animals were anesthetized and the lower limb was stabilized at 90° of knee flexion (tibia parallel to the benchtop) using a custom made alignment jig (**Supplemental Figure 1**). The ankle was flexed to 90° and the foot was secured (surgical tape) to the lever arm of a dual-mode muscle lever systems (Aurora Scientific, Ontario, Canada,). To isolate the contribution of the TA during force measurement, distal tenotomies were performed on the extensor digitorum longus (EDL) and extensor hallucis longus (EHL). TA peak isometric tetanic force was measured by stimulating the peroneal nerve with the aid of a physiological stimulator (Grass; S88). Optimal voltage (2 – 5

V) was determined using a series of tetanic contractions (150Hz, 0.1 ms pulse width, 400 ms train). Average peak tetanic force for each animal was calculated from an average of 5 contractions. All contractions were separated by one minute of rest. Raw peak tetanic contractile force (N) was recorded from both the treated and contralateral control limb of each animal and normalized to animal weight (N/kg). The weight normalized force data (N/kg) is reported in the results section. At the conclusion of electrophysiological testing, all animals were euthanized through carbon dioxide inhalation in accordance with guidelines provided by the 2013 AVMA Panel on Euthanasia of Animals.

Tissue Histology

Unrepaired and repaired TA muscles along with contralateral untreated TA muscles were harvested and trimmed to remove the periosteum and tendon. EDL muscles were also collected and weighed for comparison between treated and contralateral control limbs. Muscles were rinsed in sterile PBS, dabbed dry, and then weighed. Muscles were then immediately flash frozen in liquid nitrogen cooled isopentane. Frozen TA tissue samples (n=4/experimental group) were sectioned (7 μ m) transversely through the mid-portion of the defect site with the aid of a cryostat. Sections were mounted onto microscopic slides and immuno-stained for the presence of myosin heavy chain (α MHC, 1:40, Iowa Hybridoma Bank), a muscle specific protein marker, collagen type I (α ColI, 1:750, Sigma), collagen type III (α ColIII, 1:000, Abcam) or laminin 1 (α Ln, 500:1, Sigma) followed by incubation in the appropriate fluorescently labeled secondary antibodies (Alexfluor, 500:1, Life Technologies). Additional tissue sections were stained using a commercial Masson's Trichrome kit following manufacturers guidelines (Sigma). All sections were mounted onto microscope slides and digitally imaged. Treated sections were evaluated for

myofiber formation and organization as well as the formation and extent of repair tissue formation for comparison to untreated contralateral muscle tissue sections.

Measures of collagen type I accumulation, a potential indicator of diffuse muscle fibrosis, in tissue regions away from the VML defect area were estimated from collagen I immunoreactivity and guided by published methods (Bedair, Liu et al. 2007). Tissue immunoreactivity to collagen I was calculated from fluorescent microscopic images (200X) using image analysis software (Image J). A total of three non-consecutive tissue sections collected from three representative animals (n=3/treatment group) were used for all calculations. From each section, three images were obtained from the posterior half of the TA muscle at regions located distant to (> 3 mm) the anterior defect/repair site. A total of nine images were analyzed for each animal. All images were converted to 8-bit, grey scale, and uniformly thresholded across all samples to isolate collagen type I positive tissue regions. From these images the percent collagen type I positive tissue area was calculated for all treatment and control sections.

MyoD and ECM Gene Expression

Real-time PCR was performed using the protocol described in Washington et al. (Washington, Brown et al. 2013) Tissue samples (approximately 30mg) collected from the defect/repair site (n=4/sample group) were homogenized with Trizol (Ambion, Carlsbad, CA), chloroform (Sigma Aldrich, St. Louis, MO), and treated with DNase (Invitrogen, Carlsbad, CA). RNA was extracted using the RNeasy kit (Invitrogen, Carlsbad, CA). RNA concentration and purity was determined by UV spectrophotometry. RNA with a 260-to-280-nm ratio ≥ 1.8 was used for subsequent analysis. cDNA was reverse transcribed from 1 μ g of total RNA using the

Superscript Vilo cDNA synthesis kit (Life Technologies, Carlsbad, CA, USA). cDNA was amplified in a 25 μ L reaction containing appropriate primer pairs and TaqMan Universal Mastermix (Applied Biosystems, Grand Island, NY). Commercially available TAQMAN primers (Invitrogen, Carlsbad, CA) for MyoD, Timp-1, Collagen I, Collagen III, TGF- β 1, MMP2, and 18s ribosomal housekeeping were used to quantify the expression of desired matrix and matrix regulatory genes. Samples were incubated at 95°C for 4 minutes, followed by 40 cycles of denaturation, annealing, and elongation at 95°C, 55°C, and 72°C, respectively. TaqMan fluorescence was measured at the end of the extension step each cycle. Experimental group samples were normalized to 18s and then referenced to the contralateral normal limb. Gene expression levels are reported as fold change using the $2^{-(\Delta \Delta Ct)}$ method.

Data Analysis

Based on an *a priori* power analysis, the implantation of 8 animals per group was determined to be sufficient to detect a 15% increase in contractile force between treatment and control animals. This level of detection was designed to detect physiologically relevant and functionally meaningful increases in muscle contractile force. Pilot testing mean and standard deviation contractile force values (2.10 ± 0.15 N/kg) collected from intact TA muscle samples were used. All data **are** represented by the mean and standard error unless noted. Data were tested for normality using the Shapiro-Wilk Test. Comparisons between treatment groups (VML, DSM, and DSM+MM) for each of the outcome measures (peak force, muscle mass, collagen I % area, and gene expression) were evaluated with a one-way ANOVA using a commercial statistical software package (JMP). Post hoc comparisons were made using Tukey's test. A standard 0.05 level of significance was used for all statistical tests.

C. Results

Average DSM sample DNA content (1.0 ± 0.1 ng of DNA / mg of tissue) was well below the preferred implantation threshold (< 50 - 70 ng/mg) reported by others (Zhang, He et al. 2009, Crapo, Gilbert et al. 2011). Isolated DSM implantation took approximately 30 minutes to complete. The addition of MM preparation and coating steps added approximately 10 minutes to the procedure. Both DSM and DSM+MM treatment groups tolerated the implantation surgery well. All animals gained weight throughout the observation period at a rate (8.3 ± 0.5 and 8.5 ± 0.3 grams/week) that was not significantly different from un-repaired VML defect animals (8.8 ± 0.6 grams/week). There were no signs of post-surgical infection. At one week post-implantation, all animals were fully ambulatory with no noticeable gait differences between groups. Carprofen dietary gel cups were typically consumed within the first 3 days of surgery (effective dosage 5 mg/kg/day). All animals reached the 12-week study end point without complications.

After the 12-week recovery period, bilateral measurements of the isometric TA muscle tetanic contractile force were obtained. Tetanic contraction plots for all muscles were characterized by a sharp rise in force, followed by a plateau at the peak force, and then a return to a no force resting state (**Figure 3**). The average peak tetanic force produced by normal contralateral TA muscles was 2.0 ± 0.1 N/kg when normalized to animal mass. Following VML injury without repair, the average peak tetanic force dropped to 1.4 ± 0.1 N/kg, which is equivalent to $62 \pm 3\%$ of normal contralateral TA muscles values, a statistically significant reduction ($p < 0.05$). Following repair with isolated DSM, TA muscles produced an average contractile force of 1.5 ± 0.1 N/kg, which represents a 17% recovery of the peak force when compared to the unrepaired VML muscle group. Although elevated, the peak force recovery following isolated DSM repair was not statistically significant when compared to the unrepaired

VML group. In response to repair with combined DSM+MM, the average peak tetanic force increased to $1.7\pm 0.2\text{N/kg}$, which represents a 50% recovery in force production when compared to unrepaired VML values. The recovery of peak tetanic force following DSM+MM repair was statistically significant when compared to the unrepaired VML group ($p<0.05$).

For all muscles harvested there was no evidence of implant site infection or gross deformity at the treatment site following 12 weeks of recovery. Generally, each of the treatment group muscles appeared smaller than contralateral normal muscle and the defect site could often be identified grossly (**Figure 4**). The muscles repaired with DSM and DSM+MM appeared to have less fibrosis at the treatment site and less atrophy overall when compared to the unrepaired muscles, but still had a less organized surface morphology at the treatment site when compared to the ordered striations of normal muscle. Untreated VML sample animals had a body weight normalized average TA mass of $1.27\pm 0.1\text{ g/kg}$, which is $79\pm 3\%$ of the contralateral normal TA mass. TA muscle defects repaired with isolated DSM had an average normalized mass of $1.33\pm 0.1\text{g/kg}$, which is $82\pm 3\%$ of contralateral normal muscle mass and represents a 14% recovery in muscle mass when compared to the unrepaired VML group. The group of TA muscles repaired with combined DSM+MM had an average mass of $1.40\pm 0.1\text{g/kg}$, which is equivalent to $88\pm 3\%$ of contralateral normal values. DSM+MM muscle mass was significantly increased when compared to the unrepaired VML treatment group ($p<0.05$), but not significantly greater than the isolated DSM repair group. On average, DSM+MM treated muscles recovered 43% of the muscle mass lost following VML injury (79% vs. 88% of normal). Of note, EDL muscles collected from the treated limb were on average larger than contralateral EDL muscles for each treatment group (VML, DSM, and DSM+MM), suggesting compensatory hypertrophy.

At 12 weeks post surgery, the defect sites were detectable in histological sections prepared from all treatment groups. Transverse histological images of the defect sites for all treatment groups were characterized by the accumulation of repair tissue at the muscle surface (**Figure 5**). Unrepaired VML and isolated DSM repair defect site tissues were strongly immunoreactive to collagen type I, suggesting collagen-enriched connective tissue deposition (fibrosis) at the defect/repair site. Additional ECM proteins, including fibronectin, collagen type III, and laminin were each detected within the repair tissue (**Figure 6**). While the general composition of the repair tissue layer was similar across all treatment groups, the size/thickness of the layer was notably different between groups. Specifically, it was generally noted that the repair tissue layer observed in DSM+MM treated samples layer was distinctly thinner than both unrepaired VML and isolated DSM repair groups. The repair layer was often difficult to locate in many tissue sections. For all treatment groups, MHC positive muscle fibers were present up to the border of the repair layer, but were not observed within the layer itself. For all groups, the collagen dense repair layer was notably thinner (50-500um) than the original VML defect (3mm), suggesting atrophy of the transected muscle tissue proximal and distal to the defect site.

The Masson's trichrome staining revealed signs of increased collagen deposition (blue staining) around muscle fibers in tissue regions that extended beyond the defect site for both unrepaired VML and isolated DSM repaired tissue sections. Similar qualitative increases in collagen staining were not observed in DSM+MM Masson's stained tissue sections. Subsequent quantitative analysis of collagen type I immunoreactivity supported the Masson's Trichrome observations. When measured using tissue sections prepared from normal contralateral skeletal muscle samples, collagen I positive immunostaining regions occupied, on average, $6.2 \pm 1.3\%$ of the total tissue section area (**Figure 7**). For sections prepared from unrepaired VML and isolated

DSM repaired samples the percent surface area increased to $6.5\pm 0.8\%$, and $8.6\pm 0.5\%$, of the total surface area respectively. The elevated collagen type I area values detected following isolated DSM repair represents a 33% increase over normal tissue values. Alternatively, DSM+MM repair group collagen I percent area ($5.4\pm 0.7\%$) was below all other groups including normal muscle. On average, DSM+MM treated collagen I percent area values were 12% and 37% below VML and isolated DSM repair values respectively. The difference between DSM+MM and isolated DSM values was statistically significant.

Six key genes associated with ECM structural proteins (collagen I and III), ECM regulatory cytokines (TGF- β 1, MMP2, and TIMP-1) and myogenesis (MyoD) were examined with the aid of rt-PCR. (**Figure 8**). Muscle tissue samples collected from both unrepaired VML defect sites and isolated DSM repair sites produced approximately one tenth the relative expression of MyoD when compared to normal contralateral TA muscle, with fold changes of 0.08 ± 0.04 and 0.14 ± 0.06 respectively. Alternatively, the DSM+MM repaired muscle group produced a statistically significant increase ($p<0.05$) in the expression of MyoD with a fold change of 2.95 ± 0.47 when compared to normal TA muscle samples. Analysis of tissue collected from both the VML and isolated DSM repair groups revealed modestly increased structural and regulatory ECM gene expression values when compared to normal tissue controls. Collagen type I expression levels measured from unrepaired VML, and isolated DSM, muscle samples were 1.55 ± 0.14 and 2.60 ± 0.89 of normal muscle respectively. The expression pattern for each of the ECM regulatory genes followed a similar trend; MMP2, TGF- β , and TIMP-1 expression was typically doubled within VML and Isolated DSM repair tissue samples. Expression levels for each of the structural and regulatory ECM genes were markedly increased in response to combined DSM+MM repair. The expression level for DSM+MM repaired samples exceeded

both the VML and isolated DSM treatment groups by statistically significant margins for each of the genes examined ($p < 0.05$) and were generally an order or magnitude greater than normal contralateral TA tissue expression values.

The gene expression ratios for each of the five ECM genes to the MyoD gene (e.g. Col I:MyoD) were calculated across all treatment groups for comparison to normal muscle (**Figure 9**). Generally, normal muscle samples produced ECM to MyoD expression ratios that clustered around a value of 13 and ranged from a low of 10 ± 5 (Col1/MyoD) to a high of 16 ± 8 (Col3/MyoD). Unrepaired VML and isolated DSM repair gene expression ratios were all significantly elevated (3 to 4 fold) in comparison to normal muscle values, and clustered between values of 30 and 50. Alternatively, DSM+MM gene expression values were generally lower than normal muscle values ranging from a low of 4 ± 2 (TGFB1;MyoD) to a high of 11 ± 5 (Col1/MyoD). DSM+MM gene expression ratios calculated for Col I and Col III to MyoD were closely matched to normal muscle values and represented the only ratio values across all treatment groups that were not significantly different from normal muscle. The main outcome measures for each of the treatment groups are summarized in **Table 1**.

D. Discussion

The key findings from this study suggest that the use of an acellular DSM scaffold improved functional recovery from a VML injury and the addition of a MM paste further enhanced regeneration. Specifically, the combination of a DSM scaffold with MM paste restored approximately half the contractile force that was lost to VML injury, a finding that was consistent with the measured increases in TA muscle weight following DSM+MM repair.

Secondary findings suggest that the presence of the MM increases myogenesis, indirectly assessed through MyoD expression analysis, and decreased the accumulation of collagen enriched repair tissue at the site of the defect. When taken together the electrophysiological, histological, and gene expression data provided evidence suggesting that the addition of MM to a DSM graft can be utilized to improve muscle regeneration following VML injury.

The infusion bioreactor utilized in this project is a new approach developed by our lab to accelerate muscle tissue decellularization. Although perfusion decellularization has been performed on the entire forelimb of a rat (Jank, Xiong et al. 2015) and whole organs, such as the liver (Uygun, Soto-Gutierrez et al. 2010), heart (Ott, Matthiesen et al. 2008), kidneys (Sullivan, Mirmalek-Sani et al. 2012), and lungs (Ott, Clippinger et al. 2010), muscle tissue lacks the easily accessible vasculature needed for perfusion, motivating a different approach whereby decellularization solution was infused into the bulk tissue via a needle. In our recently published work, it was demonstrated that DSM scaffolds produced through infusion decellularization retain the composition, mechanics, and architecture of native muscle ECM. The major advantage of our infusion device is that it produces a decellularized scaffold in under 10 hours compared to standard diffusion based (incubation with agitation) methods that can take up to two weeks for a similarly sized muscle (Merritt, Cannon et al. 2010). Moving forward, a single needle system could be scaled up to create a multi-needle infusion device capable of decellularizing bulkier muscle samples needed for large animal models or eventually human tissue for clinical studies. Furthermore, while we currently don't use the infusion process during the DNase and rinse steps, we could certainly anticipate utilizing the system to accelerate all process steps. Ultimately, we believe the infusion prepared DSM scaffolds are an appropriate material from which to explore VML repair strategies.

The MM co-delivery with DSM was initially motivated by findings reported by Corona et al (Corona, Garg et al. 2013). The harvest of MM autografts in a clinical setting makes it an intriguing source of implantable satellite cells for co-delivery with DSM. Rather than utilizing satellite cells which are first harvested, purified, expanded, and then ultimately implanted using a two stage surgical strategy, MM can be acquired and delivered along with allogeneic DSM in a single stage procedure. While a single procedure strategy may simplify surgical planning, we clearly recognize that the MM volume (25% of the defect mass) utilized in this study, although far less than the full defect size, would still produce harvest challenges and donor site morbidity concerns. To minimize morbidity, it may be possible to collect subcritical muscle biopsies from contralateral muscle sources. Ultimately, the use of a MM grafting may have the greatest utility for the repair of smaller muscles like those of the face (Cardenas-Mejia, Covarrubias-Ramirez et al. 2015) and hands (Lin, Zhu et al. 2012) where a therapeutic volume of MM muscle could be harvested from the larger muscle of the lower limbs in a manner consistent with the harvest or the middle third of the patellar tendon during anterior cruciate ligament reconstruction (McGuire and Wolchok 1997).

The encouraging signs of functional regeneration that were observed in response to minced muscle implantation hint at additional cellular implantation factors that may enhance myogenesis within DSM implants. Specifically, the use of minced muscle may do more to enhance muscle regeneration than simply increase the available pool of satellite cells at the injury site. Following muscle sprains and strains, the presence of injured myocytes within the wound site provides pro-regenerative cues. Specifically, it is understood that signaling cascades initiated in response to myofiber injury activate inflammatory and myogenic cells that stimulate the muscle repair process during the essential early phases of regeneration (McClung, Davis et

al. 2007). Inclusion of the signaling cues initiated by myofibers injury may provide opportunities for novel repair strategies. These cues could be provided directly through seeding of DSM scaffolds with myofibers (minced muscle) as was examined in this study, or alternatively by identifying the key chemical signals produced in response to myofiber injury and engineering them into a biomimetic repair strategy.

The selection of a MM graft prepared using 25% of the VML defect mass was motivated by Corona's recent work showing that MM seeded in a collagen hydrogel did not effectively repair VML injury when the mass of MM was prepared using less than 50% of the tissue collected from the muscle defect (Ward, Ji et al. 2015). Others have utilized the entire defect to produce significant regenerative results (Corona, Garg et al. 2013). By exploring the use of a 25% volume MM graft, the low end of what has been explored by others thus far, we hoped to determine whether DSM scaffolds could improve the muscle regenerative performance of MM autografts beyond that which has been achieved to date. The lack of an isolated MM implantation controls group was a regrettable shortcoming to this study. It would have been valuable to know the contribution of the MM graft, and help elucidate whether the improved functional recovery measured following combined DSM+MM delivery was simply additive or whether there were interaction effects that enhanced regenerative performance when combined. Yet, while the effect of isolated MM was not evaluated in this study, what is clear, is two strategies that showed modest effectiveness when used separately (isolated DSM or <50% MM grafting) stimulated significant functional muscle recovery when used in combination, suggesting to us that infusion prepared DSM material is a MM carrier scaffold worthy of continued investigation.

Towards this end, an improved understanding of the interactions between the MM paste and DSM scaffold is warranted. In particular, it would be of interest to know whether the DSM scaffolds are serving as simply a carrier material for the delivery of satellite cells, or whether the scaffold creates a pro-myogenic environment that enhances satellite cell expansion. DSM+MM interactions could be explored over the short term using in-vitro models, or in-vivo utilizing earlier time points. The longer 12-week time point used in this study, while appropriate for the detection of force recovery, missed the key regenerative events that occur during early wound healing. Research suggests that a one-week time point may be more appropriate for the detection of regenerative satellite cell activity (Tian, Jiang et al. 2016).

The increased effectiveness of the DSM+MM scaffold when compared to the collagen hydrogel + MM examined by Corona could potentially be attributed to the architecture of the DSM scaffold. Scaffolds composed of decellularized skeletal muscle, including the infusion prepared scaffolds explored in this study, are unique because they retain the parallel alignment of the native muscle from which they were obtained (Hinds, Bian et al. 2011). We, as well as others, anticipate that scaffolds with muscle mimetic network alignment will improve muscle regeneration by providing the appropriate topographical cues during healing (Bian and Bursac 2009, Lam, Huang et al. 2009). In whole muscle, ECM surrounds and supports multinucleated myofibers which are highly aligned in the direction of muscle contraction. The individual fibers range from 5 to 100 um in diameter, and can be as long as several centimeters (Maier and Bornemann 1999). During implantation we were careful to orient the DSM scaffolds in the direction of TA contraction. In-vitro models indicate that muscle progenitor cells utilize alignment cues during myogenesis (Jana, Leung et al. 2014, Patel, Mukundan et al. 2016). Similar alignment-sensitive responses have been reported for other cells, including cardiac

muscle and tendons (English, Azeem et al. 2015, Morez, Nosedá et al. 2015). Yet, while the many in-vitro alignment studies support the motivation of aligned regenerative scaffolds, we recognize that in-vivo evidence indicating that scaffold alignment is critical to muscle implant success does not yet exist. The lack of in-vivo data supporting the importance of scaffold alignment in muscle regenerative therapies would appear to motivate future studies.

VML repair with DSM+MM dramatically increased gene expression for each of the structural and regulatory ECM genes explored in this study. However, the histological appearance of defect/repair site tissue for both VML and isolated DSM repair groups would suggest that ECM deposition and gene expression should be increased in these groups when compared to the DSM+MM group. We suspect that ECM gene expression levels for both VML and isolated DSM groups were elevated during earlier time points; an expression pattern that is consistent with muscle fibrosis (Davis, Korn et al. 2015). Once a stable fibrotic scar was formed, the genes returned to the lower expression values we measured at 12 weeks. It is also important to note that the collagen I immunoreactivity and PCR analysis were conducted on samples taken from different tissue regions. Collagen immunoreactivity was assessed within tissue regions located distant to the repair/defect site, while the tissue used for PCR analysis was collected from the repair site. As a result, the collagen immunoreactivity measures are likely an indicator of tissue wide ECM adaptation to differences in force generation and transmission between treatment groups (Hjorth, Norheim et al. 2015), while the PCR results are indicative of the regenerative and remodeling processes occurring at the site of repair.

The PCR data suggests that the addition of MM to DSM scaffolds prolongs myogenesis and ECM production at the repair site following VML injury repair. The increased expression of ECM related genes and MyoD at 12 weeks could be indicative of active remodeling and

adaptation at the defect site in response to muscle activity (Hyldahl, Nelson et al. 2015).

Alternatively, the prolonged upregulation of ECM genes at 12 weeks could be indicative of ongoing fibrosis (Mann, Perdiguero et al. 2011). To determine whether the expression patterns we observed at 12-weeks are beneficial or pathological, longer recovery time points may need to be explored to determine whether contractile recovery is maintained. Additionally, it may be of interest to explore gene expression profiles both within and away from the repair site to gain a better understanding of muscle wide responses to each repair scheme.

We explored the ratio of the relative gene expression for each of the ECM genes to MyoD in order to elucidate differences that may exist between normal muscle homeostasis and each of the treatment groups. The relationships between key repair genes may provide additional insights into the repair process, and in fact gene expression ratios have been utilized to examine tissue healing trends in musculoskeletal tissues including bone (Chow, Leung et al. 2014) and ligament (Canseco, Kojima et al. 2012). In this study, normal TA muscle tissue ratios (ECM:MyoD) ranged between 10 and 15 for each of the ECM genes measured. Repair strategies that increase expression ratios away from normal TA values might suggest a shift in the repair process towards increased ECM production and/or decreased myogenesis. In contrast, repair strategies that cause expression ratios to fall below normal TA values might alternatively suggest a shift towards decreased ECM production and/or increased myogenesis. With that hypothesis in mind, the DSM+MM repaired muscle groups expressed ratios that were at or below normal muscle for each of the genes tested. Conversely, muscles that received VML defects and those that were repaired with isolated DSM had ratios ranging from 32.9-51.5 and 28.6-38.1 respectively. Potentially, these and other gene expression ratios could be used to evaluate VML

repair strategies in future animal models, and may provide insights into treatment strategies that target gene pairs.

The co-delivery of DSM with MM restored approximately half of the peak contractile force lost following VML injury (81% versus 62%). The question then remains; what additional strategies could be utilized to restore the last twenty percent? Existing animal studies show that physical rehabilitation in the form of voluntary wheel running after VML injury and subsequent minced muscle transplant can improve maximal isometric torque, without causing significant damage to healing muscle (Corona, Garg et al. 2013). These results suggest that the application of force to the repair site during healing can contribute to muscle regeneration. This is supported by in-vitro findings that have shown force and substrate strain enhances muscle progenitor cell myogenesis (Egusa, Kobayashi et al. 2013, Heher, Maleiner et al. 2015). Motivated by a desire to closely replicate previously reported MM treatment strategies, DSM implants were not sutured to the surrounding TA muscle tissue during implantation. In the future we plan to incorporate surgical attachment into the repair strategy, as it will enable the transfer of contractile force through the repair site during healing and regeneration. In addition to physical stimuli, the delivery of soluble stimuli in the form of growth factors has been found to enhance functional recovery after muscle injury. Specifically, fibroblast growth factor (bFGF), insulin growth factor (IGF), and nerve growth factor (NGF) have been shown to aid in muscle regeneration (Baoge, Van Den Steen et al. 2012). If necessary these key molecules could be injected into the repair site at the time of surgery to deliver short-term effects, or physically linked to DSM scaffolds to potentially prolong their myogenic activity (Ramazanoglu, Lutz et al. 2013).

The Fischer 344 rats used in this study had not reached skeletal maturity and continued to gain weight throughout the recovery period. As a result, the findings reported in this study might

more accurately model the response of young adults to VML repair with DSM and MM implants. Surgical muscle removal resulting from soft tissue sarcoma resection is another anticipated target for VML repair strategies like that described in this study (Fischer, Soimaru et al. 2015). This group of patients is typically older, and to date the regenerative response of MM in an aged model has not been investigated. Age related changes in muscle biology might be a limiting factor for MM usage in older patients. It is well established that muscle resident satellite cells account for the majority of skeletal muscle's regenerative capacity (Conboy and Rando 2005). However, aging leads to an overall decrease in myogenic capacity mostly in part due to reduced satellite cell activity (Snow 1977, Conboy and Rando 2005, Brack and Rando 2007). In future studies it would be useful to understand whether the regenerative benefits of MM autografts are maintained when harvested from aged muscle. Yet, while the use of MM autografts may not be suitable for all VML repair scenarios, the findings reported herein add to the growing body of evidence supporting its potential as a VML treatment strategy that warrants continued investigation.

E. Conclusions

The key findings of this study suggest that:

1. The addition of MM to DSM significantly increased peak TA tetanic contractile force when compared to unrepaired VML controls.
2. DSM+MM repair significantly increased TA muscle mass, restoring approximately half of the muscle mass lost to VML injury.

3. Histological analysis revealed a reduced fibrotic response at the repair site in response to DSM+MM repairs, when compared to either unrepaired VML or isolated DSM repair strategies.
4. MyoD, ECM (Col I and Col III), and ECM regulatory (TGFB1, CTGF, and TIMP-1) gene expression levels were significantly increased over all other treatment groups in response to DSM+MM repair.
5. Analysis of gene expression ratios may provide a useful indicator of VML treatment efficacy and restoration of normal muscle homeostasis.

References:

- Aurora, A., J. L. Roe, B. T. Corona and T. J. Walters (2015). "An acellular biologic scaffold does not regenerate appreciable de novo muscle tissue in rat models of volumetric muscle loss injury." Biomaterials **67**: 393-407.
- Baoge, L., E. Van Den Steen, S. Rimbaut, N. Philips, E. Witvrouw, K. F. Almqvist, G. Vanderstraeten and L. C. Vanden Bossche (2012). "Treatment of skeletal muscle injury: a review." ISRN Orthop **2012**: 689012.
- Bedair, H., T. T. Liu, J. L. Kaar, S. Badlani, A. J. Russell, Y. Li and J. Huard (2007). "Matrix metalloproteinase-1 therapy improves muscle healing." J Appl Physiol (1985) **102**(6): 2338-2345.
- Bian, W. and N. Bursac (2009). "Engineered skeletal muscle tissue networks with controllable architecture." Biomaterials **30**(7): 1401-1412.
- Brack, A. S. and T. A. Rando (2007). "Intrinsic changes and extrinsic influences of myogenic stem cell function during aging." Stem Cell Rev **3**(3): 226-237.
- Canseco, J. A., K. Kojima, A. R. Penrose, J. D. Ross, H. Obokata, A. H. Gomoll and C. A. Vacanti (2012). "Effect on ligament marker expression by direct-contact co-culture of mesenchymal stem cells and anterior cruciate ligament cells." Tissue Eng Part A **18**(23-24): 2549-2558.
- Cardenas-Mejia, A., J. V. Covarrubias-Ramirez, A. Bello-Margolis and S. Rozen (2015). "Double innervated free functional muscle transfer for facial reanimation." J Plast Surg Hand Surg **49**(3): 183-188.
- Chiron, S., C. Tomczak, A. Duperray, J. Laine, G. Bonne, A. Eder, A. Hansen, T. Eschenhagen, C. Verdier and C. Coirault (2012). "Complex interactions between human myoblasts and the surrounding 3D fibrin-based matrix." PLoS One **7**(4): e36173.
- Chow, S. K., K. S. Leung, L. Qin, F. Wei and W. H. Cheung (2014). "Callus formation is related to the expression ratios of estrogen receptors-alpha and -beta in ovariectomy-induced osteoporotic fracture healing." Arch Orthop Trauma Surg **134**(10): 1405-1416.
- Conboy, I. M. and T. A. Rando (2005). "Aging, stem cells and tissue regeneration: lessons from muscle." Cell Cycle **4**(3): 407-410.
- Corona, B. T., K. Garg, C. L. Ward, J. S. McDaniel, T. J. Walters and C. R. Rathbone (2013). "Autologous minced muscle grafts: a tissue engineering therapy for the volumetric loss of skeletal muscle." Am J Physiol Cell Physiol **305**(7): C761-775.
- Corona, B. T., C. L. Ward, H. B. Baker, T. J. Walters and G. J. Christ (2014). "Implantation of in vitro tissue engineered muscle repair constructs and bladder acellular matrices partially restore in

vivo skeletal muscle function in a rat model of volumetric muscle loss injury." Tissue Eng Part A **20**(3-4): 705-715.

Crapo, P. M., T. W. Gilbert and S. F. Badylak (2011). "An overview of tissue and whole organ decellularization processes." Biomaterials **32**(12): 3233-3243.

Davis, M. E., M. A. Korn, J. P. Gumucio, J. A. Harning, A. L. Saripalli, A. Bedi and C. L. Mendias (2015). "Simvastatin reduces fibrosis and protects against muscle weakness after massive rotator cuff tear." J Shoulder Elbow Surg **24**(2): 280-287.

Egusa, H., M. Kobayashi, T. Matsumoto, J. Sasaki, S. Uraguchi and H. Yatani (2013). "Application of cyclic strain for accelerated skeletal myogenic differentiation of mouse bone marrow-derived mesenchymal stromal cells with cell alignment." Tissue Eng Part A **19**(5-6): 770-782.

English, A., A. Azeem, K. Spanouides, E. Jones, B. Tripathi, N. Basu, K. McNamara, S. A. Tofail, N. Rooney, G. Riley, A. O'Riordan, G. Cross, D. Hutmacher, M. Biggs, A. Pandit and D. I. Zeugolis (2015). "Substrate topography: A valuable in vitro tool, but a clinical red herring for in vivo tenogenesis." Acta Biomater **27**: 3-12.

Fischer, S., S. Soimaru, T. Hirsch, M. Kueckelhaus, C. Seitz, M. Lehnhardt, O. Goertz, H. U. Steinau and A. Daigeler (2015). "Local tendon transfer for knee extensor mechanism reconstruction after soft tissue sarcoma resection." J Plast Reconstr Aesthet Surg **68**(5): 729-735.

Heher, P., B. Maleiner, J. Pruller, A. H. Teuschl, J. Kollmitzer, X. Monforte, S. Wolbank, H. Redl, D. Runzler and C. Fuchs (2015). "A novel bioreactor for the generation of highly aligned 3D skeletal muscle-like constructs through orientation of fibrin via application of static strain." Acta Biomater **24**: 251-265.

Hinds, S., W. Bian, R. G. Dennis and N. Bursac (2011). "The role of extracellular matrix composition in structure and function of bioengineered skeletal muscle." Biomaterials **32**(14): 3575-3583.

Hjorth, M., F. Norheim, A. J. Meen, S. Pourteymour, S. Lee, T. Holen, J. Jensen, K. I. Birkeland, V. N. Martinov, T. M. Langleite, K. Eckardt, C. A. Drevon and S. O. Kolset (2015). "The effect of acute and long-term physical activity on extracellular matrix and serglycin in human skeletal muscle." Physiol Rep **3**(8).

Hurd, S. A., N. M. Bhatti, A. M. Walker, B. M. Kasukonis and J. C. Wolchok (2015). "Development of a biological scaffold engineered using the extracellular matrix secreted by skeletal muscle cells." Biomaterials **49**: 9-17.

Hyldahl, R. D., B. Nelson, L. Xin, T. Welling, L. Groscost, M. J. Hubal, S. Chipkin, P. M. Clarkson and A. C. Parcell (2015). "Extracellular matrix remodeling and its contribution to protective adaptation following lengthening contractions in human muscle." FASEB J **29**(7): 2894-2904.

Jana, S., M. Leung, J. Chang and M. Zhang (2014). "Effect of nano- and micro-scale topological features on alignment of muscle cells and commitment of myogenic differentiation." Biofabrication **6**(3): 035012.

Jank, B. J., L. Xiong, P. T. Moser, J. P. Guyette, X. Ren, C. L. Cetrulo, D. A. Leonard, L. Fernandez, S. P. Fagan and H. C. Ott (2015). "Engineered composite tissue as a bioartificial limb graft." Biomaterials **61**: 246-256.

Juhas, M., G. C. Engelmayr, Jr., A. N. Fontanella, G. M. Palmer and N. Bursac (2014). "Biomimetic engineered muscle with capacity for vascular integration and functional maturation in vivo." Proc Natl Acad Sci U S A **111**(15): 5508-5513.

Kasukonis, B., J. Kim, T. Washington and J. Wolchok (2016). "Development of an infusion bioreactor for the accelerated preparation of decellularized skeletal muscle scaffolds." Biotechnol Prog.

Kim, J. T., B. M. Kasukonis, L. A. Brown, T. A. Washington and J. C. Wolchok (2016). "Recovery from volumetric muscle loss injury: A comparison between young and aged rats." Exp Gerontol **83**: 37-46.

Lam, M. T., Y. C. Huang, R. K. Birla and S. Takayama (2009). "Microfeature guided skeletal muscle tissue engineering for highly organized 3-dimensional free-standing constructs." Biomaterials **30**(6): 1150-1155.

Lin, C. H., Z. S. Zhu, C. H. Lin, C. C. Hsu, J. T. Yeh and Y. T. Lin (2012). "Primary free functioning muscle transfer for fingers with accompanying tendon transfer for thumb provide one-stage upper extremity composite reconstruction in acute open wound." J Trauma Acute Care Surg **72**(3): 737-743.

Maier, F. and A. Bornemann (1999). "Comparison of the muscle fiber diameter and satellite cell frequency in human muscle biopsies." Muscle Nerve **22**(5): 578-583.

Mann, C. J., E. Perdiguero, Y. Kharraz, S. Aguilar, P. Pessina, A. L. Serrano and P. Munoz-Canoves (2011). "Aberrant repair and fibrosis development in skeletal muscle." Skelet Muscle **1**(1): 21.

Mase, V. J., Jr., J. R. Hsu, S. E. Wolf, J. C. Wenke, D. G. Baer, J. Owens, S. F. Badylak and T. J. Walters (2010). "Clinical application of an acellular biologic scaffold for surgical repair of a large, traumatic quadriceps femoris muscle defect." Orthopedics **33**(7): 511.

McClung, J. M., J. M. Davis and J. A. Carson (2007). "Ovarian hormone status and skeletal muscle inflammation during recovery from disuse in rats." Exp Physiol **92**(1): 219-232.

McGuire, D. A. and J. C. Wolchok (1997). "Consistent and accurate graft passage and interference screw guide wire placement during single incision anterior cruciate ligament reconstruction." Arthroscopy **13**(4): 526-529.

- Merritt, E. K., M. V. Cannon, D. W. Hammers, L. N. Le, R. Gokhale, A. Sarathy, T. J. Song, M. T. Tierney, L. J. Suggs, T. J. Walters and R. P. Farrar (2010). "Repair of traumatic skeletal muscle injury with bone-marrow-derived mesenchymal stem cells seeded on extracellular matrix." Tissue Eng Part A **16**(9): 2871-2881.
- Morez, C., M. Nosedá, M. A. Paiva, E. Belian, M. D. Schneider and M. M. Stevens (2015). "Enhanced efficiency of genetic programming toward cardiomyocyte creation through topographical cues." Biomaterials **70**: 94-104.
- Oishi, S. N. and M. Ezaki (2010). "Free gracilis transfer to restore finger flexion in Volkmann ischemic contracture." Tech Hand Up Extrem Surg **14**(2): 104-107.
- Ott, H. C., B. Clippinger, C. Conrad, C. Schuetz, I. Pomerantseva, L. Ikonou, D. Kotton and J. P. Vacanti (2010). "Regeneration and orthotopic transplantation of a bioartificial lung." Nat Med **16**(8): 927-933.
- Ott, H. C., T. S. Matthiesen, S. K. Goh, L. D. Black, S. M. Kren, T. I. Netoff and D. A. Taylor (2008). "Perfusion-decellularized matrix: using nature's platform to engineer a bioartificial heart." Nat Med **14**(2): 213-221.
- Patel, A., S. Mukundan, W. Wang, A. Karumuri, V. Sant, S. M. Mukhopadhyay and S. Sant (2016). "Carbon-based hierarchical scaffolds for myoblast differentiation: Synergy between nano-functionalization and alignment." Acta Biomater.
- Perniconi, B., A. Costa, P. Aulino, L. Teodori, S. Adamo and D. Coletti (2011). "The pro-myogenic environment provided by whole organ scale acellular scaffolds from skeletal muscle." Biomaterials **32**(31): 7870-7882.
- Ramazanoglu, M., R. Lutz, P. Rusche, L. Trabzon, G. T. Kose, C. Prechtel and K. A. Schlegel (2013). "Bone response to biomimetic implants delivering BMP-2 and VEGF: an immunohistochemical study." J Craniomaxillofac Surg **41**(8): 826-835.
- Sicari, B. M., J. P. Rubin, C. L. Dearth, M. T. Wolf, F. Ambrosio, M. Boninger, N. J. Turner, D. J. Weber, T. W. Simpson, A. Wyse, E. H. Brown, J. L. Dziki, L. E. Fisher, S. Brown and S. F. Badylak (2014). "An acellular biologic scaffold promotes skeletal muscle formation in mice and humans with volumetric muscle loss." Sci Transl Med **6**(234): 234ra258.
- Snow, M. H. (1977). "The effects of aging on satellite cells in skeletal muscles of mice and rats." Cell Tissue Res **185**(3): 399-408.
- Sullivan, D. C., S. H. Mirmalek-Sani, D. B. Deegan, P. M. Baptista, T. Aboushwareb, A. Atala and J. J. Yoo (2012). "Decellularization methods of porcine kidneys for whole organ engineering using a high-throughput system." Biomaterials **33**(31): 7756-7764.

Terada, N., S. Takayama, H. Yamada and T. Seki (2001). "Muscle repair after a transection injury with development of a gap: an experimental study in rats." Scand J Plast Reconstr Surg Hand Surg **35**(3): 233-238.

Terzis, J. K. and V. K. Kostopoulos (2010). "Free muscle transfer in posttraumatic plexopathies: part 1: the shoulder." Ann Plast Surg **65**(3): 312-317.

Tian, Z. L., S. K. Jiang, M. Zhang, M. Wang, J. Y. Li, R. Zhao, L. L. Wang, S. S. Li, M. Liu, M. Z. Zhang and D. W. Guan (2016). "Detection of satellite cells during skeletal muscle wound healing in rats: time-dependent expressions of Pax7 and MyoD in relation to wound age." Int J Legal Med **130**(1): 163-172.

Uygun, B. E., A. Soto-Gutierrez, H. Yagi, M. L. Izamis, M. A. Guzzardi, C. Shulman, J. Milwid, N. Kobayashi, A. Tilles, F. Berthiaume, M. Hertl, Y. Nahmias, M. L. Yarmush and K. Uygun (2010). "Organ reengineering through development of a transplantable recellularized liver graft using decellularized liver matrix." Nat Med **16**(7): 814-820.

Vekris, M. D., A. E. Beris, M. G. Lykissas, A. V. Korompilias, A. D. Vekris and P. N. Soucacos (2008). "Restoration of elbow function in severe brachial plexus paralysis via muscle transfers." Injury **39 Suppl 3**: S15-22.

Ward, C. L., L. Ji and B. T. Corona (2015). "An Autologous Muscle Tissue Expansion Approach for the Treatment of Volumetric Muscle Loss." Biores Open Access **4**(1): 198-208.

Washington, T. A., L. Brown, D. A. Smith, G. Davis, J. Baum and W. Bottje (2013). "Monocarboxylate transporter expression at the onset of skeletal muscle regeneration." Physiol Rep **1**(4): e00075.

Wilson, K., A. Terlouw, K. Roberts and J. C. Wolchok (2016). "The characterization of decellularized human skeletal muscle as a blueprint for mimetic scaffolds." J Mater Sci Mater Med **27**(8): 125.

Wolf, M. T., K. A. Daly, J. E. Reing and S. F. Badylak (2012). "Biologic scaffold composed of skeletal muscle extracellular matrix." Biomaterials **33**(10): 2916-2925.

Wu, X., B. T. Corona, X. Chen and T. J. Walters (2012). "A standardized rat model of volumetric muscle loss injury for the development of tissue engineering therapies." Biores Open Access **1**(6): 280-290.

Zhang, Y., Y. He, S. Bharadwaj, N. Hammam, K. Carnagey, R. Myers, A. Atala and M. Van Dyke (2009). "Tissue-specific extracellular matrix coatings for the promotion of cell proliferation and maintenance of cell phenotype." Biomaterials **30**(23-24): 4021-4028.

Acknowledgments:

Research reported in this publication was supported by the National Institute Of Arthritis And Musculoskeletal And Skin Diseases of the National Institutes of Health under Award Number R15AR064481 and the Arkansas Biosciences Institute.

Author Disclosure Statement:

No competing financial interests exist for any of the authors.

Figure Legend

Figure 1: DSM scaffolds were infusion decellularized using a custom-built infusion bioreactor. During decellularization, SDS solution was delivered via a hypodermic needle (A) which was positioned into the wide mid-belly region of the TA muscle (B). SDS solution was infused via a syringe pump (5 ml/hr for 12 hours) through each muscle and outflowed to waste collection. The bioreactor was designed to accommodate four side-by-side decellularization units each capable of accommodating a single muscle tissue sample (C). Representative whole TA muscle appearance prior to and following infusion decellularization treatment (D & E), illustrates the dramatic color change (red to white) following removal of intracellular myoglobin. Infusion prepared DSM scaffolds, when viewed in thin section (scale bar = 100um) with H&E staining, retained the highly aligned architecture of native muscle ECM (F). (arrow = direction of contraction)

Figure 2: To create the VML injury model, the mid-belly region of the TA muscle in a Fischer 344 rat was visualized through a 1-2cm incision (A) and approximately 20% of the TA muscle (average defect weight = 94 ± 6 mg) was excised using an 8mm biopsy punch inserted to a depth of 3mm (B-D). During isolated DSM repair a single scaffold was cut to size and implanted into the TA defect (E). To prepare each MM autograft, 25% of the previously removed defect plug was minced with a scalpel and scissors and then used to coat the surface of a single DSM scaffold (F). The combined DSM scaffold and MM paste construct was implanted into the TA defect (G). The deep fascia and skin (H). were closed separately using absorbable sutures.

Figure 3: Twelve-weeks after treatment, TA peak contractile force was assessed for both unrepaired and DSM repaired groups (n=8/group). Representative tetanic force responses for

normal, unrepaired VML, DSM, and DSM+MM repaired TA muscles (A). Peak tetanic force was normalized to animal weight (N/kg) and computed as a percentage of the untreated contralateral limb for each animal tested (B). Box and whisker plot values shown are the median, 1st and 3rd quartile, as well as maximum and minimum. The increase in peak contractile force in response to DSM+MM implantation was statically significant when compared to both un-repaired VML and isolated DSM repaired samples. (n=7-8 / sample group). # distinguishes significant difference from VML group. p<0.05; ANOVA with post hoc Tukey's test.

Figure 4: Gross morphology of normal, unrepaired VML, DSM, and DSM+MM repaired whole TA muscles harvested 12 weeks post treatment (A). TA weight, calculated as the percent normal contralateral muscle, was significantly increased in response to repair with combined DSM+MM implants (B). The EDL muscle mass was similarly increased in response to treatment, suggesting compensatory hypertrophy. Box and whisker plot values shown are the median, 1st and 3rd quartile, as well as maximum and minimum. (n=8/sample); # distinguishes significant difference from VML group, p<0.05; ANOVA with post hoc Tukey's test.

Figure 5: Representative normal (A, E, I), unrepaired VML (B, F, J), DSM (C, G, K) and DSM+MM (D, H, L) repaired histological sections (panel E inset indicates approximate section location). Sections were stained with either Masson's Trichrome or immunostained for the presence of MHC (red) and collagen type I (green). The defect/repair site (*) for unrepaired VML and isolated DSM repaired samples showed evidence of a thick, collagen enriched, connective tissue repair layer. DSM+MM repair site tissue showed markedly less connective tissue formation than VML or DSM groups. Dotted line highlights the boundary between collagen dense repair

tissue and MHC positive muscle tissue . Scale bar = 250um unless noted Arrow indicates anterior direction.

Figure 6: Representative normal (A, E), unrepaired VML (B, F), DSM (C, G) and DSM+MM (D, H) tissue sections. Repair site tissue was immunoreactive to antibodies directed against collagen I and III (A-D) as well as laminin and fibronectin (E-F). Scale bar = 100um. Arrow indicates anterior direction.

Figure 7: Representative DSM (A) and DSM+MM repaired (B) tissue sections immunostained for the presence of collagen type I. The sectional area immunoreactive to collagen type I was calculated using sections prepared from tissue regions located at least 3mm away from the anterior surface of the muscle. Tissue samples collected from DSM+MM repair samples exhibited a significantly lower immunoreactivity to collagen type I when compared to isolated DSM repair samples. Scale bar = 100um; n=3/sample group; * distinguishes significant difference from the DSM treatment group; p<0.05 ANOVA with Tukey's

Figure 8. RT-PCR results (fold change compared to normal muscle) for the ECM structural proteins Collagen I and III, the ECM regulatory cytokines TGFB1, MMP2, and TIMP-1, and the myogenic marker MyoD Values shown are mean+sem; n=4/sample group;. # distinguishes significant difference from both VML and DSM groups; p<0.05 ANOVA with Tukey's test.

Figure 9: Collagen I to MyoD gene expression ratio versus percent normal contractile force (A) for VML, DSM, DSM+MM, and normal TA sample groups. The average expression ratios

calculated for VML and DSM samples clustered near an elevated value of 30, while the DSM+MM repair sample ratio was better aligned with normal TA muscle. Average expression ratios (B) for each of the ECM structural and ECM regulatory genes to MyoD. Expression ratio values shown are mean+sem; n=4/sample group.

Supplemental Figure 1: To record peak tetanic contractile force, the hind foot of an anesthetized rat was secured to a foot plate with the knee was immobilized at 90° (A). A tenotomy was performed on the distal tendons of the EDL and EHL (B & C) to isolate the contribution of TA muscle to force production. Needle electrodes were used to stimulate the peroneal nerve (D). During stimulation, ankle dorsiflexion force in Newtons versus time was recorded.

Figures

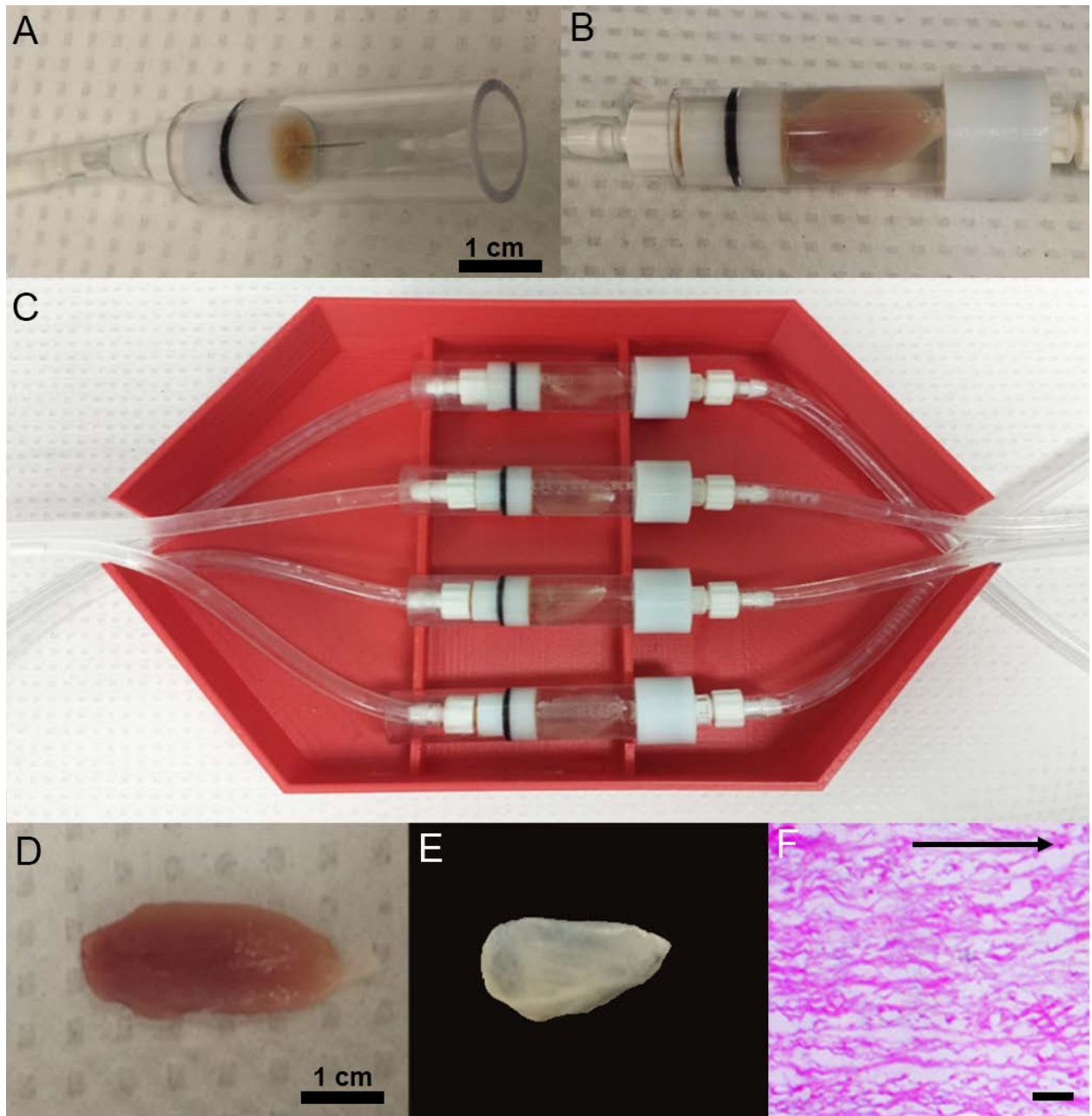


Figure 1

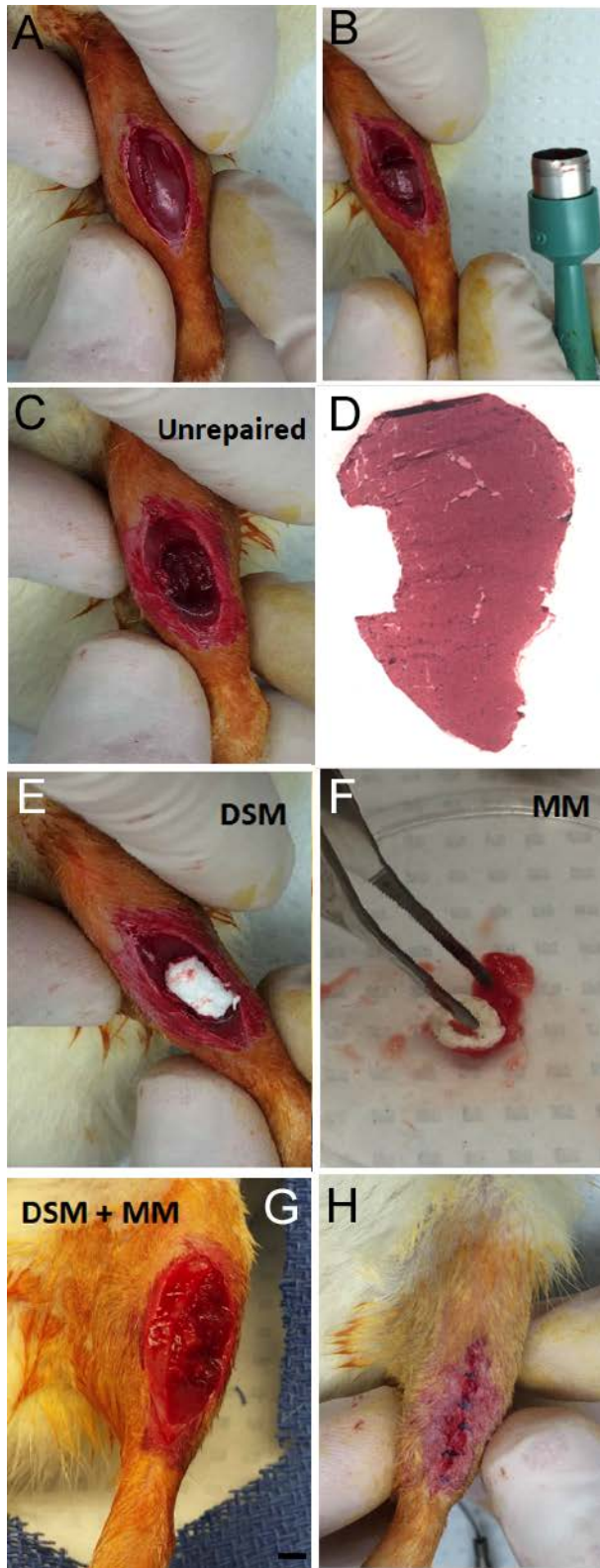


Figure 2

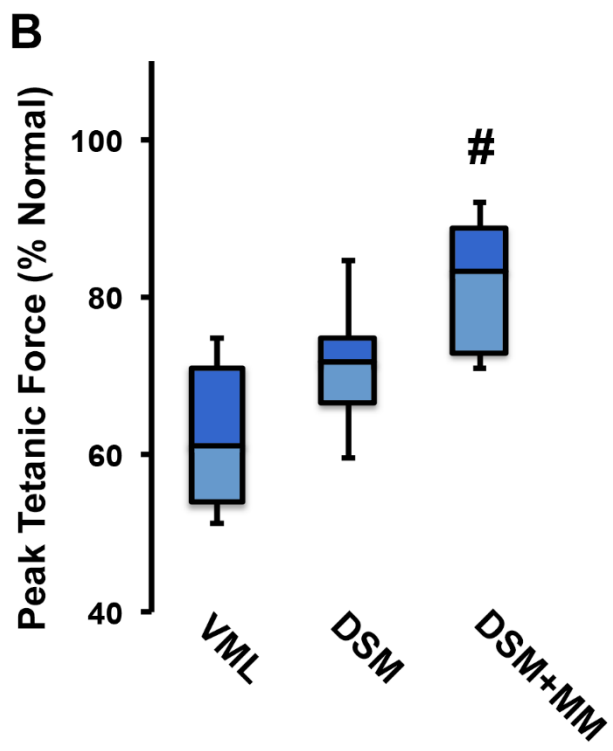
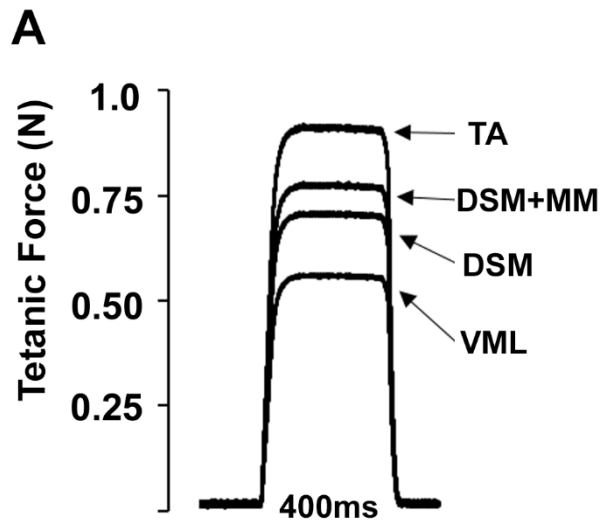


Figure 3

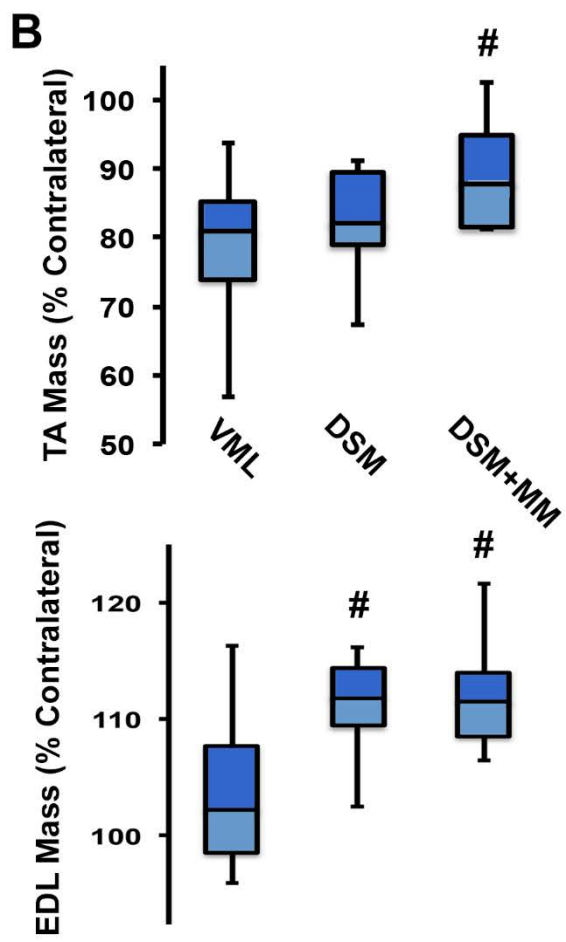
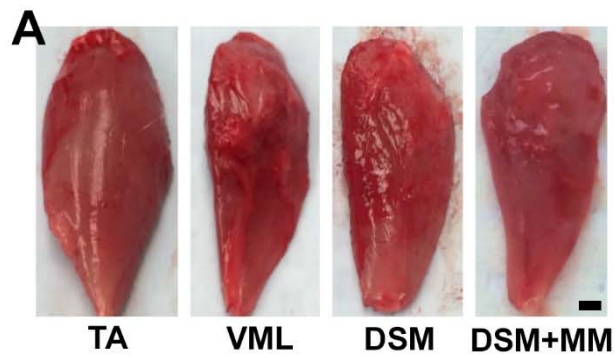


Figure 4

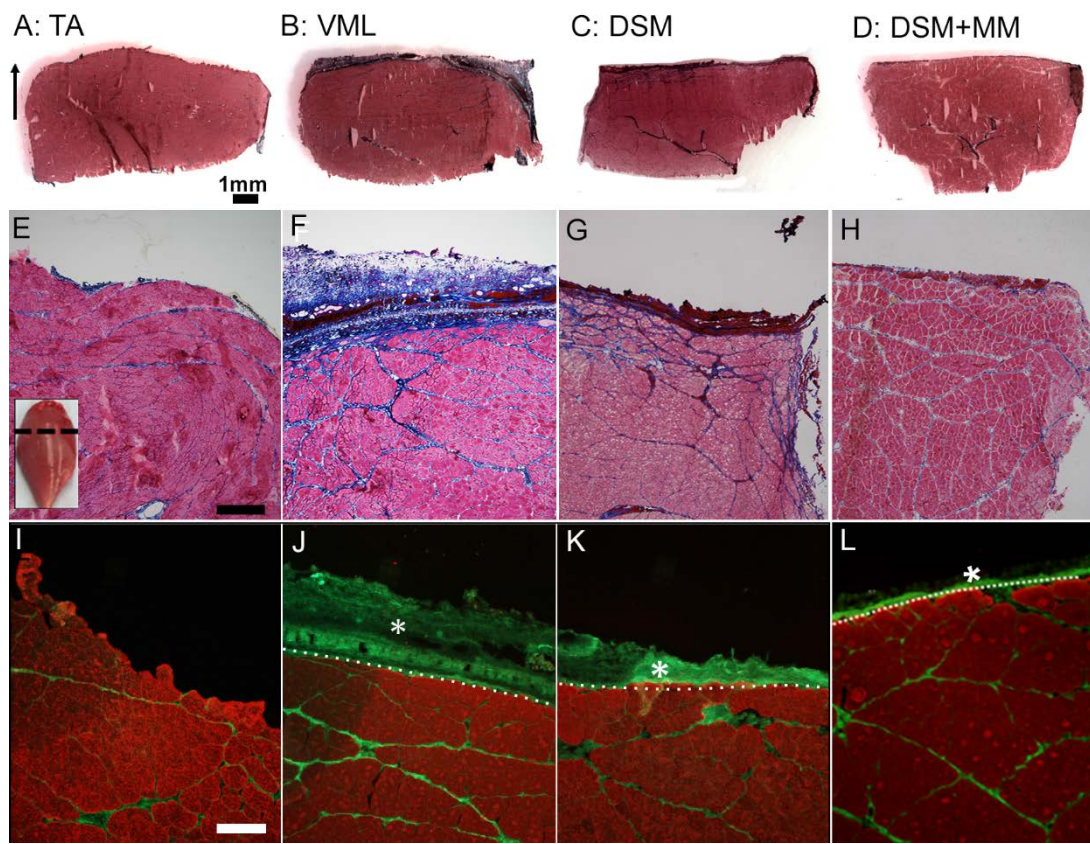


Figure 5

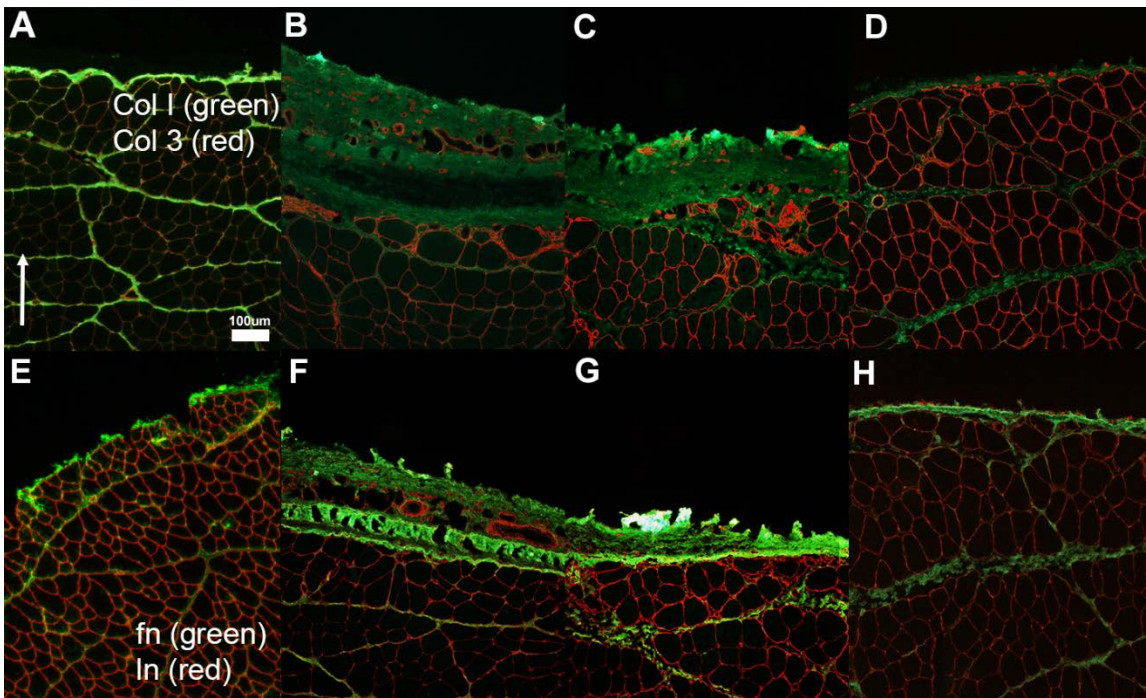


Figure 6

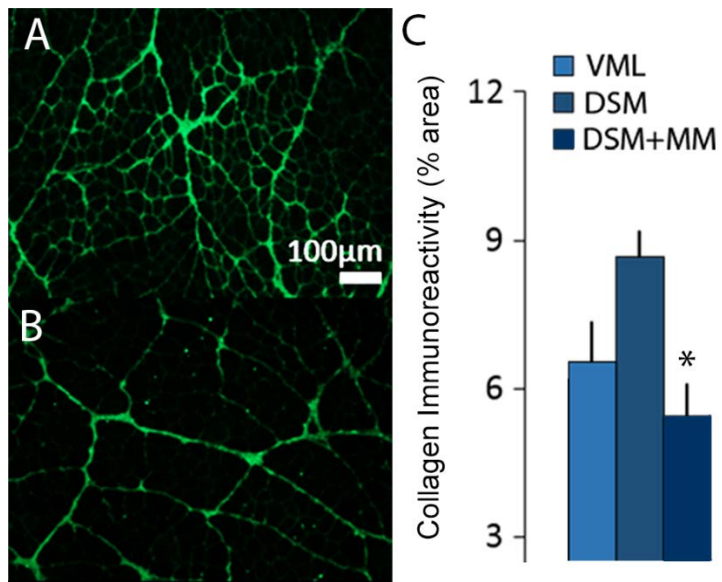


Figure 7

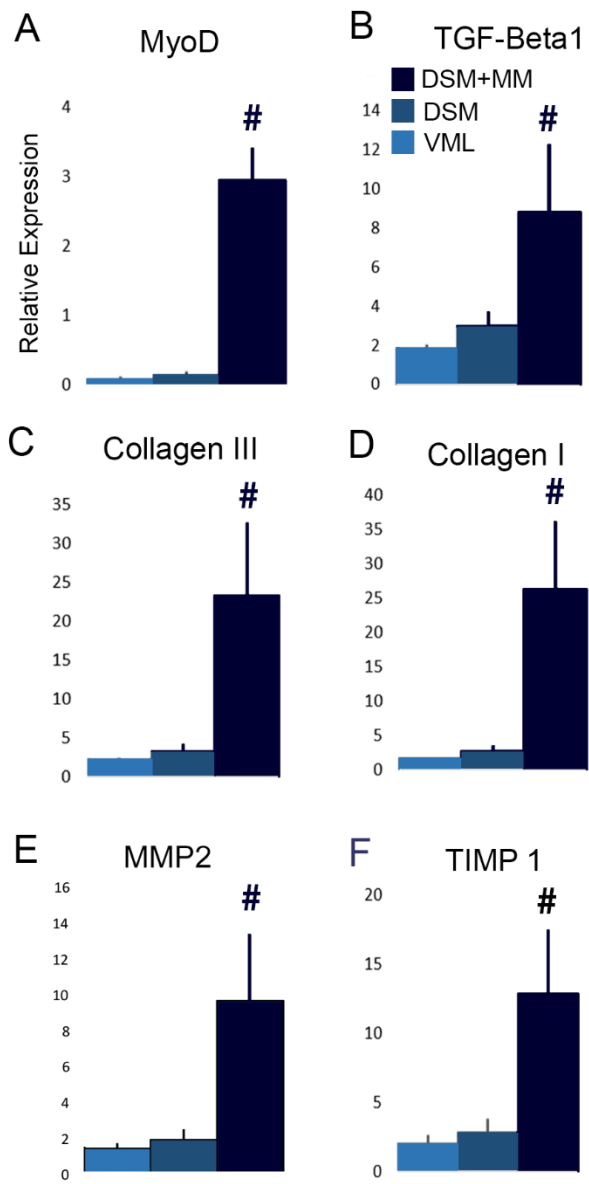
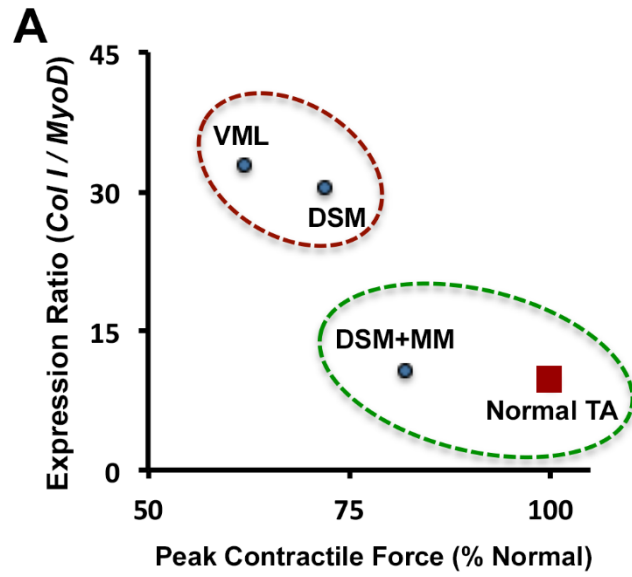


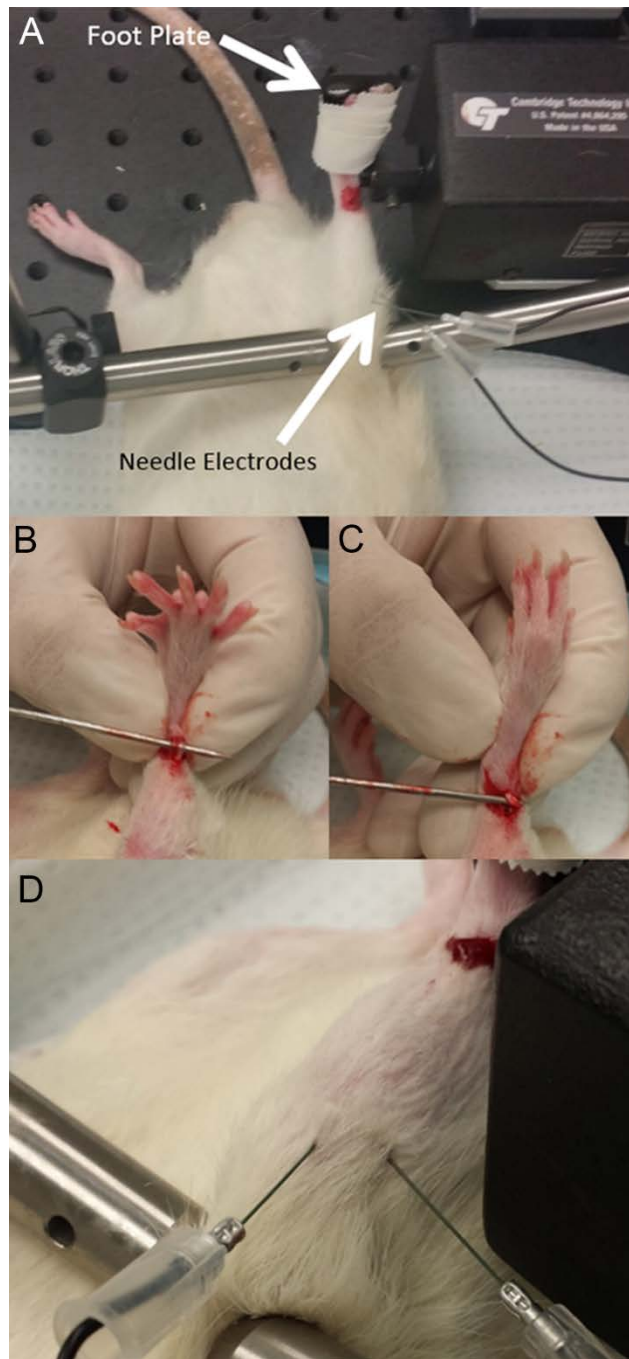
Figure 8



B

	TA	VML	DSM	DSM+MM
TGF- β 1 / MyoD	13.7 \pm 6.8	41.9 \pm 18.0	34.6 \pm 12.3	3.6 \pm 1.7
Col I / MyoD	9.8 \pm 5.3	32.9 \pm 10.5	30.3 \pm 15.5	10.6 \pm 4.5
Col III / MyoD	15.6 \pm 7.8	47.1 \pm 15.8	38.1 \pm 15.3	9.4 \pm 4.2
Timp-1 / MyoD	14.6 \pm 8.3	45.9 \pm 25.2	30.8 \pm 12.5	4.9 \pm 1.6

Figure 9



Supplemental Figure 1

Chapter 4

Autograft Relative Alignment Impacts the Regenerative Response of Skeletal Muscle After Volumetric Muscle Loss in a Rat Model

To be submitted as an original article by:

Ben Kasukonis¹, John Kim¹, Tyrone Washington², and Jeffrey Wolchok¹

¹ Department of Biomedical Engineering, College of Engineering, University of Arkansas, Fayetteville, AR

² Department of Health, Human Performance, and Recreation, College of Education and Health Professions, University of Arkansas, Fayetteville, AR

Abstract:

Minor trauma, such as contusions and small lacerations, to a skeletal muscle has no lasting effect on the force production or morphological structure of the tissue due to the self-repair capabilities of skeletal muscle. When trauma is severe and results in a decrease of bulk tissue, the characteristic repair mechanisms are overwhelmed resulting in permanent fibrosis and reduction in contractile force production. Tissue engineering has yielded several cell and scaffold based therapies, and many scaffolds or tissue constructs used in VML repair mimic the parallel alignment of myofibers and underlying ECM in skeletal muscle tissue. While the alignment of the biomaterial or engineered muscle is addressed in many studies, the relative alignment between the tissue engineering construct and the myofibers of the damaged muscle has not been thoroughly investigated. This goal of this study was to provide evidence towards the hypothesis that the relative alignment of an autograft used to repair VML in an animal model will affect the regenerative response of the damaged skeletal muscle tissue. A rat VML model was used with 3 treatment groups: aligned, 45° unaligned, and 90° unaligned studied at 2 time points: 2 weeks (n=6/group) and 12 weeks (n=9) of recovery. We observed significant upregulation of MyoD (2.5 fold increase) and Pax7 (1.7 fold increase) expression at 2 weeks post-implantation in VML defected muscles repaired with aligned autografts, which provides evidence that congruent alignment of a scaffold within a defect contributes to the myogenic response of the repaired tissue. After 12 weeks, aligned autografts had greater functional recovery (74.8±10.5%) when compared to 45° and 90° unaligned autografts (63.7±10.2% and 60±11.0%, respectively). The importance of relative alignment has been demonstrated with this study but the underlying mechanisms require further exploration.

A. Introduction

Volumetric muscle loss (VML) is a skeletal muscle injury in which more than 20% of a muscle's volume is lost to traumatic injury. (Grogan et al., 2011) Innate mechanisms to repair skeletal muscle are overwhelmed and patients are left with permanent fibrosis and functional deficiencies. The current standard of care for patients presenting with a VML injury is the use of muscle flap autografts. However, there are currently multiple therapeutic interventions being developed and tested in animal models, as well as two small clinical studies. Some of the more successful strategies include the use of ECM scaffolds. The source of the ECM varies from decellularized skeletal muscle (DSM) to porcine small intestine submucosa (SIS). There are several differences between the two scaffolds including: pore size, pore alignment, and embedded growth factors. Skeletal muscle is a highly aligned tissue with a hierarchical arrangement of ECM, and after decellularization the resulting scaffold is anisotropic. (Meyer & Lieber, 2011; Wilson et al., 2016) The architecture and mechanical properties of the ECM are important not only to provide structure to myofibers, but to transmit mechanical stimuli to the myofibers. (Kjaer, 2004) Perhaps more importantly from the standpoint of muscle regeneration, mechanical stimuli are imperative for the differentiation of satellite cells and the fusion of myoblasts. (Grossi et al., 2007; Tidball et al., 1998)

Skeletal muscle tissue is highly aligned and the force production of a muscle is heavily influenced by the muscle's architecture. Muscle architecture, the arrangement of muscle fibers in relation to the axis of force generation, is constrained by the length of the muscle, the length of myofibers, the pennation angle, and the physiological cross sectional area (PCSA). (Lieber & Friden, 2000) Even in pennate muscles, adjacent myofibers have parallel alignment and the

surrounding ECM is highly uniform in direction. When designing bioreactors for tissue engineered skeletal muscle, researchers are deliberate in developing alignment within their constructs.(Aubin et al., 2010; Aviss et al., 2010; Huang et al., 2010b; Vandeburgh & Karlisch, 1989) Parallel alignment of myofibers has been shown to be important for developing phenotypically normal muscle tissue under *in vitro* conditions.(Aubin et al., 2010; Lam et al., 2009; Vandeburgh & Karlisch, 1989; Wang et al., 2015) Researchers obtain parallel alignment through micropatterning(Cimetta et al., 2009; Flaibani et al., 2009; Huang et al., 2010a; Shimizu et al., 2009), aligned deposition of fibers(Aviss et al., 2010; Choi et al., 2008b; Wang et al., 2015), or by selecting a scaffold that has native parallel alignment. Myofiber alignment indicative of a mature muscle phenotype has also been induced *in vitro* using bioreactors that deliver mechanical or electrical stimulation to cells and/or tissue constructs.(Ahadian et al., 2013; Boonen et al., 2010a; Donnelly et al., 2010; Flaibani et al., 2009; Grossi et al., 2007; Langelaan et al., 2011; Powell et al., 2002; Vandeburgh & Karlisch, 1989)

It has been suggested that parallel alignment is not only necessary for efficient contractile force production, but for the arrangement of blood vessels and nerves as well as the migration of macrophages, fibroblasts, and muscle progenitor cells during muscle repair. In response to sarcolemma damage, satellite cells activate and migrate to the site of tissue insult. Satellite cells are capable of migrating across the ECM to adjacent myofibers, but are more likely to travel down the length of a myofiber.(Siegel, Atchison, Fisher, Davis, & Cornelison, 2009b) Migration of satellite cells is dependent on the release of matrix metalloproteases (MMPs) to degrade the basal lamina to allow for efficient chemotaxis to the site of injury.(Kaar et al., 2008) The action of MMPs is attenuated by tissue inhibitors of metalloproteases (TIMPs) allowing for increased

cell migration, while limiting the degradation of the supportive ECM.(Karalaki et al., 2009; Nishimura et al., 2008)

The effects of alignment and misalignment on the regenerative response of skeletal muscle, especially in cases of VML, are not understood and have not been explored. The alignment of a biomaterial when selecting a therapeutic intervention for VML injuries is a parameter that many researchers acknowledge.(Merritt et al., 2010; Perniconi et al., 2011b; Wang, Johnson, Chang, & Zhang, 2013; Wolf et al., 2012) In another study, researchers used autografts to repair VML in an animal model and attributed variance within treatment groups to misalignment of the myofibers of the autograft with the myofibers of the VML defected tissue.(M. T. A. Li, Willett, Uhrig, Guldborg, & Warren, 2014a) As the field of skeletal muscle tissue engineering progresses towards effective treatment options for VML, the effect of relative alignment must be understood.

This goal of this study is to provide evidence towards the hypothesis that the relative alignment of an autograft used to repair VML in an animal model will affect the regenerative response of the damaged skeletal muscle tissue. More specifically, aligned autografts will have greater functional recovery and myogenic activity and decreased fibrosis when compared to unaligned autografts. A rat model for VML will be used to assess the effect relative autograft alignment has on VML repair.(Wu, Corona, Chen, & Walters, 2012b) Functional recovery will be assessed through *in vivo* electrophysiological testing and repaired muscle mass which will be compared to contralateral unaffected limbs. Evidence of myogenesis and fibrosis will be ascertained using RT-PCR for quantitative measures of relative gene expression and histological analysis will be used for qualitative assessment of the regenerative response of the defected muscle. The two time points selected for this study will allow us to explore the initial fibrotic and

myogenic response to alignment or misalignment of an autograft and the long-term recovery outcomes for VML defected muscles repaired with aligned or unaligned autografts.

B. Methods

Animal Implantation

The implantation of 9 animals per group at 12 weeks was determined to be sufficient to detect a 15% increase in contractile force between treatment and control animals using a power analysis. This level of detection was designed to detect physiologically relevant and functionally meaningful increases in muscle contractile force. Pilot testing mean and standard deviation contractile force values (1.7 ± 0.3 N/kg and 1.4 ± 0.3 N/kg) collected from repaired and unrepaired VML-injured TA samples, respectively, were used for the 2 sample equivalence test.

Fischer 344 rats (Harlan, Indianapolis, IN), weighing approximately 300-325g were used as the animal model for all implantation studies. Surgical procedures and DSM implant preparation methods were performed in accordance with protocols approved by the University of Arkansas IACUC (protocol #14044) and guided by published methods (Wu, Corona et al. 2012, Kasukonis, Kim et al. 2016). Anesthesia was induced using isoflurane (1-3%) in oxygen. The implant site was surgically exposed through a 1-2 cm incision running parallel to the tibia. The TA was identified and a sterile surgical marker was used to draw a thin line indicating the dominant alignment of the myofibers. A partial thickness VML defect (8 mm diameter x 3 mm deep) was created using a sterile biopsy punch (Figure 2). The muscle tissue removed from the defect site was weighed (Average defect weight = 93.4 mg). Muscle defect mass values (20% of

TA mass) were based on pilot study TA muscle mass measurements (average TA mass = 470±17 mg). Animals were randomly assigned to one of three treatment groups at

Group 1: VML repaired with an aligned autograft

Group 2: VML repaired with a 45° unaligned autograft

Group 3: VML repaired with a 90° unaligned autograft

Muscle defect plugs were immediately implanted in the defect site and sutured in place with four interrupted stiches with 6-0 polypropylene sutures (Redilene, MYCO Medical, Cary, NC). The contralateral limb was left untreated to serve as an internal comparative control. The deeper fascia and surface skin layers were separately closed using an interrupted stich with a 5-0 absorbable suture (Vicryl, Ethicon, Summerville, MA). A single surgeon (BK) performed all implantation procedures including the preparation of MM autografts. Postoperative analgesia consisted of 0.1mg/kg buprenorphine administered subcutaneously via injection twice daily for two days. Animals also had access to the anti-inflammatory medication (Carprofen) via a single dietary gel cup (Medigel CPF, ClearH₂O, Westbrook, ME) added to each cage following surgery. Animal consumption of the gel was voluntary and any uneaten gel was removed from the cage at 1-week post surgery. Following surgery, animals were housed in standard-sized rat cages with unrestricted movement. The animals were allowed to bear weight on the operative extremity as tolerated. All animals were housed for a 2 or 12 week recovery period.

Contractile Force Measurement

At the completion of the assigned 2 or 12 week recovery period, the peak tetanic contractile force was measured in situ as described in Corona et al (Corona, Garg et al. 2013).

Animals were anesthetized and the lower limb was stabilized at 90° of knee flexion (tibia parallel to the benchtop) using a custom made alignment jig (Supplemental Figure 1). The ankle was flexed to 90° and the foot was secured (surgical tape) to the lever arm of a dual-mode muscle lever systems (Aurora Scientific, Ontario, Canada,). To isolate the contribution of the TA during force measurement, distal tenotomies were performed on the extensor digitorum longus (EDL) and extensor hallucis longus (EHL). TA peak isometric tetanic force was measured by stimulating the peroneal nerve with the aid of a physiological stimulator (Grass; S88). Optimal voltage (2 – 5 V) was determined using a series of tetanic contractions (150Hz, 0.1 ms pulse width, 400 ms train). Average peak tetanic force for each animal was calculated from an average of 5 contractions. All contractions were separated by one minute of rest. Raw peak tetanic contractile force (N) was recorded from both the treated and contralateral control limb of each animal and normalized to animal weight (N/kg). The weight normalized force data (N/kg) is reported in the results section. At the conclusion of electrophysiological testing and hindlimb muscle harvest, all animals were euthanized through a two-part procedure with 4% isoflurane to induce anesthesia followed by immediate carbon dioxide inhalation in accordance with guidelines provided by the 2013 AVMA Panel on Euthanasia of Animals.

Tissue Histology

Autograft repaired TA muscles along with contralateral untreated TA muscles were harvested and trimmed to remove the periosteum and tendon. EDL muscles were also collected and weighed for comparison between treated and contralateral control limbs. Muscles were rinsed in sterile PBS, dabbed dry, and then weighed. Muscles were then immediately flash frozen in liquid nitrogen cooled isopentane. 12 week frozen TA tissue samples (n=4/experimental

group) were sectioned (10 μ m) transversely through the mid-portion of the defect site with the aid of a cryostat. Sections were mounted onto microscopic slides and immuno-stained for the presence of collagen type III (α ColIII, 1:500, Abcam) followed by incubation in the appropriate fluorescently labeled secondary antibody (Alexfluor, 1:500, Life Technologies). These sections were analyzed using ImageJ to determine the average myofiber area. Other 12 week transverse sections were stained with H&E (VWR) using standard protocols. Tissue sections from 2 week time points were obtained by slicing the frontal plane of whole muscle. These 10 μ m sections were stained using a commercial Masson's Trichrome kit following manufacturers guidelines (Sigma). All sections were mounted onto microscope slides and digitally imaged. Treated sections were evaluated for myofiber formation and organization as well as the formation and extent of repair tissue formation for comparison to untreated contralateral muscle tissue sections.

Myogenesis and ECM Gene Expression

Real-time PCR was performed using the protocol described in Washington et al. (Washington, Brown et al. 2013) Tissue samples (approximately 30mg) collected from the defect/repair site (n=4/sample group/time point) were homogenized with Trizol (Ambion, Carlsbad, CA), chloroform (Sigma Aldrich, St. Louis, MO), and treated with DNase (Invitrogen, Carlsbad, CA). RNA was extracted using the RNeasy kit (Invitrogen, Carlsbad, CA). RNA concentration and purity was determined by UV spectrophotometry. RNA with a 260-to-280-nm ratio ≥ 1.8 was used for subsequent analysis. cDNA was reverse transcribed from 1 μ g of total RNA using the Superscript Vilo cDNA synthesis kit (Life Technologies, Carlsbad, CA, USA). cDNA was amplified in a 25 μ L reaction containing appropriate primer pairs and TaqMan Universal Mastermix (Applied Biosystems, Grand Island, NY). Commercially available TAQMAN primers (Invitrogen, Carlsbad, CA) for MyoD, Pax7, Timp-1, Collagen I, Collagen

III, TGF- β 1, MMP2, and 18s ribosomal housekeeping were used to quantify the expression of desired matrix and matrix regulatory genes. Samples were incubated at 95°C for 4 minutes, followed by 40 cycles of denaturation, annealing, and elongation at 95°C, 55°C, and 72°C, respectively. TaqMan fluorescence was measured at the end of the extension step each cycle. Experimental group samples were normalized to 18s and then referenced to the contralateral normal limb. Gene expression levels are reported as fold change using the $2^{-(\Delta \Delta Ct)}$ method.

Data Analysis

All data are represented by the mean and standard error unless noted. Data were tested for normality using the Shapiro-Wilk Test. Each time point was considered separately and no comparisons were made between treatment groups of different recovery times. Comparisons between treatment groups (Aligned, 45° Unaligned, and 90° Unaligned) for each of the outcome measures (peak force, muscle mass, and gene expression) were evaluated with a one-way ANOVA using a commercial statistical software package (JMP). Post hoc comparisons were made using Tukey's HSD. A standard 0.05 level of significance was used for all statistical tests.

C. Results

Defect Creation and Autograft Implantation

The defect creation and autograft implantation took approximately 40 minutes to complete. (Figure 2) All autograft treatment groups tolerated the implantation surgery well. All animals gained weight throughout the first two weeks at a rate of 7.1 ± 4.0 grams/week. Animals

gained an average of 7.2 ± 1.1 grams/week over the long-term recovery period (12 weeks). There were no signs of post-surgical infection. At one week post-implantation, all animals were fully ambulatory with no noticeable gait differences between groups. Carprofen dietary gel cups were typically consumed within the first 3 days of surgery (effective dosage (5/mg/kg/day)). All animals reached the assigned 2-week or 12-week study end point without complications.

Contractile Force Measurement

After the 2-week or 12-week recovery period, bilateral measurements of the isometric TA muscle tetanic contractile force were obtained. Tetanic contraction plots for all muscles were characterized by a sharp rise in force, followed by a plateau at the peak force, and then a return to a no force resting state (Figure 3). The average peak tetanic force produced by normal contralateral TA muscles was 2.5 ± 0.1 N/kg at 2 weeks post-implantation when normalized to animal mass and 2.5 ± 0.2 N/kg after 12 weeks. Following VML injury with aligned autograft repair, the average peak tetanic force dropped to 1.2 ± 0.2 N/kg after two weeks, which is equivalent to $48 \pm 8\%$ of normal contralateral TA muscles values, a statistically significant reduction ($p < 0.05$). However, after 12 weeks of recovery, muscles repaired with aligned autografts produced 1.8 ± 0.3 N/kg of force, representing $75 \pm 11\%$ of the peak tetanic contractile force of normal muscle. Following repair with 45° unaligned autografts, TA muscles produced an average contractile force of 1.3 ± 0.3 N/kg after two weeks, which represents $51 \pm 11\%$ of the peak force of the control muscle group. After 12 weeks, the muscles repaired with 45° unaligned autografts had 1.6 ± 0.2 N/kg of force when normalized to body mass, representing $64 \pm 10\%$ of force of normal muscle at the same time point. In response to repair with 90° unaligned autografts, the average peak tetanic force increased to only 1.5 ± 0.3 N/kg after 12 weeks of

recovery compared to 1.3 ± 0.3 N/kg of force at 2 weeks, which represents 61% and 53% of the force production of body mass normalized control muscle peak contractile force at the same time points.

Muscles harvested at 2 weeks of recovery showed remarkable morphological differences between all treatment groups and all treatment groups compared to the contralateral control muscles. (Figure 4) There was minimal fibrosis around the polypropylene stitches and no evidence of ineffective approximation of defect-autograft margins. Muscles repaired with a 90° unaligned autograft displayed the most deformity at the defect site. A fibrotic strip of tissue which occupied the entire defect vertically (8mm) and about 2-3mm in the horizontal direction was observed in all of the 90° unaligned autograft treatment group at 2 weeks post-implantation (Figure 4). The muscles repaired with the 45° unaligned autografts did not display any distinctive features, but the defect site appeared to be generally more disorganized and fibrotic than normal contralateral muscle. The defect site of muscles receiving the aligned autograft were closest to contralateral muscle at 2 weeks post-implantation and the margins of the autograft were just visible with the naked eye. For all muscles harvested following 12 weeks of recovery, there was no evidence of implant site infection or gross deformity at the treatment site. There was no obvious patterns of fibrosis in any of the treatment groups, although there appeared to be progressively more atrophy as degree of misalignment increased. The muscles repaired with aligned autografts appeared to have less atrophy at the treatment site and less disorganization overall when compared to the unaligned autograft repaired muscles. Although the aligned treatment group displayed evidence of repair at the defect site, treated muscle was remarkably similar to contralateral normal muscle. At 12 weeks post-implantation, 45° and 90° unaligned treatment groups were undistinguishable from each other and general appearance at the defect

site was characterized by degenerated tissue and disorder of myofibers. Aligned treatment animals had a body weight normalized average TA mass of 1.37 ± 0.1 g/kg at 2 weeks and 1.39 ± 0.1 g/kg at 12 weeks, which is $82\pm 5\%$ and $89\pm 7\%$ of the contralateral normal TA mass at the respective time points. Two weeks after defect creation and repair, TA muscle defects repaired with 45° unaligned autografts had an average normalized mass of 1.37 ± 0.1 g/kg, which is $82\pm 5\%$ of contralateral normal muscle mass and after 12 weeks the muscles had an average mass of 1.37 ± 0.1 g/kg, which is $88\pm 7\%$ of contralateral normal muscle mass when normalized to body weight. The group of TA muscles repaired with 90° unaligned autografts had an average mass of 1.30 ± 0.2 g/kg after 2 weeks and 1.35 ± 0.1 g/kg after 12 weeks, which is equivalent to $78\pm 9\%$ and $86\pm 8\%$ of contralateral normal values at the respective time points. All treatment group muscle masses were significantly decreased when compared to contralateral control groups of their respective time points ($p < 0.05$), but were not significantly different from other treatment groups of the same recovery length.

Six key genes associated with ECM structural proteins (collagen I and III), ECM regulatory cytokines (TGF- β 1, MMP2, and TIMP-1) and 2 genes related to myogenesis (MyoD & Pax7) were examined with the aid of rt-PCR. (Figure 5). The muscles recovered at two weeks post-implantation had an across the board upregulation of ECM associated genes for all treatment groups. For TGF- β expression, the fold change was 4.4 ± 0.8 , 2.6 ± 0.4 , and 3.3 ± 1.4 for aligned, unaligned 45° , and unaligned 90° , respectively. Collagen I expression in the autograft repaired muscles had the greatest fold change compared to normal muscle expression with aligned having 11.6 ± 4.2 fold change, unaligned 45° with a 8.1 ± 1.7 fold change, and unaligned 90° had a 12.0 ± 7.4 fold change. Collagen III expression in the autograft repaired muscles had significant increases compared to normal muscle expression with aligned having 9.1 ± 2.7 fold

change, unaligned 45° with a 7.5±1.8 fold change, and unaligned 90° had a 7.6±4.1 fold change. MMP2 had a significant increase in expression in all treatment groups compared to the uninjured control muscle expression levels with fold changes of 7.3±1.4, 6.6±1.4, and 6.5±2.9 for aligned, unaligned 45°, and unaligned 90°, respectively. Timp-1, an MMP inhibitor, also had significantly increased expression in all treatment groups compared to uninjured muscle expression with aligned having 10.2±3.5 fold change, unaligned 45° with a 7.9±2.1 fold change, and unaligned 90° had a 8.1±4.6 fold change. Alternatively, the aligned autograft repaired muscle group produced a statistically significant increase ($p < 0.05$) in the expression of MyoD with a fold change of 2.5±0.7 and of Pax7 with a fold change of 1.7±0.1 when compared to normal TA muscle samples. The unaligned repaired muscle expression did not have a significant difference with the uninjured TA expression of myogenic genes. After 12 weeks of recovery, the autograft repaired muscle did not have any significant difference in ECM or myogenic gene expression when compared to the relative expression of uninjured TA muscle.

At 2 weeks post-implantation, Masson's trichrome staining revealed signs of increased collagen deposition (blue staining) at the defect site in all treatment groups. The locations and amount of collagen varied between treatment groups. (Figure 6) Muscles repaired with aligned autografts had increased collagen at the margins of the defect but evidence of myofibers at the most interior parts of the autograft. Alignment of the myofibers appeared to be in-line with surrounding myofibers of the TA. Unaligned autograft repair led to an increase in collagen deposition when compared to the aligned repair. Unaligned 90° repaired muscles were the most fibrotic with defect sites characterized by disorganization and lack of myofibers. Collagen deposition was not limited to the defect site but was more prevalent through most of the muscle. Unaligned 45° repair had an intermediate amount of fibrosis at the defect site and there was

evidence of myofibers at the defect with alignment incongruent with the surrounding tissue orientation. As observed in the unaligned 90° repaired muscles, the unaligned 45° repair had evidence of increased collagen deposition beyond the margins of the defect. The defect sites all retained a small number of myofibers in the original implanted alignment.

At 12 weeks post surgery, the defect sites were detectable in histological sections prepared from all treatment groups. There was evidence of fibrotic tissue at the surface of the defect site for all treatment groups with little deviation between groups. (Figure 7) The average fiber diameter was not significantly different between groups, suggesting that any functional improvement observed in muscles repaired with aligned autografts was not due to hypertrophy. (Figure 7)

D. Discussion

The results from this study indicate that the alignment of an autograft has a significant effect on the regenerative response of the surviving muscle. By varying only the alignment of fibers relative to the damaged muscle, we ensured that only relative fiber alignment could generate differences between the treatment groups. After the creation of the VML injury and weighing the autograft, the autograft was immediately placed back into the defect site while the margins of the defected muscle were still bleeding. The autograft was aligned according to the relative angle between the TA myofibers and the myofibers of the autograft as indicated by the line drawn prior to defect creation. The alignment of the autografts was straightforward for the aligned and 90° treatment groups, the 45° treatment group was an intermediate treatment between the aligned and 90° groups. Although the angle was not measured, the intermediate

nature of the 45° treatment group would allow us to determine if the repair response was proportional to the relative alignment or, as was seen in contractile force measurements, histological analysis, and gene expression data, muscle only regenerated in response to aligned autografts and responded to any degree of misalignment with increased fibrosis and atrophy resulting in a functional deficit.

Polypropylene sutures served as anchors to maintain the relative alignment of the autografts and to allow for mechanical force transduction through the autograft and to the distal myofibers which were severed upon creation of the VML injury. Four sutures were determined to be the minimum required to preserve the prescribed alignment or misalignment while limiting the incidence of foreign body response and encapsulation by the host immune system, which is a concern for non-resorbable biomaterials.(Anderson et al., 2008) Polypropylene sutures were selected as they would provide consistent and effective mechanotransduction through the autograft. Mechanotransduction, the conversion of mechanical stimuli through tissue into biochemical signals by cells, is known to improve myogenesis *in vitro* and *in vivo*.(Boonen et al., 2010b; Martineau & Gardiner, 2001) Mechanotransduction may contribute to the response of the host skeletal and immune systems to therapeutic interventions with varying mechanical properties. Scaffolds and tissue constructs with mechanical properties incongruent to native skeletal muscle could deliver mechanical stimuli outside the thresholds necessary for myogenesis.(Courtney, Sacks, Stankus, Guan, & Wagner, 2006; Takaza, Moerman, Gindre, Lyons, & Simms, 2013)

The fibrotic strip observed in the gross morphological analysis of the 90° unaligned treatment group after 2 weeks of recovery provides evidence of ineffective skeletal muscle repair. Studying the formation and subsequent disappearance of this feature could facilitate an

investigation into the mechanisms by which relative misalignment affects the regenerative response of VML injured muscle. Although the fibrotic strip was not clearly visible with Masson's trichrome stain, other staining protocols may yield better results. The increased collagen deposition outside the margins of the defect may obfuscate a collagen-rich feature as was observed with the Masson's trichrome stained sections.

The significant upregulation of myogenic genes during the first 2 weeks of recovery and the near significant improvement in peak tetanic contractile force after 12 weeks, provides evidence that the relative alignment between an autograft and myofibers of a VML injured muscle is significant to the determination of a fibrotic or myogenic response by the damaged skeletal muscle. This cannot be extrapolated to conclude that a significant difference exists between the regenerative response to anisotropic scaffolds with mechanical properties similar to skeletal muscle, such as DSM,(Wilson et al., 2016) and to isotropic scaffolds, such as SIS or UBM. Evidence published recently suggests that there is no significant differences with respect to the regenerative capacity of repair with DSM compared to UBM, although the study used an abdominal wall model which does not have the same design requirements and challenges as extremity VML injury models with respect to volumetric repair and desired functional outcomes.(Wolf et al., 2012)

The results of RT-PCR give evidence of a transient remodeling phase which was present at 2 weeks as evidenced by the upregulation of ECM related genes in all treatment groups and a return to baseline levels of gene expression after 12 weeks of recovery. The significant upregulation of MyoD and the upward trend of Pax7 expression in VML defected muscles repaired with aligned autografts provides evidence that congruent alignment of a scaffold within a defect contributes to the myogenic response of the repaired tissue. There did not appear to be a

continuum of responses in gene expression with respect to the relative angle of misalignment. The unaligned scaffolds performed similarly to each other with upregulation of ECM related genes at the 2 week time point and a return to baseline levels after 12 weeks. The disorganization of the defect site in both unaligned treatment groups was evident at 2 and 12 weeks of recovery

The mechanisms by which alignment contributes to the regenerative response of host muscle after VML cannot be elucidated by the methods of this current study. Further studies at intermediate time points could track the facilitation or retardation of blood vessel in growth or the infiltration of the autograft by macrophages, muscle progenitor cells, and myofibroblasts. The use of GFP+ rats could provide a platform to investigate autograft fate, including cells and damaged myofibers, after being implanted into a volumetric defect. An autograft from the creation of a VML defect in a GFP+ rat could be implanted into the VML defect of a GFP- rat and the reverse could be performed simultaneously. The use of an inbred strain of rat, such as Fischer 344 rats, would eliminate the host rejection response and allow for innate regenerative responses to predominate over foreign cell immune reactions. There still exists a knowledge gap into the mechanisms that cause fibrosis at the defect site, yet allow for significant functional recovery. The hypothesis of a functional fibrotic repair deserves further exploration, especially exploring the muscle as a whole instead of limiting research simply to the defect site. The use of unaligned grafts may help clarify the fibrotic response the VML repair and help guide more effective strategies.

E. Conclusions

The key findings of this study suggest that:

1. VML defected TA muscles repaired with aligned autografts had improved peak tetanic force production over muscles repaired with unaligned autografts after 12 weeks of recovery.
2. There was no significant difference in TA mass between aligned and unaligned treatment groups at short-term or long-term recovery time points
3. At two weeks post-implantation, only muscles repaired with aligned autografts displayed increased expression of myogenic genes (MyoD & Pax7), while all treatment groups had increased expression of ECM/fibrotic genes (Col I, Col III, TGF- β , MMP2, and Timp-1)
4. By 12 weeks post-implantation, muscles had reached base line levels for all gene expression and were morphologically similar with respect to fibrosis at the surface of the defect site.
5. The differences seen histologically at 2 weeks of recovery between aligned and 90° unaligned autograft treated muscle warrant further study as to the mechanisms leading to a fibrotic vs. myogenic regenerative response.

References

- Ahadian, S., Ramon-Azcon, J., Ostrovidov, S., Camci-Unal, G., Kaji, H., Ino, K., . . . Matsue, T. (2013). A contactless electrical stimulator: Application to fabricate functional skeletal muscle tissue. *Biomedical Microdevices*, *15*(1), 109-115. doi:10.1007/s10544-012-9692-1; 10.1007/s10544-012-9692-1
- Anderson, J. M., Rodriguez, A., & Chang, D. T. (2008). Foreign body reaction to biomaterials. *Seminars in Immunology*, *20*(2) 86-100.
- Aubin, H., Nichol, J. W., Hutson, C. B., Bae, H., Sieminski, A. L., Crokek, D. M., . . . Khademhosseini, A. (2010). Directed 3D cell alignment and elongation in microengineered hydrogels. *Biomaterials*, *31*(27), 6941-6951.
- Awiss, K. J., Gough, J. E., & Downes, S. (2010). Aligned electrospun polymer fibres for skeletal muscle regeneration. *Euro. Cells and Mater.*, *19*, 193-204.
- Boonen, K. J., Langelaan, M. L., Polak, R. B., van der Schaft, Daisy WJ, Baaijens, F. P., & Post, M. J. (2010a). Effects of a combined mechanical stimulation protocol: Value for skeletal muscle tissue engineering. *Journal of Biomechanics*, *43*(8), 1514-1521.
- Boonen, K. J., Langelaan, M. L., Polak, R. B., van der Schaft, D. W., Baaijens, F. P., & Post, M. J. (2010b). Effects of a combined mechanical stimulation protocol: Value for skeletal muscle tissue engineering. *Journal of Biomechanics*, *43*(8), 1514-1521. doi:10.1016/j.jbiomech.2010.01.039; 10.1016/j.jbiomech.2010.01.039
- Choi, J. S., Lee, S. J., Christ, G. J., Atala, A., & Yoo, J. J. (2008). The influence of electrospun aligned poly(epsilon-caprolactone)/collagen nanofiber meshes on the formation of self-aligned skeletal muscle myotubes. *Biomaterials*, *29*(19), 2899-2906. doi:10.1016/j.biomaterials.2008.03.031; 10.1016/j.biomaterials.2008.03.031
- Cimetta, E., Pizzato, S., Bollini, S., Serena, E., De Coppi, P., & Elvassore, N. (2009). Production of arrays of cardiac and skeletal muscle myofibers by micropatterning techniques on a soft substrate. *Biomedical Microdevices*, *11*(2), 389-400.
- Courtney, T., Sacks, M. S., Stankus, J., Guan, J., & Wagner, W. R. (2006). Design and analysis of tissue engineering scaffolds that mimic soft tissue mechanical anisotropy. *Biomaterials*, *27*(19), 3631-3638.
- Donnelly, K., Khodabukus, A., Philp, A., Deldicque, L., Dennis, R. G., & Baar, K. (2010). A novel bioreactor for stimulating skeletal muscle in vitro. *Tissue Engineering. Part C, Methods*, *16*(4), 711-718. doi:10.1089/ten.TEC.2009.0125; 10.1089/ten.TEC.2009.0125
- Flaibani, M., Boldrin, L., Cimetta, E., Piccoli, M., Coppi, P. D., & Elvassore, N. (2009). Muscle differentiation and myotubes alignment is influenced by micropatterned surfaces and exogenous electrical stimulation. *Tissue Engineering Part A*, *15*(9), 2447-2457.

- Grogan, B. F., Hsu, J. R., & Skeletal Trauma Research Consortium. (2011). Volumetric muscle loss. *The Journal of the American Academy of Orthopaedic Surgeons*, *19 Suppl 1*, S35-7. doi:19/suppl_1/S35 [pii]
- Grossi, A., Yadav, K., & Lawson, M. A. (2007). Mechanical stimulation increases proliferation, differentiation and protein expression in culture: Stimulation effects are substrate dependent. *Journal of Biomechanics*, *40*(15), 3354-3362.
- Huang, N. F., Lee, R. J., & Li, S. (2010a). Engineering of aligned skeletal muscle by micropatterning. *American Journal of Translational Research*, *2*(1), 43-55.
- Huang, N. F., Lee, R. J., & Li, S. (2010b). Engineering of aligned skeletal muscle by micropatterning. *American Journal of Translational Research*, *2*(1), 43-55.
- Kaar, J. L., Li, Y., Blair, H. C., Asche, G., Koepsel, R. R., Huard, J., & Russell, A. J. (2008). Matrix metalloproteinase-1 treatment of muscle fibrosis. *Acta Biomaterialia*, *4*(5), 1411-1420.
- Karalaki, M., Fili, S., Philippou, A., & Koutsilieris, M. (2009). Muscle regeneration: Cellular and molecular events. *In Vivo (Athens, Greece)*, *23*(5), 779-796. doi:23/5/779 [pii]
- Kjaer, M. (2004). Role of extracellular matrix in adaptation of tendon and skeletal muscle to mechanical loading. *Physiological Reviews*, *84*(2), 649-698. doi:10.1152/physrev.00031.2003 [doi]
- Lam, M. T., Huang, Y. C., Birla, R. K., & Takayama, S. (2009). Microfeature guided skeletal muscle tissue engineering for highly organized 3-dimensional free-standing constructs. *Biomaterials*, *30*(6), 1150-1155. doi:10.1016/j.biomaterials.2008.11.014; 10.1016/j.biomaterials.2008.11.014
- Langelaan, M. L., Boonen, K. J., Rosaria-Chak, K. Y., van der Schaft, Daisy WJ, Post, M. J., & Baaijens, F. (2011). Advanced maturation by electrical stimulation: Differences in response between C2C12 and primary muscle progenitor cells. *Journal of Tissue Engineering and Regenerative Medicine*, *5*(7), 529-539.
- Li, M. T. A., Willett, N. J., Uhrig, B. A., Guldborg, R. E., & Warren, G. L. (2014). Functional analysis of limb recovery following autograft treatment of volumetric muscle loss in the quadriceps femoris. *Journal of Biomechanics*, *47*(9), 2013-2021.
- Lieber, R. L., & Friden, J. (2000). Functional and clinical significance of skeletal muscle architecture. *Muscle & Nerve*, *23*, 1647-1666.
- Martineau, L. C., & Gardiner, P. F. (2001). Insight into skeletal muscle mechanotransduction: MAPK activation is quantitatively related to tension. *Journal of Applied Physiology (Bethesda, Md.: 1985)*, *91*(2), 693-702.

- Merritt, E. K., Cannon, M. V., Hammers, D. W., Le, L. N., Gokhale, R., Sarathy, A., . . . Farrar, R. P. (2010). Repair of traumatic skeletal muscle injury with bone-marrow-derived mesenchymal stem cells seeded on extracellular matrix. *Tissue Engineering.Part A*, *16*(9), 2871-2881. doi:10.1089/ten.TEA.2009.0826; 10.1089/ten.TEA.2009.0826
- Meyer, G. A., & Lieber, R. L. (2011). Elucidation of extracellular matrix mechanics from muscle fibers and fiber bundles. *Journal of Biomechanics*, *44*(4), 771-773.
doi:<http://dx.doi.org/10.1016/j.jbiomech.2010.10.044>
- Nishimura, T., Nakamura, K., Kishioka, Y., Kato-Mori, Y., Wakamatsu, J., & Hattori, A. (2008). Inhibition of matrix metalloproteinases suppresses the migration of skeletal muscle cells. *Journal of Muscle Research and Cell Motility*, *29*(1), 37-44.
- Perniconi, B., Costa, A., Aulino, P., Teodori, L., Adamo, S., & Coletti, D. (2011). The pro-myogenic environment provided by whole organ scale acellular scaffolds from skeletal muscle. *Biomaterials*, *32*(31), 7870-7882. doi:10.1016/j.biomaterials.2011.07.016; 10.1016/j.biomaterials.2011.07.016
- Powell, C. A., Smiley, B. L., Mills, J., & Vandeburgh, H. H. (2002). Mechanical stimulation improves tissue-engineered human skeletal muscle. *American Journal of Physiology.Cell Physiology*, *283*(5), C1557-65. doi:10.1152/ajpcell.00595.2001 [doi]
- Shimizu, K., Fujita, H., & Nagamori, E. (2009). Alignment of skeletal muscle myoblasts and myotubes using linear micropatterned surfaces ground with abrasives. *Biotech. and Bioeng.*, *103*, 631-638.
- Siegel, A. L., Atchison, K., Fisher, K. E., Davis, G. E., & Cornelison, D. (2009). 3D timelapse analysis of muscle satellite cell motility. *Stem Cells*, *27*(10), 2527-2538.
- Takaza, M., Moerman, K. M., Gindre, J., Lyons, G., & Simms, C. K. (2013). The anisotropic mechanical behaviour of passive skeletal muscle tissue subjected to large tensile strain. *Journal of the Mechanical Behavior of Biomedical Materials*, *17*, 209-220.
- Tidball, J. G., Lavergne, E., Lau, K. S., Spencer, M. J., Stull, J. T., & Wehling, M. (1998). Mechanical loading regulates NOS expression and activity in developing and adult skeletal muscle. *The American Journal of Physiology*, *275*(1 Pt 1), C260-6.
- Vandeburgh, H. H., & Karlisch, P. (1989). Longitudinal growth of skeletal myotubes in vitro in a new horizontal mechanical cell stimulator. *In Vitro Cellular & Developmental Biology*, *25*(7), 607-616.
- Wang, L., Wu, Y., Guo, B., & Ma, P. X. (2015). Nanofiber yarn/hydrogel Core-Shell scaffolds mimicking native skeletal muscle tissue for guiding 3D myoblast alignment, elongation, and differentiation. *ACS Nano*, *9*(9), 9167-9179.

Wang, L., Johnson, J. A., Chang, D. W., & Zhang, Q. (2013). Decellularized musculofascial extracellular matrix for tissue engineering. *Biomaterials*, 34(11), 2641-2654. doi:<http://dx.doi.org/10.1016/j.biomaterials.2012.12.048>

Wilson, K., Terlouw, A., Roberts, K., & Wolchok, J. C. (2016). The characterization of decellularized human skeletal muscle as a blueprint for mimetic scaffolds. *Journal of Materials Science: Materials in Medicine*, 27(8), 1-15.

Wolf, M. T., Daly, K. A., Reing, J. E., & Badylak, S. F. (2012). Biologic scaffold composed of skeletal muscle extracellular matrix. *Biomaterials*, 33(10), 2916-2925. doi:10.1016/j.biomaterials.2011.12.055

Wu, X., Corona, B. T., Chen, X., & Walters, T. J. (2012). A standardized rat model of volumetric muscle loss injury for the development of tissue engineering therapies. *BioResearch Open Access*, 1(6), 280-290. doi:10.1089/biores.2012.0271; 10.1089/biores.2012.0271

Acknowledgments:

Research reported in this publication was supported by the National Institute Of Arthritis And Musculoskeletal And Skin Diseases of the National Institutes of Health under Award Number R15AR064481 and the Arkansas Biosciences Institute.

Author Disclosure Statement:

No competing financial interests exist for any of the authors.

Figure Legend

Figure 1: Experimental abstract. A VML defect was created in the left TA of Fisher 344 rats. The defect was repaired with autografts from one of three treatment groups: Aligned, 45°, or 90°. Autografts were secured in place with polypropylene sutures to maintain prescribed alignment. Animals were assigned to one or two recovery periods, 2 weeks (n=6/group) or 12 weeks (n=9/group). Electrophysiological data was collected for both the repaired TA muscle and the contralateral control TA muscle. TA muscles were harvested, weighed, and prepared for RT-PCR or histological analysis.

Figure 2: Surgical procedure. A ~1.5cm incision parallel to tibia was made in the left hind limb of Fischer 344 rats (A). The skin and fascia was dissected to reveal the TA and a mark was drawn onto the TA with a sterile surgical marker to indicate the direction of the myofiber alignment (B). An 8mm biopsy punch was used to create a volumetric defect in the TA. A PDMS ring was used to ensure a defect depth of 3mm (C). The defect plug was weighed and then placed into defect as an autograft at the assigned alignment (90° unaligned pictured) (D). The autograft was sutured in place using polypropylene sutures to maintain appropriate alignment or misalignment (E). The wound was closed using double layer closure of the fascia and skin utilizing absorbable sutures with interrupted stitches (F).

Figure 3: Electrophysiological data. Contraction of the TA was induced by stimulating the peroneal nerve. Force was measured by securing the foot to the foot plate of a force transducer. The average percent recovery (A) for the three treatment groups at the two time points along

with the body weight normalized (N/kg) mean peak tetanic force produced (B) is shown for the three treatment groups and control TA muscles at the two recovery time points. A representative force profile for each treatment group is shown (C). $n = 6/\text{group}$ at 2 weeks and $n = 9/\text{group}$ at 12 weeks. Values are mean + SD.

Figure 4: Gross morphology. Representative samples of the autograft repaired muscles are shown immediately after being secured into the VML defect ($t = 0$) and after being harvested at either 2 or 12 weeks for each of the three treatment groups: Aligned, 45° , or 90° (A). TA muscles were harvested, weighed, and the mass was normalized to body weight (g/kg) for each of the treatment groups (B). $n = 6/\text{group}$ at 2 weeks and $n = 9/\text{group}$ at 12 weeks. Values are mean + SD. * indicates significant difference from the body weight normalized control TA at the same time point. ($p < 0.05$ with ANOVA with Tukey's HSD)

Figure 5: Gene expression. RT-PCR was used to determine the relative expression of ECM related structural proteins and regulatory factors Collagen I and III, TGF β , MMP2, Timp1 and myogenic markers MyoD and Pax7. $n = 4/\text{group}$ at 2 weeks and $n = 4/\text{group}$ at 12 weeks. Values are mean + SE. * indicates significant difference from the relative expression of that gene for the control TA at the same time point. ($p < 0.05$ with ANOVA with Tukey's HSD)

Figure 6: Histology. Representative whole muscle sections of autograft repaired TA muscles at 2 weeks stained with Masson's trichrome for aligned (A), 45° (B), 90° (C). Representative samples stained with Masson's trichrome showing relative alignment of autograft still present at

2 weeks for aligned (D), 45° (E), 90° (F). * indicates myofibers still in their implanted alignment. Black scale bar = 1mm. White scale bar = 100µm.

Figure 7: Long-term recovery. Representative transverse sections at the surface of the defect site of muscle repaired with aligned (A), 45° unaligned (B), and 90° unaligned (C) autografts stained with H&E. Representative transverse sections of muscle repaired with aligned (D), 45° unaligned (E), and 90° unaligned (F) autografts immunostained for Collagen III. Average myofiber area (G). Values are mean + SD. Black scale bar = 100µm. White scale bar = 100µm.

Figures

3 experimental groups

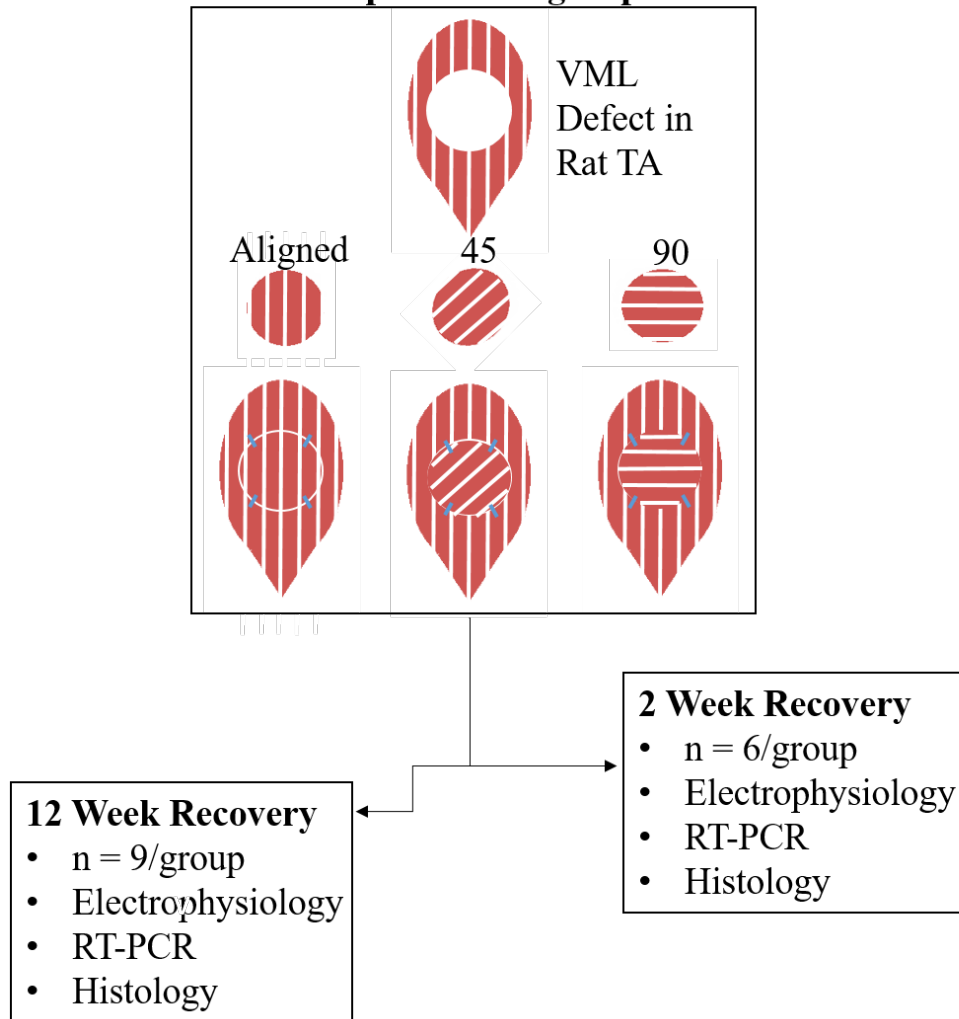


Figure 1

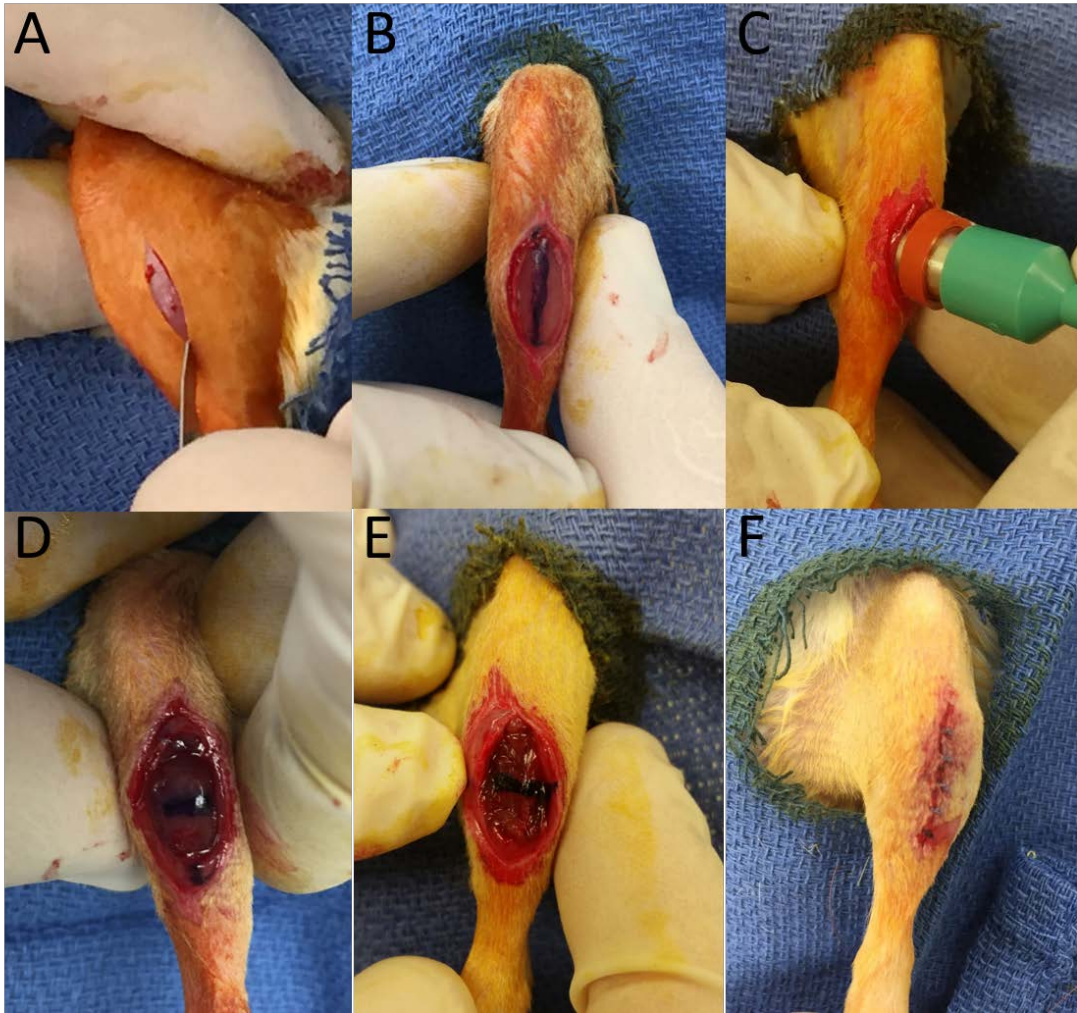


Figure 2

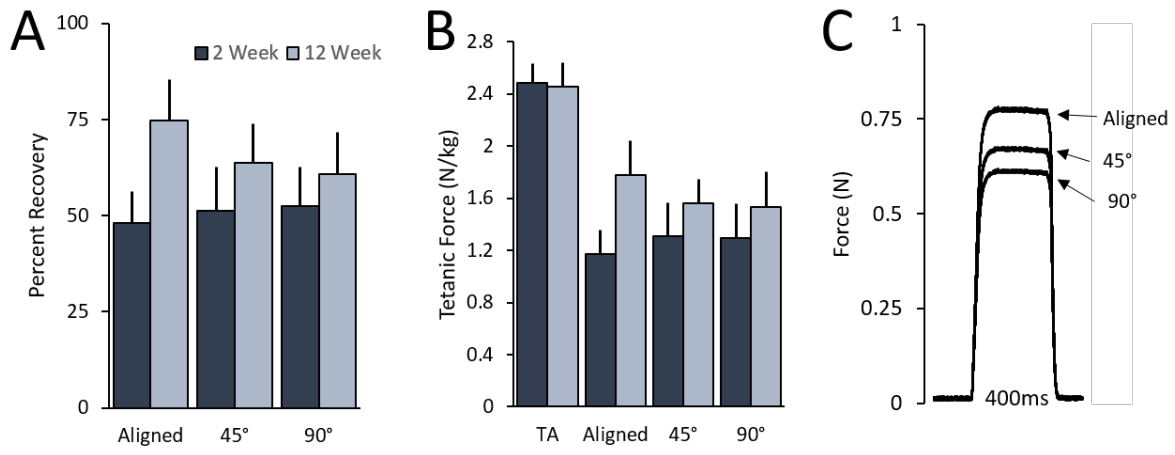


Figure 3

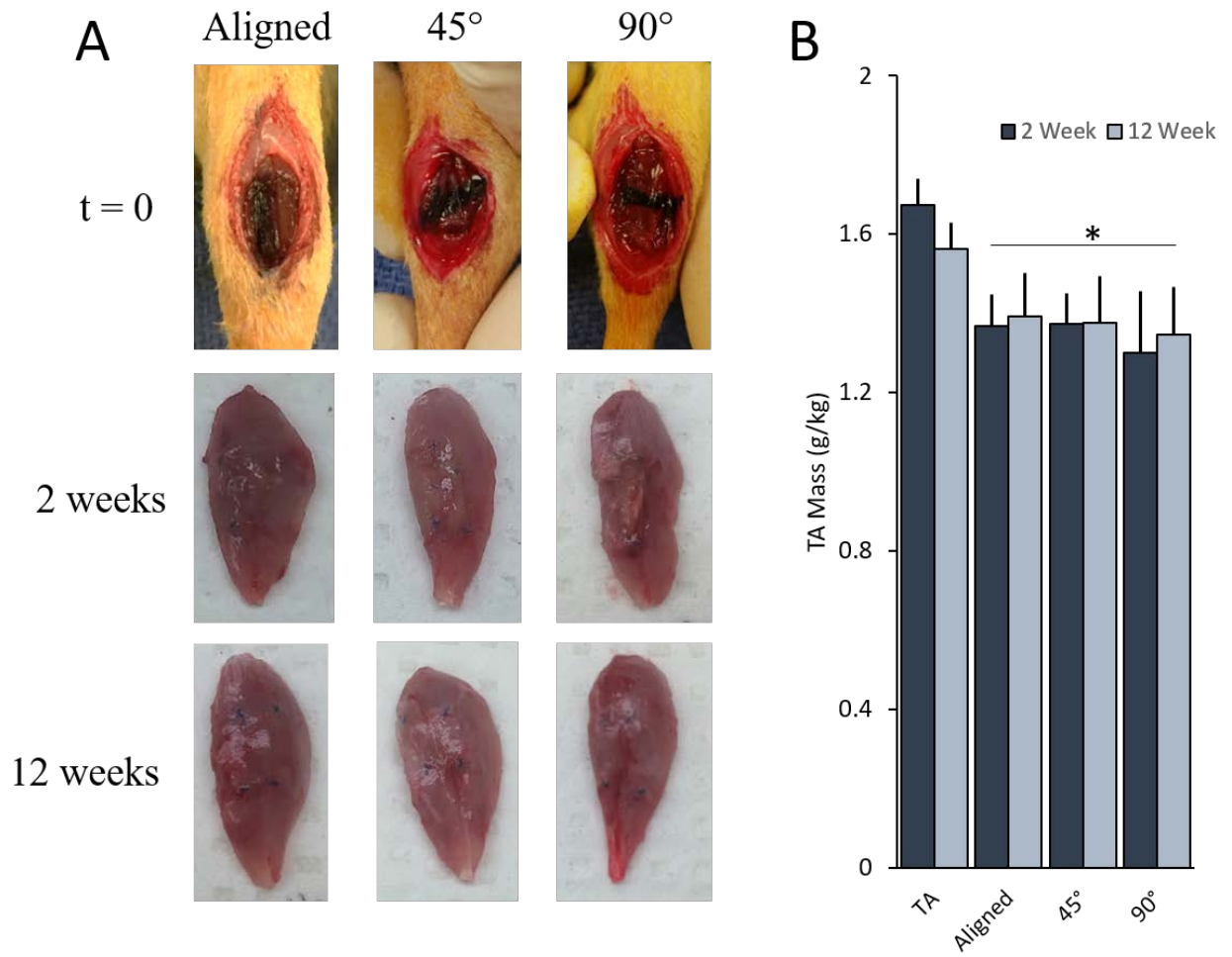


Figure 4

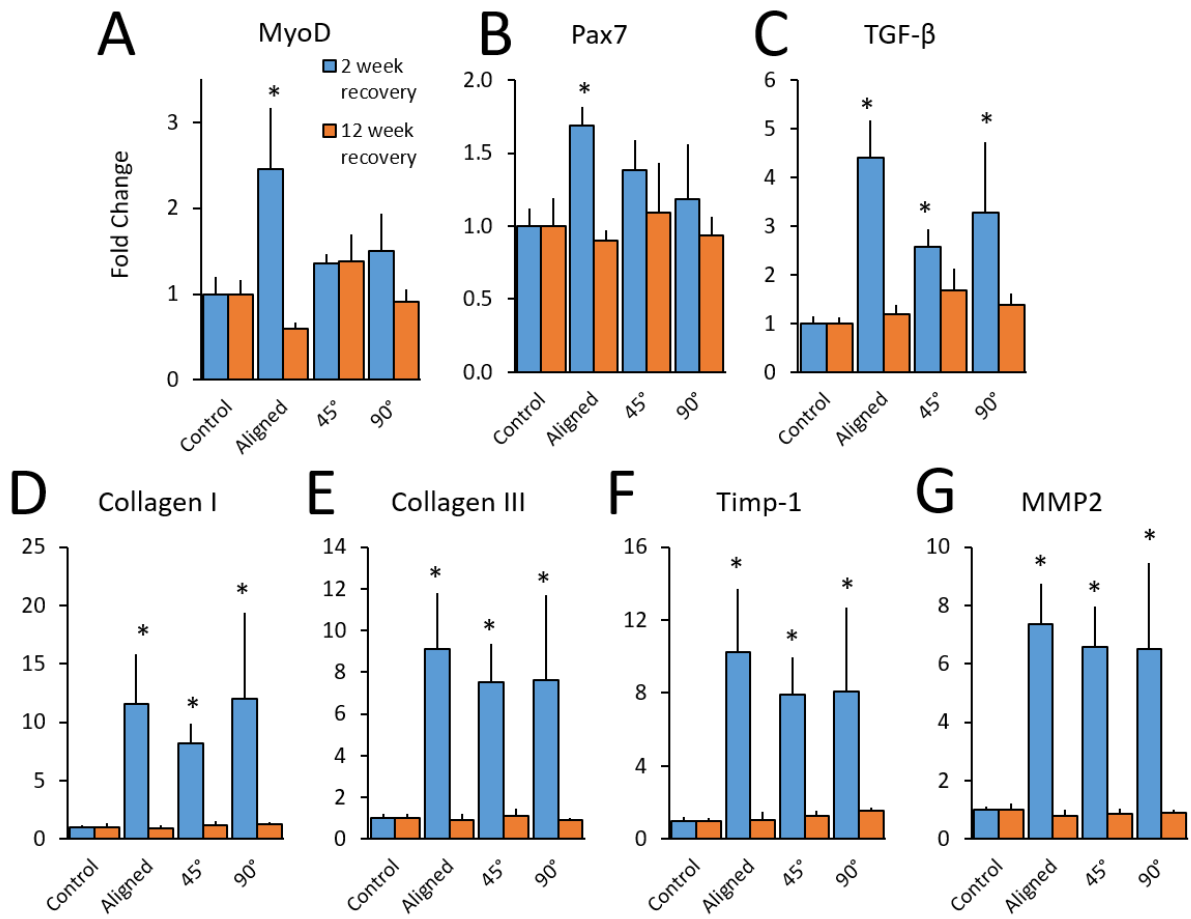


Figure 5

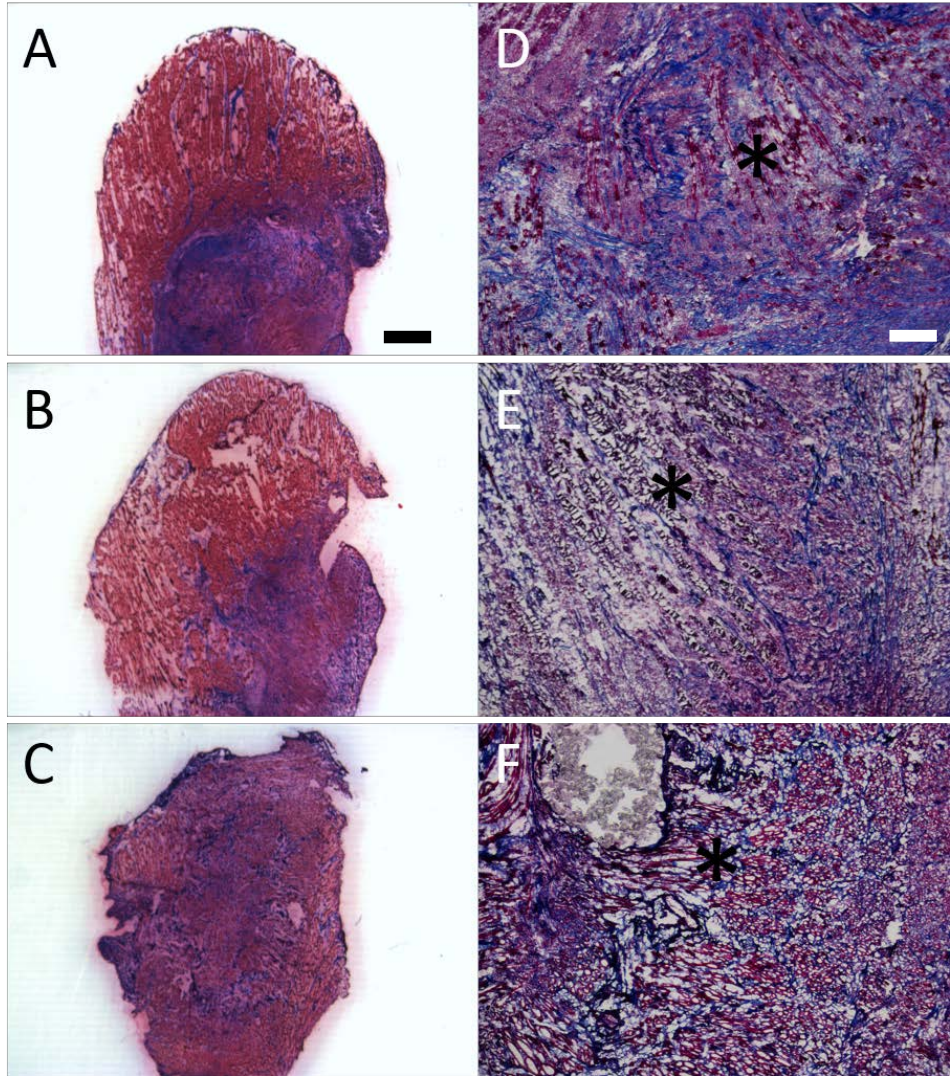


Figure 6

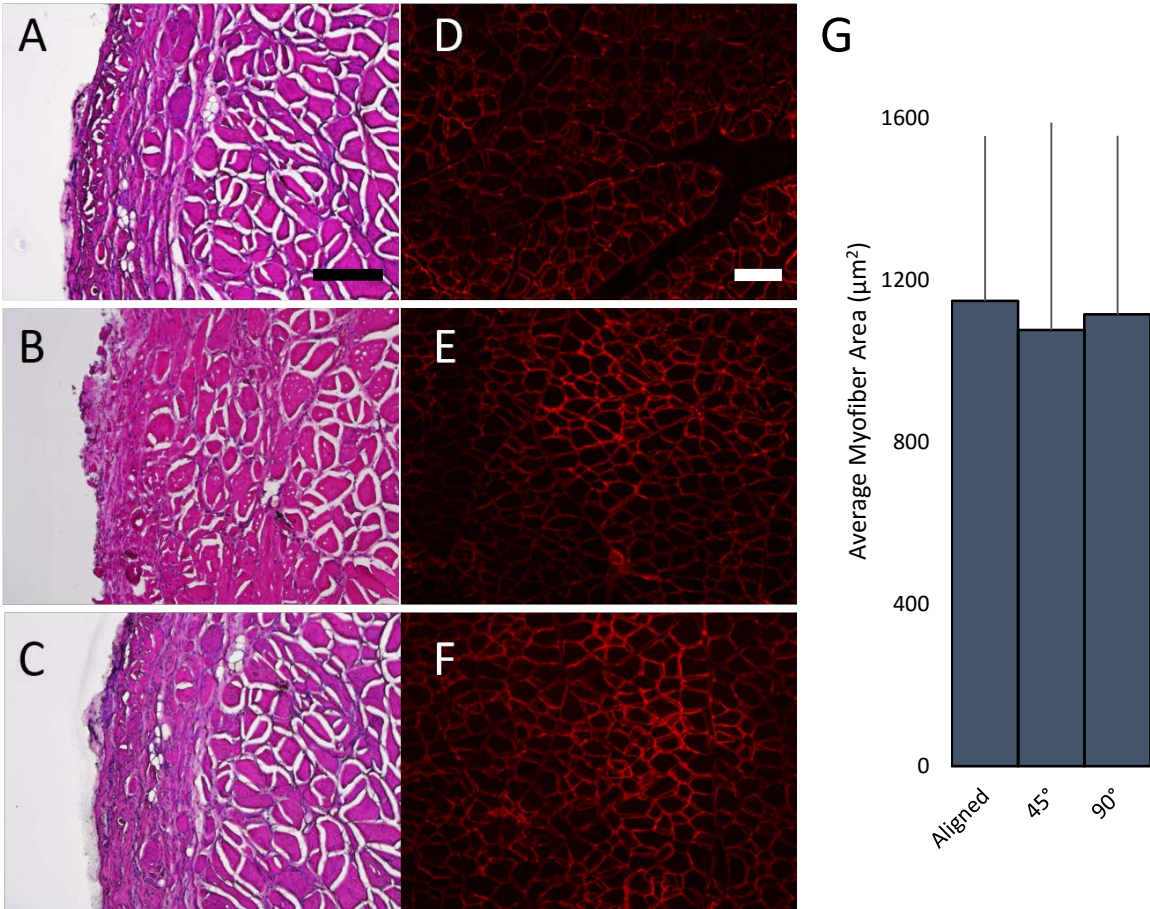


Figure 7

Chapter 5

Conclusion

A. Evaluation of Muscle Regeneration

Skeletal muscle tissue engineering is still a relatively new field within biomedical research, although evidence of initial explorations into the plasticity and “repairability” of muscle date back more than a century.(Bursac et al., 2015; Thompson, 1971) The fact that physicians still have few options when it comes to repairing VML necessitates further innovation. The most successful strategies so far have combined scaffold and cell-based approaches to deliver a construct that directs innate repair mechanisms towards a myogenic response rather than fibrosis.(Aurora et al., 2015; Merritt et al., 2010; Page et al., 2011; Ward et al., 2015) Moving forward, researchers should first start with a consensus of what constitutes success in a strategy or technique to improve tissue regeneration after muscle trauma.

Contractile force measurements

The first and primary measure of success in skeletal muscle repair must be anchored in the contractility of the repaired tissue. Skeletal muscle without contractility ceases to perform its role within the human body and eventually develops into fibrotic tissue. Cosmetic appearances are certainly important from a clinical perspective and improvements in patient satisfaction after a traumatic injury are needed.(Mase et al., 2010) Likewise, other parameters used to evaluate skeletal muscle repair and regeneration after traumatic injury, such as histological and biomolecular measurements and observations, are very important from a research standpoint as they allow investigators to elucidate mechanisms involved in the repair process and serve as

snapshot of a certain aspect of regeneration. However, the priority needs to be placed on the functional recovery from a traumatic injury that negatively impacts the patient's freedom and quality of life.

There are several methods for measuring contractile force in animal models and human patients. In animal models there seems to be a consensus around the use of *in vivo* or *in situ* peak tetanic contractile force as adequate measure of skeletal muscle function.(Corona, Ward, Baker, Walters, & Christ, 2013; Grasman, Do, Page, & Pins, 2015; Han et al., 2016; M. T. A. Li, Willett, Uhrig, Guldberg, & Warren, 2014b; Merritt et al., 2010; Mintz, Passipieri, Lovell, & Christ, 2016; Page et al., 2011; Valentin, Turner, Gilbert, & Badylak, 2010) Peak tetanic contractile force is obtained by immobilizing the joint proximal to the defected muscle and electrodes are positioned to stimulate the nerve responsible for innervating the muscle of interest. The appendage distal to the defected muscle is secured to a force transducer and when the muscle is stimulated using parameters known to induce peak contraction, the force produced by the muscle is measured. Peak tetanic contractile force is not the only *in vivo* measure of force used, other studies have used twitch force(Han et al., 2016) and others have selected fatigue testing.(Corona et al., 2013b; M. T. A. Li et al., 2014b) All protocols produce physiological relevant data for evaluating the functional recovery of muscle from a VML injury.

Histology

Histological data provides researchers with data to elucidate spatial differences in VML animal repair models. Direct measurements of morphological features and physiological adaptations to the VML repair microenvironment are possible through thin sectioning of repaired

skeletal muscle tissue. Appropriate staining protocols and visualization techniques allow researchers to investigate the following broad categories: myogenesis, fibrosis, vascularization, and innervation. Protocols for the histological analysis of *in vivo* myogenesis include immunofluorescent stains for transcription factors such as Pax7, MyoD, and Ki67, and for sarcomeric features such as embryonic-myosin heavy chain. Another technique for determining myogenic activity is to observe sections for centrally located nuclei and other morphological features indicative of differentiating muscle progenitor cells. Fibrosis within histological samples can be determined through any staining protocol that locates the deposition of collagen and other ECM constituents. The presence of collagen can be observed with techniques for brightfield microscopy such as Masson's trichrome or immunohistochemical staining. Immunofluorescence can also be used to locate collagen. If care is taken to ensure that thin muscle sections have exact exposure times (i.e. batch processing), quantitative data can be obtained from these histological techniques.

Biomolecular Response

Another area of methods for gathering quantitative and qualitative data in the field of skeletal muscle tissue engineering and regenerative medicine is to use protocols that provide data on the biomolecular response of skeletal muscle tissue. The techniques could broadly include: Western blotting, ELISA, biomolecular assays, RT-PCR, and gel electrophoresis. While Western blots, gel electrophoresis, and ELISA techniques are not typically found in studies concerned with investigating VML repair, RT-PCR is used in many studies to give researchers evidence of cellular responses to regenerative therapies. Most published papers in the field generally examine genes related to fibrosis (Collagen I & III, TGF- β , MMP1 & 2 & 9, Timp-1, CTGF) and

myogenesis (MyoD, myogenin, Myf5, Pax3, Pax7). RT-PCR is an excellent tool to facilitate investigations into the mechanisms of repair in skeletal muscle since it provides researchers with snapshots of cellular activity at the prescribed timepoint.

Effect of Age

Almost all studies investigating skeletal muscle after VML in a rat model have been performed on young (< 6 months old) rats. There has only been one study involving VML in an aged rat model.(J. T. Kim, Kasukonis, Brown, Washington, & Wolchok, 2016) Regeneration after VML was markedly decreased for all aged animals and preliminary results have shown that DSM +MM repaired muscles had no significant improvements in contractile force recovery compared to VML controls. Studies have suggested the decrease in the regenerative capacity of satellite cells in aged muscle is due to age-related changes in the microenvironment of the muscle and not necessarily due to age-related changes intrinsic to the cell.(Conboy, Conboy, Smythe, & Rando, 2003; Conboy et al., 2005) Further studies should be performed in aged animal VML models to validate techniques that have demonstrated success in younger animal models.

B. Further Characterization

A study presented previously in this dissertation used DSM and MM together as a construct for skeletal muscle regeneration after VML. Previous studies have shown that a DSM

scaffold alone and a MM autograft made up of 25% of the defect volume with enough collagen gel to completely fill the defect were not effective treatments for inducing muscle regeneration in animal VML models.(Kasukonis et al., 2016; Sicari et al., 2014; Ward et al., 2015) In addition to determining the optimal ratio of DSM:MM to repair VML, further work should be done to investigate each constituent for more complete characterization and to ensure future clinical studies have maximum regenerative potential.

Advantages of DSM

Although it has been established that DSM or any other acellular scaffold alone is not sufficient to regenerate skeletal muscle after VML, DSM can be a component in an effective strategy for repairing VML.(Kasukonis et al., 2016; Merritt et al., 2010) DSM maintains an advantage over other acellular ECM scaffolds in that DSM is composed of aligned ECM, contains skeletal muscle specific ECM-bound growth factors, and cadaveric skeletal muscle is plentiful. With techniques similar to the one outlined previously in this dissertation, production of DSM scaffolds for large VML injuries would be possible.(Kasukonis, Kim, Washington, & Wolchok, 2016) There are still several studies that should be performed to further characterize DSM, not only as a scaffold but as a template for engineered ECM constructs that by using ECM harvested from cell cultures, would eliminate the need for donor tissue.(Hurd, Bhatti, Walker, Kasukonis, & Wolchok, 2015)

These future avenues of research include determining if the source of the ECM has any effect on the regenerative response of the host tissue. Previous studies have shown that there are differences in the starting composition of ECM derived from different muscles, but the challenge

is to discover if those differences correspond to increased or decreased regenerative potential. Another question that needs to be answered is, does the degradation of ECM scaffolds before they are implanted have any effect on their regenerative potential in the context of VML repair. Decellularization protocols have been developed to lessen the degradation of ECM during the process of lysing and stripping cells, but does that matter in the VML wound niche?(Gillies et al., 2010) During the initial inflammatory response, macrophages will dismantle the donor ECM as remodeling begins within the wound site. If the scaffold has been preconditioned with various levels of degradation, will the remodeling response follow more myogenic or more fibrotic pathways? Conversely, can the ECM scaffold be “functionalized” with growth factors in order to affect the regenerative response of the host tissue? Continued exploration along these lines could help push scaffold based therapies from 80-85% force recovery to 90-95% recovery. In summary, even though in isolation DSM scaffolds will not generate an effective myogenic response, further improvements to the scaffold should be investigated.

Advantages of MM

The use of MM as a constituent in a repair strategy appears to be the most promising method of delivering cells and physiological cues to the site of VML.(Corona et al., 2013b; Kasukonis et al., 2016) Autologous MM has an advantage over any allogeneic cell transplant in that it does not require immunosuppressant drugs. It has an advantage over any isolated autologous stem cell line because it is as close to off-the-shelf as cells can be with current technologies. Most surgical suites do not contain the necessary apparatus for cell culture. In addition, and more importantly, isolation and proliferation of a stem cell line would require a preliminary procedure to harvest cells and several days or weeks to isolate the stem cells and

expand them to a therapeutic level. This additional procedure to harvest cells could lead to increased chance of infection and patient discomfort. Conversely, harvesting and mincing tissue is certainly within the current skillset of surgeons and nurses within an operating room and could be a procedure that is performed with concurrent to VML repair.(Ward et al., 2016) MM should also be preferred to isolated stem cells or other muscle progenitor cells because it also delivers pro-inflammatory and pro-myogenic factors to the defect site at the time of implantation. The studies completed by the US Army Institute of Surgical Research team have shown the response of surviving tissue to MM autografts is favorable for *de novo* formation of myofibers in the defect area.(Corona et al., 2013b; Ward et al., 2015) Several questions remain regarding the characterization of the initial MM but also the spatiotemporal response of the surviving muscle and immune system to the MM autograft. Much as the innate regenerative processes of muscle can be broken down into timelines of minutes and hours, then days and weeks, the response of the initial immune and long-term fibrotic vs. myogenic remodeling that follows implantation should be further studied. Evidence presented earlier in this dissertation indicates that even though MM appears to induce myogenesis there appears to be long-term upregulation of genes associated with fibrosis.(Kasukonis et al., 2016) MM has already shown potential as an autograft and further characterization could potentially lead to a reduced donor volume being necessary if scaffolds could be preconditioned with growth factors or cytokines after their relative importance to muscle regeneration in a VML injury niche is determined.

Other studies should explore the effect the location of source muscle has on the regenerative capacity of MM. Related studies must be done to determine the most effective harvesting technique. One possibility is maximize the amount of donor tissue while minimizing donor site morbidity or fibrosis could be to “mesh” biopsy a donor muscle similar to methods

used to prepare autologous skin grafts.(Tanner, Vandeput, & Olley, 1964) Instead of taking a smaller surface of skin and meshing it to stretch to the desired surface area, donor muscle would be left in place and several small volume biopsies could be taken to give the desired quantity.

This leads to the next avenue of inquiry: What is the smallest biopsy that can be taken from a muscle such that it suffers no long-term negative effects? A recent study to investigate the regenerative potential of isolated MSC delivered with a fibrin glue inadvertently found that a 5mm biopsy from the TA of a rat was insufficient to produce an irrecoverable defect.(Pereira et al., 2014) When force measurements were obtained 35 days after the creation of a defect, there was no significant difference between the peak tetanic force produced by the defected muscle and uninjured muscle.(Pereira et al., 2014) Of course further studies should be performed to determine if multiple biopsies from a donor muscle will afford researchers enough donor MM without any deleterious effects on the donor tissue.

Effects of Alignment

Although micropatterning and aligned engineered scaffolds induce myoblast and myofiber alignment under *in vitro* conditions, (Avis et al., 2010; Choi et al., 2008b; Hinds, Bian, Dennis, & Bursac, 2011; Huang et al., 2010b; Lam et al., 2009) it has been demonstrated that mechanical and electrical stimuli also produce aligned myofibers under the same conditions.(Boonen et al., 2010b; Donnelly et al., 2010; Langelaan et al., 2011; Pennisi, Olesen, de Zee, Rasmussen, & Zachar, 2011; Tatsumi, 2010; Vandeburgh & Karlisch, 1989)

One aspect about the effect of fiber alignment on skeletal muscle repair that needs to be determined is whether the location of the defect has any bearing on how much alignment matters.

Many of the studies that used porcine SIS and other scaffolds with no alignment seem to have success repairing abdominal wall defects.(Prevel et al., 1995; Valentin et al., 2010) While this could be due to the “functional fibrosis” described by a different group, it could also be due to the location of the injury.(Corona et al., 2013a) If abdominal wall injuries and extremity muscle injuries respond differently to fiber alignment, more specific strategies could be developed to suit each injury niche.

C. Future Directions for VML

Rehabilitation

When human patients suffer musculoskeletal trauma, the standard of care in almost all cases involves physical rehabilitation. However, post-implantation protocols in small animal models do not consistently include exercise such as voluntary running wheels. Some studies have included physical rehabilitation in both VML model and in stem cell based interventions for myopathies such as DMD.(Ambrosio et al., 2009; Bouchentouf, Benabdallah, Mills, & Tremblay, 2006; Corona et al., 2013b) Rehabilitation was shown to improve outcomes in the cases of stem cell transplants and there were mixed results with the exercise treatment group in the VML animal model.

A different study indirectly highlights the effect rehabilitation can have on muscle that suffers traumatic injury. A murine model in which myotoxin-induced direct muscle damage and hind limb ischemia were used for skeletal muscle trauma.(Cezar et al., 2016) Cyclic mechanical compression was applied through a pressure cuff or a biphasic ferrogel scaffold which was

implanted at the injection site of myotoxin and actuated with an external permanent magnet. Decreased fibrosis and increased oxygen perfusion was reported in the muscle treated with the biphasic ferrogel scaffold.(Cezar et al., 2016) Although the study did not make comparisons to normal muscle, the authors did report a two fold increase in contractile force when compared to injured muscle that did not receive any therapeutic interventions.(Cezar et al., 2016) This study was not performed in a VML model, however, cyclic mechanical compression through a biphasic ferrogel scaffold could potentially be used to decrease fibrosis and improve regeneration in animal models for VML

Whole muscle replacement and scaling up

Currently, most animal models used for VML repair investigations are rodents. While animal models are a necessary tool for preclinical investigations, in certain instances size differences can outweigh any physiological similarities when studying a small animal model. VML is typically presented as an injury where 20% of the muscles volume is absent after trauma. A 20% reduction in the TA of a rat will result in a loss of mass of ~100mg and a volume less than 0.5 cm³. Large defects in the skeletal muscle of humans could be >200cm³ depending on the affected muscle. This difference in scale matters as the diffusion of oxygen into a scaffold immediately after implantation can sustain a greater proportion of the cells in a rodent model than in a human patient.

A very recent study by Ward et al. demonstrated that autologous MM could provide significant functional recovery in a porcine VML model.(Ward et al., 2016) By creating a 3cm x 3cm x 1.5cm defect in the peroneous tertius, they reduced the maximum tetanic force by 43%. In

muscles repaired with autologous MM, the PT only suffered a 27% reduction in peak tetanic contractile force, which represents a 35% increase over the nonrepaired muscles. The recovery in the larger porcine model was diminished from the recovery observed in rat VML models, where force recovery is generally around 80-85%. (Corona et al., 2013b; Merritt et al., 2010) Ward et al. attributed this difference to the size discrepancy between the defect size in the two animal models. They also observed an increased inflammatory and fibrotic response in the porcine model which hindered revascularization and axonal regeneration. Further studies using larger animal models and more specifically, larger defect sizes will accelerate the development of effective therapies and strategies for treating VML.

The two clinical studies currently published do provide evidence for use of porcine SIS or UBM in VML repair, but there needs to be a more systemic approach when there are multiple injury sites and various comorbidities that complicate results observed in these initial studies. (J. Dziki et al., 2016; Sicari et al., 2014) Skeletal muscle tissue engineering still has several specific challenges that will have to be addressed before a new standard of care emerges for the treatment of VML.

F. Remaining Challenges

Vascularization

One of the biggest challenges for any translational tissue engineering application to overcome, especially scaffold-based therapies, is the challenge of vascularization. Scaffolds by their nature have material that separates one portion of damaged tissue from another portion.

Scaffolds used to repair VML and regenerate skeletal muscle have seemingly opposing design requirements in that one requirement the scaffold should occupy the space left by the volumetric defect and the other is that it allow for in the infiltration of host inflammatory and myogenic cells into all points within the defect void.

Engineered skeletal muscle constructs offer an alternative approach to the use of scaffolds, but the scale of the current generation of engineered muscle constructs is too small to have an application in VML repair.(Juhas, Ye, & Bursac, 2016; Juhas, Engelmayr, Fontanella, Palmer, & Bursac, 2014; VanDusen, Syverud, Williams, Lee, & Larkin, 2014b; Williams, Kostrominova, Arruda, & Larkin, 2013) Although the Larkin group has used engineered constructs to repair VML in animal models, the defect sizes are thus far not clinically relevant.(VanDusen et al., 2014b; Williams et al., 2013) In order to serve as a new standard for the treatment of VML, engineered constructs would have to have sufficient vasculature with functional capillary beds before implantation and would need to have relatively large arteries and veins to connect to systemic circulation of the host. This is in addition to scaling engineered constructs up to a volume sufficient to repair or even replace whole muscle which has suffered a VML injury. However, engineered skeletal muscle has other important applications in biomedical research, including as *in vitro* models for pharmacological investigations and diseased tissue surrogates.(Juhas et al., 2016)

Fibrosis vs. Myogenesis

The final challenge to be discussed in this dissertation is specific to skeletal muscle tissue engineering. The advancement of the field should be focused on: (1) understanding the response of the host immune and muscle tissue to direct cellular activity to myogenesis or fibrosis and (2) how to manipulate scaffold based therapies to maximize the myogenic and regenerative response

of the host tissue. As discussed previously, further characterization of DSM and MM along with characterization of the *in vivo* response to a combined construct in a VML injury niche will be key to developing an effective therapy that is ready for clinical study. Although fibrotic repair can provide some functional benefit, therapeutic success should be defined as maximizing myogenesis for permanent 100% contractile force recovery. In order to successfully repair and regenerate skeletal muscle after a VML injury, researchers should have a clear understanding of the differences between innate muscle repair for minor injuries and attempts at self-repair by muscle after it has suffered a VML injury. The cellular, biochemical, and mechanical cues that are unique to VML injuries should be elucidated to direct researcher toward developing therapies that induce a robust myogenic response.

References

- Ambrosio, F., Ferrari, R. J., Fitzgerald, G. K., Carvell, G., Boninger, M. L., & Huard, J. (2009). Functional overloading of dystrophic mice enhances muscle-derived stem cell contribution to muscle contractile capacity. *Archives of Physical Medicine and Rehabilitation*, *90*(1), 66-73.
- Aurora, A., Roe, J. L., Corona, B. T., & Walters, T. J. (2015). An acellular biologic scaffold does not regenerate appreciable de novo muscle tissue in rat models of volumetric muscle loss injury. *Biomaterials*, *67*, 393-407.
- Aviss, K. J., Gough, J. E., & Downes, S. (2010). Aligned electrospun polymer fibres for skeletal muscle regeneration. *Euro. Cells and Mater.*, *19*, 193-204.
- Boonen, K. J., Langelaan, M. L., Polak, R. B., van der Schaft, D. W., Baaijens, F. P., & Post, M. J. (2010). Effects of a combined mechanical stimulation protocol: Value for skeletal muscle tissue engineering. *Journal of Biomechanics*, *43*(8), 1514-1521. doi:10.1016/j.jbiomech.2010.01.039; 10.1016/j.jbiomech.2010.01.039
- Bouchentouf, M., Benabdallah, B. F., Mills, P., & Tremblay, J. P. (2006). Exercise improves the success of myoblast transplantation in mdx mice. *Neuromuscular Disorders*, *16*(8), 518-529.
- Bursac, N., Juhas, M., & Rando, T. A. (2015). Synergizing engineering and biology to treat and model skeletal muscle injury and disease. *Annual Review of Biomedical Engineering*, *17*, 217-242. doi:10.1146/annurev-bioeng-071114-040640 [doi]
- Cezar, C. A., Roche, E. T., Vandeburgh, H. H., Duda, G. N., Walsh, C. J., & Mooney, D. J. (2016). Biologic-free mechanically induced muscle regeneration. *Proceedings of the National Academy of Sciences of the United States of America*, *113*(6), 1534-1539. doi:10.1073/pnas.1517517113 [doi]
- Choi, J. S., Lee, S. J., Christ, G. J., Atala, A., & Yoo, J. J. (2008). The influence of electrospun aligned poly(epsilon-caprolactone)/collagen nanofiber meshes on the formation of self-aligned skeletal muscle myotubes. *Biomaterials*, *29*(19), 2899-2906. doi:10.1016/j.biomaterials.2008.03.031; 10.1016/j.biomaterials.2008.03.031
- Conboy, I. M., Conboy, M. J., Smythe, G. M., & Rando, T. A. (2003). Notch-mediated restoration of regenerative potential to aged muscle. *Science (New York, N.Y.)*, *302*(5650), 1575-1577. doi:10.1126/science.1087573 [doi]
- Conboy, I. M., Conboy, M. J., Wagers, A. J., Girma, E. R., Weissman, I. L., & Rando, T. A. (2005). Rejuvenation of aged progenitor cells by exposure to a young systemic environment. *Nature*, *433*(7027), 760-764. doi:nature03260 [pii]

- Corona, B. T., Ward, C. L., Baker, H. B., Walters, T. J., & Christ, G. J. (2013). Implantation of in vitro tissue engineered muscle repair constructs and bladder acellular matrices partially restore in vivo skeletal muscle function in a rat model of volumetric muscle loss injury. *Tissue Engineering Part A*, 20(3-4), 705-715.
- Corona, B. T., Wu, X., Ward, C. L., McDaniel, J. S., Rathbone, C. R., & Walters, T. J. (2013a). The promotion of a functional fibrosis in skeletal muscle with volumetric muscle loss injury following the transplantation of muscle-ECM. *Biomaterials*, 34(13), 3324-3335.
- Corona, B. T., Garg, K., Ward, C. L., McDaniel, J. S., Walters, T. J., & Rathbone, C. R. (2013b). Autologous minced muscle grafts: A tissue engineering therapy for the volumetric loss of skeletal muscle. *American Journal of Physiology. Cell Physiology*, 305(7), C761-75. doi:10.1152/ajpcell.00189.2013 [doi]
- Donnelly, K., Khodabukus, A., Philp, A., Deldicque, L., Dennis, R. G., & Baar, K. (2010). A novel bioreactor for stimulating skeletal muscle in vitro. *Tissue Engineering. Part C, Methods*, 16(4), 711-718. doi:10.1089/ten.TEC.2009.0125; 10.1089/ten.TEC.2009.0125
- Dziki, J., Badylak, S., Yabroudi, M., Sicari, B., Ambrosio, F., Stearns, K., . . . Brown, E. H. (2016). An acellular biologic scaffold treatment for volumetric muscle loss: Results of a 13-patient cohort study. *Npj Regenerative Medicine*, 1, 16008.
- Gillies, A. R., Smith, L. R., Lieber, R. L., & Varghese, S. (2010). Method for decellularizing skeletal muscle without detergents or proteolytic enzymes. *Tissue Engineering Part C: Methods*, 17(4), 383-389.
- Grasman, J. M., Do, D. M., Page, R. L., & Pins, G. D. (2015). Rapid release of growth factors regenerates force output in volumetric muscle loss injuries. *Biomaterials*, 72, 49-60.
- Han, N., Yabroudi, M. A., Stearns-Reider, K., Helkowski, W., Sicari, B. M., Rubin, J. P., . . . Ambrosio, F. (2016). Electrodiagnostic evaluation of individuals implanted with extracellular matrix for the treatment of volumetric muscle injury: Case series. *Physical Therapy*, 96(4), 540-549. doi:10.2522/ptj.20150133 [doi]
- Hinds, S., Bian, W., Dennis, R. G., & Bursac, N. (2011). The role of extracellular matrix composition in structure and function of bioengineered skeletal muscle. *Biomaterials*, 32(14), 3575-3583. doi:10.1016/j.biomaterials.2011.01.062; 10.1016/j.biomaterials.2011.01.062
- Huang, N. F., Lee, R. J., & Li, S. (2010). Engineering of aligned skeletal muscle by micropatterning. *American Journal of Translational Research*, 2(1), 43-55.
- Hurd, S. A., Bhatti, N. M., Walker, A. M., Kasukonis, B. M., & Wolchok, J. C. (2015). Development of a biological scaffold engineered using the extracellular matrix secreted by skeletal muscle cells. *Biomaterials*, 49, 9-17.

- Juhas, M., Ye, J., & Bursac, N. (2016). Design, evaluation, and application of engineered skeletal muscle. *Methods*, 99, 81-90.
- Juhas, M., Engelmayer, G. C., Jr, Fontanella, A. N., Palmer, G. M., & Bursac, N. (2014). Biomimetic engineered muscle with capacity for vascular integration and functional maturation in vivo. *Proceedings of the National Academy of Sciences of the United States of America*, 111(15), 5508-5513. doi:10.1073/pnas.1402723111 [doi]
- Kasukonis, B., Kim, J., Brown, L., Jones, J., Ahmadi, S., Washington, T., & Wolchok, J. (2016). Codelivery of infusion decellularized skeletal muscle with minced muscle autografts improved recovery from volumetric muscle loss injury in a rat model. *Tissue Engineering Part A*, 22(19-20), 1151-1163.
- Kasukonis, B., Kim, J., Washington, T., & Wolchok, J. (2016). Development of an infusion bioreactor for the accelerated preparation of decellularized skeletal muscle scaffolds. *Biotechnology Progress*, doi:10.1002/btpr.2257 [doi]
- Kim, J. T., Kasukonis, B. M., Brown, L. A., Washington, T. A., & Wolchok, J. C. (2016). Recovery from volumetric muscle loss injury: A comparison between young and aged rats. *Experimental Gerontology*, 83, 37-46.
- Lam, M. T., Huang, Y. C., Birla, R. K., & Takayama, S. (2009). Microfeature guided skeletal muscle tissue engineering for highly organized 3-dimensional free-standing constructs. *Biomaterials*, 30(6), 1150-1155. doi:10.1016/j.biomaterials.2008.11.014; 10.1016/j.biomaterials.2008.11.014
- Langelaan, M. L., Boonen, K. J., Rosaria-Chak, K. Y., van der Schaft, Daisy WJ, Post, M. J., & Baaijens, F. (2011). Advanced maturation by electrical stimulation: Differences in response between C2C12 and primary muscle progenitor cells. *Journal of Tissue Engineering and Regenerative Medicine*, 5(7), 529-539.
- Li, M. T. A., Willett, N. J., Uhrig, B. A., Guldberg, R. E., & Warren, G. L. (2014). Functional analysis of limb recovery following autograft treatment of volumetric muscle loss in the quadriceps femoris. *Journal of Biomechanics*, 47(9), 2013-2021.
- Mase, V. J., Hsu, J. R., Wolf, S. E., Wenke, J. C., Baer, D. G., Owens, J., . . . Walters, T. J. (2010). Clinical application of an acellular biologic scaffold for surgical repair of a large, traumatic quadriceps femoris muscle defect. *Orthopedics*, 33(7)
- Merritt, E. K., Cannon, M. V., Hammers, D. W., Le, L. N., Gokhale, R., Sarathy, A., . . . Farrar, R. P. (2010). Repair of traumatic skeletal muscle injury with bone-marrow-derived mesenchymal stem cells seeded on extracellular matrix. *Tissue Engineering. Part A*, 16(9), 2871-2881. doi:10.1089/ten.TEA.2009.0826; 10.1089/ten.TEA.2009.0826
- Mintz, E. L., Passipieri, J. A., Lovell, D. Y., & Christ, G. J. (2016). Applications of in vivo functional testing of the rat tibialis anterior for evaluating tissue engineered skeletal muscle

repair. *Journal of Visualized Experiments : JoVE*, (116). doi(116), 10.3791/54487.
doi:10.3791/54487 [doi]

- Page, R. L., Malcuit, C., Vilner, L., Vojtic, I., Shaw, S., Hedblom, E., . . . Dominko, T. (2011). Restoration of skeletal muscle defects with adult human cells delivered on fibrin microthreads. *Tissue Engineering.Part A*, 17(21-22), 2629-2640.
doi:10.1089/ten.TEA.2011.0024; 10.1089/ten.TEA.2011.0024
- Pennisi, C. P., Olesen, C. G., de Zee, M., Rasmussen, J., & Zachar, V. (2011). Uniaxial cyclic strain drives assembly and differentiation of skeletal myocytes. *Tissue Engineering Part A*, 17(19-20), 2543-2550.
- Pereira, T., Armada-da Silva, P. A., Amorim, I., Rema, A., Caseiro, A. R., Gartner, A., . . . Mauricio, A. C. (2014). Effects of human mesenchymal stem cells isolated from wharton's jelly of the umbilical cord and conditioned media on skeletal muscle regeneration using a myectomy model. *Stem Cells International*, 2014, 376918. doi:10.1155/2014/376918 [doi]
- Prevel, C. D., Eppley, B. L., Summerlin, D., Jackson, J. R., McCarty, M., & Badylak, S. F. (1995). Small intestinal submucosa: Utilization for repair of rodent abdominal wall defects. *Annals of Plastic Surgery*, 35(4), 374-380.
- Sicari, B. M., Rubin, J. P., Dearth, C. L., Wolf, M. T., Ambrosio, F., Boninger, M., . . . Badylak, S. F. (2014). An acellular biologic scaffold promotes skeletal muscle formation in mice and humans with volumetric muscle loss. *Science Translational Medicine*, 6(234), 234ra58.
doi:10.1126/scitranslmed.3008085 [doi]
- Tanner, J., Vandeput, J., & Olley, J. (1964). The mesh skin graft. *Plast Reconstr Surg*, 34(3), 287-292.
- Tatsumi, R. (2010). Mechano-biology of skeletal muscle hypertrophy and regeneration: Possible mechanism of stretch-induced activation of resident myogenic stem cells. *Animal Science Journal*, 81(1), 11-20.
- Thompson, N. (1971). Autogenous free grafts of skeletal muscle: A preliminary experimental and clinical study. *Plastic and Reconstructive Surgery*, 48(1), 11-27.
- Valentin, J. E., Turner, N. J., Gilbert, T. W., & Badylak, S. F. (2010). Functional skeletal muscle formation with a biologic scaffold. *Biomaterials*, 31(29), 7475-7484.
doi:10.1016/j.biomaterials.2010.06.039; 10.1016/j.biomaterials.2010.06.039
- Vandenburgh, H. H., & Karlisch, P. (1989). Longitudinal growth of skeletal myotubes in vitro in a new horizontal mechanical cell stimulator. *In Vitro Cellular & Developmental Biology*, 25(7), 607-616.

- VanDusen, K. W., Syverud, B. C., Williams, M. L., Lee, J. D., & Larkin, L. M. (2014). Engineered skeletal muscle units for repair of volumetric muscle loss in the tibialis anterior muscle of a rat. *Tissue Engineering Part A*, 20(21-22), 2920-2930.
- Ward, C. L., Ji, L., & Corona, B. T. (2015). An autologous muscle tissue expansion approach for the treatment of volumetric muscle loss. *BioResearch Open Access*, 4(1), 198-208.
- Ward, C. L., Pollot, B. E., Goldman, S. M., Greising, S. M., Wenke, J. C., & Corona, B. T. (2016). Autologous minced muscle grafts improve muscle strength in A porcine model of volumetric muscle loss injury. *Journal of Orthopaedic Trauma*, doi:10.1097/BOT.0000000000000673 [doi]
- Williams, M. L., Kostrominova, T. Y., Arruda, E. M., & Larkin, L. M. (2013). Effect of implantation on engineered skeletal muscle constructs. *Journal of Tissue Engineering and Regenerative Medicine*, 7(6), 434-442.

Appendix



UNIVERSITY OF
ARKANSAS

Office of Research Compliance

MEMORANDUM

TO: Jeffrey Wolchok

FROM: Craig N. Coon, Chairman
Institutional Animal Care and Use Committee

DATE: May 14, 2014

SUBJECT: IACUC APPROVAL
Expiration date: May 14, 2017

The Institutional Animal Care and Use Committee (IACUC) has APPROVED protocol 14044: "Engineering a Muscle Mimetic Biomaterial". We have listed the start date as May 15, 2014.

In granting its approval, the IACUC has approved only the information provided. Should there be any further changes to the protocol during the research, please notify the IACUC in writing (via the Modification form) prior to initiating the changes. If the study period is expected to extend beyond May 14, 2017 you must submit a new protocol. By policy the IACUC cannot approve a study for more than 3 years at a time.

The IACUC appreciates your cooperation in complying with University and Federal guidelines for involving animal subjects.

CNC/aem

cc: Animal Welfare Veterinarian

Administration Building 210 • 1 University of Arkansas • Fayetteville, AR 72701-1201 • 479-575-4572
Fax: 479-575-3846 • <http://vpred.uark.edu/199>
The University of Arkansas is an equal opportunity/affirmative action institution.